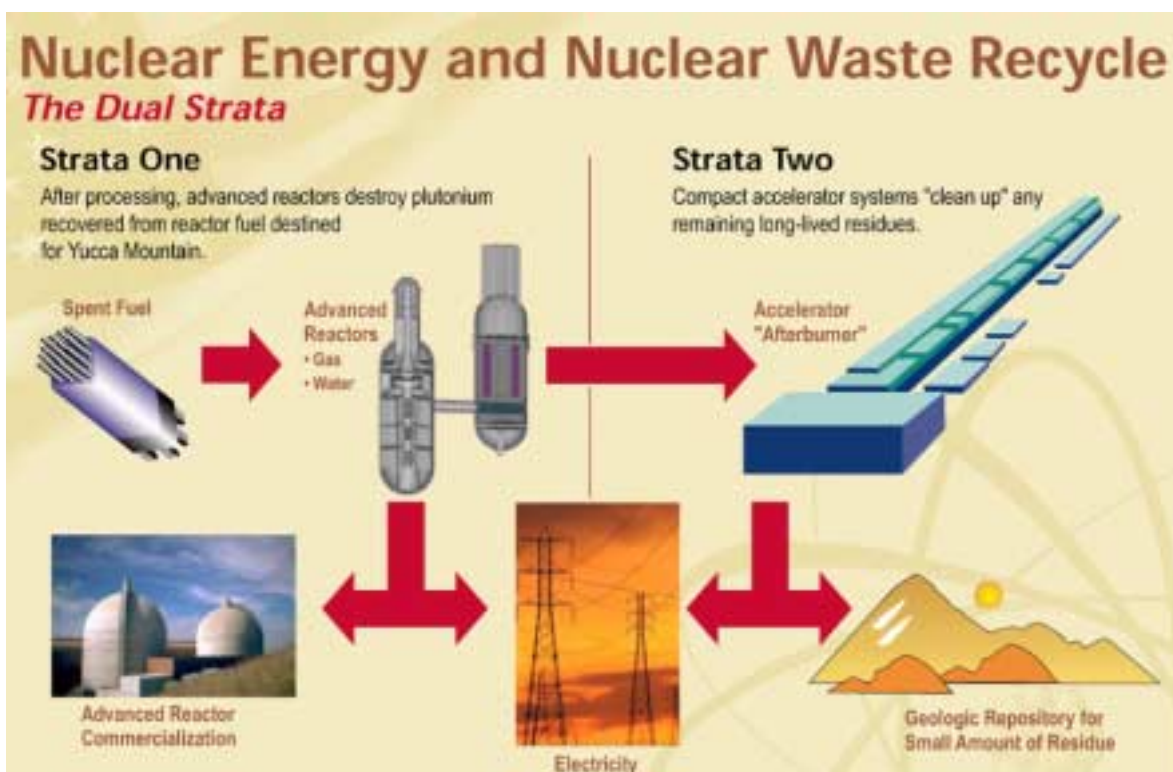




PDO-RGN-1004
AAA-PDO-GEN-01-0024
31 July 2001

AAA Quarterly Report April–June 2001

LA-UR 01-4283



Los Alamos National Laboratory, Argonne National Laboratory
Oak Ridge National Laboratory, Sandia National Laboratories
Brookhaven National Laboratory, Lawrence Livermore National Laboratory
Burns & Roe, Enterprises, Inc., General Atomics, Westinghouse Savannah River Company
University of Nevada, University of Michigan, University of California, University of Texas

This page left intentionally blank

AAA Technical Quarterly Report

April–June 2001

LA-UR 01-4283

PDO-RGN-1004

AAA-PDO-GEN-01-0024

Approval

Signature on file

Date 8/15/01

R. Bruce Matthews
AAA Program Director
Advanced Accelerator Applications

This page left intentionally blank

Table of Contents

Major Contributors	viii
Acronyms	ix
I. INTRODUCTION	1
II. HIGHLIGHTS	3
III. TECHNOLOGY DEVELOPMENT	7
1. Fuels Development	7
Scope	7
Highlights	7
Fabrication Development	8
Oxide Fuel Fabrication	8
Metal Fuel Fabrication	8
Nitride Fuel Fabrication	10
Irradiation Testing	11
ATW-1	11
ATW-3	13
Assessment of Radiation Tolerance	14
Fuel Design	15
General Discussion of Unpublished, Relevant Fuel Performance Results	16
Review of Experimental Data on He Generation in Am-Bearing Fuels	17
Evaluation of Potential He Generation Effects on Transmutation Fuel Performance	24
Modeling	26
2. Separations Technology	27
Scope	27
Highlights	27
Development of the AMUSE Code	28
Evaluation of the Stability of AHA	28
Effect of Dissolved Iron on AHA Stability	29
Development of Processes for Treatment of Oxide Transmuter Fuels	29
Ceramic-Ceramic Oxide Dispersion Fuels	29
Ceramic-Metal Oxide Dispersion Fuels	30
Extraction of Technetium in the UREX Process	30
PYRO-A Process Development	30
3. Accelerator Development	31
3.1 Low Energy Demonstration Accelerator	31
Scope	31
Major Highlights	31
Layout of the Quadrupole Magnet FODO Lattice	31
Measurements of Beam Halo in the Quadrupole Magnet Lattice	32
Measurement of the Bunched-Beam Current	35

CCDTL Post-Braze Tuning and Installation on the Hot Model Test Stand.....	36
Milestone and DDN Documentation Progress	38
3.2 High Energy Linac.....	38
Scope	38
Highlights	38
Spoke Cavity Development.....	39
Cavity Testing	41
APT SCRF DDN Work	43
4. Transmuter Development.....	43
Scope	43
Highlights	44
Analysis Support.....	44
Nuclear Codes and Data.....	45
Thermal-Hydraulic Codes	51
Laboratory Experiments	54
Irradiation Tests.....	55
5. Spallation Target Development	56
Scope	56
Highlights	57
LBE Technology – Materials Test Loop (MTL)	57
Materials Research	59
IV. ENGINEERING DESIGN & DEVELOPMENT	67
6. APT Engineering Design.....	67
Scope	67
Highlights	67
Preliminary Design Status.....	67
Top-Level Design Documents	68
System Design Descriptions (SDDs).....	68
Interface Control	69
Analysis, Calculations, and Modeling.....	69
Design Changes	71
Design Drawings	71
7. Accelerator-Driven Test Facility (ADTF).....	72
Scope	72
Highlights	73
7.1 Systems Integration	74
Overall Facility Design and Arrangement.....	74
ADTF Missions, Functions, and Requirements.....	75
Critical Decision - 0 (CD-0) Package.....	76
Cost Estimate	76
7.2 ADTF Target and Material Test (TMT) Station.....	76
Target and Material Test (TMT) Station Design	76
LBE Target Design	77

Sodium-Cooled Tungsten Target Design	81
Helium-Cooled Tungsten Target Design	81
Heat Removal System Design	82
7.3 ADTF Subcritical Multiplier - 100 MW (SCM-100) Design	84
Sodium-Cooled Fast-Spectrum SCM Design.....	86
SCM Neutron Physics Design.....	90
SCM Neutron Physics Calculations with an LBE Target	90
SCM Neutron Physics Calculations with a Solid Tungsten Target.....	92
SCM Target Designs	93
LBE Target Design	93
Solid Tungsten-Target Design	96
Thermal Fatigue Analysis.....	97
7.4 Balance of Facility Design	98
 V. PROJECT INTEGRATION	 101
 8. Systems and Technology Integration	 101
Scope	101
Highlights	101
Multi-Strata Evaluations	101
 9. University Programs.....	 103
Scope	103
Highlights	103
University Participation Program	104
 10. Collaborations.....	 104
Scope	104
Highlights	105
Meeting with CEA at Saclay.....	105
OECD/NEA Working Party on Partitioning and Transmutation	106

Major Contributors

Fuels Development:	D. Crawford (ANL) K. Chidester (LANL) M. Meyer (ANL) S. Hayes (ANL) R. Margevicius (LANL) K. McClellan (LANL)
Separations Technology:	J. Laidler (ANL)
Accelerator Development:	R. Sheffield (LANL) V. Smith (LANL) D. Chan (LANL) P. Colestock (LANL) R. Wood (LANL)
Transmuter Development:	K. Pasamehmetoglu (LANL) B. Hill (ANL) M. Chadwick (LANL) J. Spore (LANL) M. Farmer (ANL) S. Wender (LANL)
Spallation Target Development:	K. Pasamehmetoglu (LANL) N. Li (LANL) S. Maloy (LANL)
APT Engineering Design:	C. Rodriguez (BREI/GA) R. Chuebon (BREI/GA) J. Tooker (BREI/GA) A. Baxter (BREI/GA) G. Campbell (BREI/GA) D. McEachern (BREI/GA) B. Boore (WSRC) L. Parme (BREI/GA)
Accelerator-Driven Test Facility:	M. Cappiello (LANL) S. McConnell (LANL) K. Pasamehmetoglu (LANL) J. Roglans (ANL) R. Guffee (LANL) H. Cohen (BREI/GA) J. Herceg (ANL) E. Pitcher (LANL)
Systems & Technology Integration:	G. Van Tuyle (LANL) D. Bennett (LANL)
University Programs:	D. Beller (LANL) A. Hechanova (UNLV)
Collaborations:	G. Van Tuyle (LANL)

Acronyms

AAA	Advanced Accelerator Applications
ADS	Accelerator-Driven System
ADTF	Accelerator-Driven Test Facility
AES	Advanced Energy Systems (formerly Northrup-Grumman Corp.)
AET	Ability Engineering Technology
AHA	Acetohydroxamic Acid
ANL	Argonne National Laboratory
ANRC	Amarillo National Research Center
ANS	American Nuclear Society
appm	atomic parts per million
APT	Accelerator Production of Tritium
ASME	American Society of Mechanical Engineers
ATR	Advanced Test Reactor (INEEL)
ATW	Accelerator Transmutation of Waste
BBE	Backbone Beam Enable System
BCCM	Bridge-Coupler Cold Model
BCM	Beam-Current Monitor
BCP	Baseline Change Proposal
BCP	Buffered Chemical Polishing
Beta (β)	Ratio to the speed of light
BNFL	British Nuclear Fuels, Ltd
BNL	Brookhaven National Laboratory
BOL	beginning of life
BOR-60	Sodium-Cooled Fast Reactor (Dimitrovgrad, Russia)
BPM	Beam-Position Monitor
CCDTL	Coupled-Cavity Drift-Tube Linac
CCL	Coupled-Cavity Linac
CEA	Commissariat à l'Energie Atomique (France)
CEM	Cascade Exciton Model code (Model-based Monte-Carlo particle transport code)
CERCA	Compagnie Pour L'Etude Et La Realisation De Combustibles Atomiques
cercer	ceramic-ceramic
cermet	ceramic-metal
CLWR	Commercial Light Water Reactor
CMR	Chemistry and Metallurgy Research (facility at LANL)
CONCERT	COMbined Neutron Center for European Research and Technology
CTR	Cryogenic Test Rig
cw	continuous wave (100% duty factor)
DCR	Design Change Request
DDN	Design Data Need
dpa	displacements per atom
EBR	Experimental Breeder Reactor
ED&D	Engineering Development and Demonstration
EEV	English Electric Valve
EFPD	Effective Full-Power Day
EIS	Electrochemical Impedance Spectroscopy
EIS	Environmental Impact Statement
EOI	end of irradiation
EOL	end of life
EPICS	Experimental Physics and Industrial Control System
ERC	External Review Committee
ES&H	Environmental, Safety, and Health

ESS	European Spallation Source
ESSAB	Energy System Acquisition Advisory Board (DOE)
FZK	Forschungs Zentrum Karlsruhe (German Nat'l Lab)
FDD	Facility Design Description
FODO	focus-drift-defocus-drift
fpv	full power year
HCP	Hazard Control Plan
GSI	Gesellschaft für Schwerionenforschung (Darmstadt, Germany)
GT-MHR	Gas Turbine Modular Helium Reactor
HEBT	High-Energy Beam Transport
HFR	High Flux Reactor (Petten, Netherlands)
HIP	Hot Isostatic Process (for bonding materials)
HM	heavy metal
HPRF	High-Power Radio Frequency
HS/WS	halo-scraper/wire-scanner (diagnostic device)
I&C	Instrumentation and Control
ICS	Integrated Control System
IFMIF	International Fusion Materials Irradiation Facility
IFR	Integral Fast Reactor
IMS	Information Management System
IHX	Intermediate Heat Exchanger
INEEL	Idaho National Engineering and Environmental Laboratory
IOT	Inductive-Output Tube
ISTC	International Science and Technology Centre (Moscow)
JAERI	Japan Atomic Energy Research Institute
JCNNM	Johnson Controls Northern New Mexico
JLAB	Jefferson Laboratory (VA)
KEK	National Laboratory for High-Energy Physics (Tsukuba, Japan)
LAHET	Los Alamos High-Energy Transport
LANL	Los Alamos National Laboratory
LANSC	Los Alamos Neutron Science Center
LBE	Lead-Bismuth Eutectic
LBHM	Low- β Hot Model
LEBT	Low-Energy Beam Transport
LEDA	Low Energy Demonstration Accelerator
LLFP	Long-Lived Fission Product
LLNL	Lawrence Livermore National Laboratory
LLRF	Low-Level Radio Frequency
LMR	Liquid Metal Reactor
LWR	Light Water Reactor
MCNP	Monte Carlo N-Particle Transport Code
MCNPX	Merged code - Los Alamos High-Energy Transport (LAHET) and Monte Carlo N-Particle Codes (MCNP)
MEGAPIE	MEGAwatt Pilot Experiment
MOX	Mixed oxide fuel
MTL	Materials Test Loop
n/p	neutrons per proton
NDA	Non-Destructive Analyses
NEA	Nuclear Energy Agency (Paris)
NEPA	National Environmental Protection Agency
NERAC	Nuclear Energy Research Advisory Committee
NERI	Nuclear Energy Research Initiative
NFF	non-fertile fuel
O&M	Operations and Maintenance
OECD	Organization for Economic Cooperation and Development (Paris)
ORNL	Oak Ridge National Laboratory

P&ID	Piping and Instrumentation Diagram
PACS	Personnel Access Control System
PFD	Process Flow Diagram
PHENIX	Fast Reactor in France
PIE	post-irradiation examination
PNNL	Pacific Northwest National Laboratory
PPO	Plant Project Office
PRAD	Proton Radiography
PRISM	Power Reactor Innovative Small Module
PSAR	Preliminary Safety Analysis Report
PSS	Personnel Safety System
PSI	Paul Scherrer Institute (Switzerland)
PUREX	Plutonium-Uranium Extraction
PWR	Pressurized Water Reactor
PYRO	Pyrochemical Process
Q	Quality Factor
QA	Quality Assurance
QAC	<u>Quick ATW Costing</u>
RAMI	Reliability, Availability, Maintainability, and Inspectability
RERTR	Reduced Enrichment for Research and Test Reactors program
RF	Radio Frequency
RFQ	Radiofrequency Quadrupole
RCCS	Resonance-Control Cooling System
RIA	Rare Isotope Accelerator
RIAR	Russian Institute of Atomic Reactors
RRR	Residual Resistance Ratio
RTTB	Room Temperature Test Bed
SAR	Safety Analysis Report
SC	Superconducting
SCRF	Superconducting RF
SDD	System Design Description
SEM	Scanning Electron Microscopy
SINQ	Spallation Neutron Source at Paul Scherrer Institute (Switzerland)
SNL	Sandia National Laboratory
SRS	Savannah River Site
SRTC	Savannah River Technology Center
STAYSL2	A computer code used to analyze the results of the activation foil measurements in both a proton and neutron flux
STP	standard temperature and pressure
STIP	Spallation Target Irradiation Program (at PSI)
T/p	Tritons (nucleii of tritium atoms) per proton
T/B	Target / Blanket
TBP	tri- <i>n</i> -butyl phosphate or "TriButylPhosphate"
TEM	Transmission Electron Microscopy
TESLA	International Collaboration on a TeV Superconducting Linear Accelerator
TJNAF	Thomas Jefferson National Accelerator Facility
TMT	Target and Materials Test Station
TRAC	Transient Reactor Analysis Code
TRISPAL	Refers to the French APT Program
TRU	transuranics (plutonium, neptunium, americium, and curium)
TSF	Tritium Separation Facility
UFP	University Fellowship Program
UNLV	University of Nevada Las Vegas
UPP	University Participation Program
UREX	Uranium Extraction (an aqueous partitioning process)
URP	University Research Program

USQD	Unreviewed Safety Question Determination
WBS	Work Breakdown Structure
WNR	Weapons Neutron Research (facility at LANL)
WPPT	Working Party on Partitioning and Transmutation
WS/HS	Wire Scanner / Halo Scraper (beam diagnostic device)
WSRC	Westinghouse Savannah River Company
ZPPR	Zero Power Physics Reactor

Advanced Accelerator Applications

Quarterly Report

April–June 2001

I. INTRODUCTION

The Advanced Accelerator Applications (AAA) Program is a Department of Energy program commissioned last year by Congress. Los Alamos leads a national effort consisting of DOE laboratories (Los Alamos, Argonne, Savannah River, Livermore, Oak Ridge), industry (Burns and Roe Engineering Inc, General Atomics) and universities (Berkeley, Texas, Michigan, Nevada). The primary mission of the AAA Program is to develop the technology base for the transmutation of nuclear waste and to demonstrate its practicality and value for long-term waste management.

The AAA Program was constituted by combining two programs: The Accelerator Production of Tritium (APT) Program and the Accelerator Transmutation of Waste (ATW) Program. The APT Program was established in 1995 with a commercial light water reactor (CLWR) program as part of a dual-path strategy for development of a new tritium-production technology for the nation. From 1995 through 2001, Defense Programs (DOE) invested in the design and development of an accelerator to produce tritium, including a full-scale prototype of the front-end of the accelerator. In December 1998, the Department chose the CLWR as the primary technology for tritium production, assigning APT the role of a backup technology, which affords Defense Programs the opportunity to establish a robust backup technology to assure the nation's capability to produce tritium. The Accelerator Transmutation of Waste (ATW) Program, funded by Congress in FY00, has been investigating the feasibility of accelerator-driven systems to transmute long-lived toxic components of spent nuclear fuel. Together, these two programs benefit each other by integrating common technologies.

The goal of the AAA Program is to evaluate the effectiveness of transmutation of spent nuclear fuel against the following criteria:

- (1) reduce the long-term radiological impact of waste;
- (2) enable development of a simpler, cheaper repository;
- (3) reduce proliferation risk; and
- (4) improve long-term prospects of nuclear power.

Improving the long-term prospects of nuclear power means not only demonstrating through proof-of-performance the practicality of the transmutation of nuclear waste and its meaningful impact on nuclear materials, waste management, and economics, but also defining and executing activities designed to support the country's nuclear science and engineering infrastructure. In addition to these goals, the AAA Program will continue technology development and demonstration applicable to a backup tritium-production capability, should national security needs dictate.

For the short term, the AAA Program has focused its efforts on (1) evaluating the most effective systems for transmutation of spent nuclear fuel, (2) developing separations

technologies to partition long-lived radioactive waste from reusable nuclear material, (3) developing and testing potential transmutation fuels, (4) developing, constructing, and demonstrating both the low-energy portion and the superconducting RF technology for the high-energy portion of the accelerator, which is required for production of tritium and for testing transmutation fuels, (5) developing a spallation target to provide an effective environment for transmutation, (6) establishing and supporting a national university program to reenergize development and training in nuclear-related fields, and (7) collaborating in international research efforts with nations involved in evaluating nuclear waste management. Through these focused efforts, the AAA Program is defining key experiments, analyses, and facilities needed to demonstrate the technical viability of partitioning and transmutation of long-lived nuclear wastes.

A key future objective of AAA is the construction of an accelerator-driven test facility (ADTF). The goal of the facility would be to demonstrate the transmutation of nuclear waste and to function as a national nuclear science and engineering user facility.

II. HIGHLIGHTS

Fuels Development

- An americium-bearing plutonium-oxide pellet has been fabricated, a first-time achievement in transmutation fuels in the US, accomplishing a milestone.
- A potential technique for arc casting of TRU-Zr alloy fuel slugs has been developed and demonstrated with a stainless steel surrogate alloy, which should enable fabrication of metal segments of transmutation fuels for testing.
- The experiment description package for the ATW-1 Irradiation Test—a test of transmutation fuels to be irradiated in the advanced test reactor (ATR)—is nearly complete. Design and safety calculations indicate that ATW-1 test objectives can be achieved with the present scheme.

Separations Technology

- Development and optimization of the AMUSE code for modeling AAA solvent extraction processes is progressing well. This code can now be used to optimize the demonstration of the complete UREX flowsheet. Models for the extraction of U, Np, Pu and Tc have been incorporated in the code, and user-input has been enhanced for greater flexibility.
- For the UREX process reductant/complexant, the stability of acetohydroxamic acid (AHA—the reagent that suppresses plutonium and neptunium extraction in the UREX process) in nitric acid has been determined under a wide range of process operating conditions and found to be more than adequate for transmutation applications.
- Conceptual process flowsheets for the treatment of transmuter oxide fuels have been developed for the PYRO-B process. They are similar to the PYRO-A process for LWR spent fuel treatment. A commonality of process design could result in significant reductions in cost for chemical separations.
- Recent studies in the recovery of technetium confirm the expectation that Tc will extract with uranium and can be subsequently stripped with high efficiency. This should make it feasible to achieve the goal of >95% Tc recovery from LWR spent fuel.

Accelerator Development

- The beam-halo measurements performed on the Low Energy Demonstration Accelerator (LEDA) at LANL were completed, meeting a Level-1 milestone as scheduled.
- Section 2 of the coupled-cavity drift-tube linac (CCDTL) accelerating structure was tuned and installed on the hot-model test stand in the LEDA building at LANL.
- Following an external review of the Accelerator-Driven Test Facility (ADTF) linac, the review committee recommended replacing the CCDTL and CCL (coupled cavity linac) of the ADTF design with superconducting spoke cavities and $\beta=0.48$

elliptical cavities, respectively, which will result in a linear accelerator (linac) that is almost completely superconducting.

Transmuter Development

- The upgraded CEM2k code (Cascade Exciton Model code) was delivered to the MCNPX code developers, considerably improving the intra-nuclear cascade physics modeling capability of the MCNPX code.
- The liquid-metal-cooled and helium-cooled systems-modeling updates (ATW upgrades) to the Transient Reactor Analysis Code (TRAC), providing a systems-modeling capability for transmuter assessment, were incorporated into TRAC-M (the NRC version). These changes and the test results were documented and submitted to the NRC.

Spallation Target Development

- The report, *Preliminary Assessment of the Spallation Target Options for Accelerator Driven-Transmutation*, compiling the initial assessment of various target options, was published and distributed.
- The *Lead-Bismuth Eutectic Materials Test Loop Test Plan*, emphasizing the facility description for the Materials Test Loop (MTL), was issued.
- Under the APT ED&D program, Design Data Need, DDN 30, *Light Water Corrosion*, was completed.

APT Engineering Design

- The top-level APT document, *Facility Design Description* was revised and released, satisfying a significant Level-2 milestone. The APT *Safety Requirements Document*, a Level 2 milestone, was also completed on schedule.

Accelerator-Driven Test Facility

- The Critical Decision-0 (CD-0) package materials, submitted to DOE headquarters in March, was distributed and used to brief most of the DOE office directors in preparation for a formal review by the DOE Energy System Acquisition Advisory Board (ESAAB).
- The revision of the Accelerator-Driven Test Facility (ADTF) Missions, Functions, and Requirements document was completed, and a final updated draft issued for final acceptance review.
- Design review meetings were held with the French *Commissariat à l'Energie Atomique* (CEA) in June to discuss international collaborative efforts on the ATDF project.

Systems & Technology Integration

- AAA Task Force on AAA System Definition was formed, implementing a “nuclear future” approach to multi-strata evaluations.
- Multi-strata system cases have been specified, and environmental, proliferation, and economic factors are being considered in multi-strata system evaluations.

University Programs

- Ten fellowship recipients were selected by a Blue Ribbon Panel to receive funding in the AAA University Fellowship Program. Summer internship positions were established at LANL and ANL for four of the selected Fellows.
- The AAA University Participation Program was initiated at the University of Nevada Las Vegas (UNLV) with a \$3M budget. The program is providing funding for four student research proposals related to AAA work.

Collaborations

- A delegation from the AAA Program, including representatives from the DOE, LANL, and ANL, participated in meetings with the *Commissariat à l'Energie Atomique* (CEA) in France during June, and discussed a number of work packages concerning the proposed ADTF.
- A meeting of the Nuclear Energy Agency (NEA) Working Party on Partitioning and Transmutation (WPPT) met in Paris to discuss a number of issues being evaluated by AAA within an international context.

This page left intentionally blank

III. TECHNOLOGY DEVELOPMENT

1. Fuels Development

Scope

AAA fuel development activities are directed toward the development and qualification of fuels for safe transmutation of actinides at maximal rates. The objective of the effort is to provide one (or more) transmutation fuel form(s) at Technical Readiness Level (TRL) 6 at the time that transmutation technology overall is to begin integral demonstration. Thus far, requirements for such fuels include non-fertile compositions in forms suitable for fast-spectrum transmuters and a homogenous fuel cycle (i.e., all minor actinides would be maintained in the same fuel and processing stream). However, the AAA transmutation program is considering additional transmuter architectures, the use of which would imply different requirements for fuels; therefore, the fuel development program is evolving as the nature of and approach for the overall transmutation mission evolves.

The specific R&D activities include development of techniques to fabricate transmutation fuels from LWR fuel-derived actinide feed and from actinide feed recycled from transmuters. As-fabricated samples are chemically and microstructurally characterized to evaluate the success of fabrication processes and to better understand the nature of the fuel materials. Evaluation of proposed fuel forms requires irradiation testing, so near-term irradiation tests are being planned and will be performed through the course of this program. Finally, the understanding of in-service fuel behavior is best demonstrated through the development and validation of fuel behavior models that are eventually incorporated into fuel performance codes. Such models are being developed, concurrent with an effort to develop thermal models that allow calculation of fuel and cladding temperatures in service and during testing.

Highlights

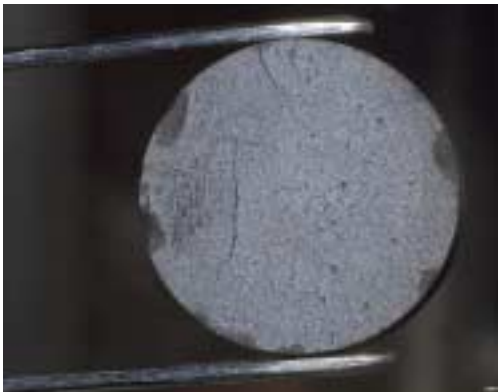
- An americium-bearing plutonium-oxide pellet has been fabricated.
- A potential technique for arc casting of TRU-Zr alloy fuel slugs has been developed and demonstrated with a stainless steel surrogate alloy.
- Sintering at temperatures suitable for AmN processing (to minimize volatilization) provides moderate mechanical integrity to ZrN pellets suggesting that such a process is amenable to low-density (TRU,Zr)N fuel-pellet fabrication.
- The Experiment Description package for the ATW-1 Irradiation Test is nearly complete. Design and safety calculations indicate that ATW-1 test objectives can be achieved with the present scheme.

- Initial heavy-ion damage results indicate that ZrN is surprisingly radiation tolerant. This result, along with uranium-nitride irradiation performance data from the SP100 program, suggests that nitride fuel pellets can show radiation tolerance behavior similar to some of the best ceramic oxides.
- Data from previous irradiation tests of high-actinide fuels and analysis of He generation indicate that He retention and release will have important effects on fuel lifetime. Specific He generation rates appear to be considerably greater than the rate of fission gas generation for fuels with relatively high amounts of Am, suggesting that fuel should be designed to retain enormous amounts of He gas, or to accommodate its release.
- Published data for nitrides with different crystal structures is providing an initial basis for development of pair potentials for atomistic modeling of (TRU)N and ZrN which begins in FY02.

Fabrication Development

Oxide Fuel Fabrication

The Actinide Ceramics team has produced a (Pu-Am) O_2 pellet. Non-destructive analyses (NDA) indicated that the Pu stock that provided the source of this material contained approximately 3.5 wt.% Am. After sintering, the pellet had lost approximately 5% of its weight. The surfaces exposed to the furnace atmosphere turned blue while the surface in contact with the furnace boat was gray (see Fig. 1). The change in color is assumed to be due to a different chemical composition on the surface. The sample has been submitted to the characterization team for optical ceramography and microprobe. Total Am content of the pellet will be measured to determine how much volatilized during the sintering process. It is likely that other volatile species (namely, K and Na) were also volatilized. Other compositions involving Pu O_2 , Am O_2 , and Np O_2 are being planned and executed.



Surface in contact with furnace boat



Surface exposed to furnace atmosphere

Fig. 1. (Pu-Am) O_2 surface in contact with furnace boat and exposed to furnace atmosphere.

Metal Fuel Fabrication

An arc casting process was developed to fabricate metal alloy fuel slugs for the ATW-1 irradiation test. This method also appears to be applicable to fabrication of longer specimens. The arc casting process uses a DC arc to melt an alloy charge, which is then gravity fed into a fuel-pin mold. The arc-melting furnace is similar to a

Tungsten Inert Gas (TIG) welder in operation—an electronic arc is struck onto a charge and moved across the sample surface until sufficient melting has taken place. The significance of this development is that arc-melting techniques have been shown to reduce the loss of volatile americium during alloying and arc casting of Pu-Am alloys¹. If this technique can be successfully applied to fabrication of metal alloy fuel slugs, then it might be possible to fabricate TRU-Zr fuel with acceptable Am volatilization. The status of development of the technique is described in the following paragraphs.

The arc-melting unit used for the testing is a commercially available, single-arc furnace. It consists of water-cooled top and bottom sections, separated by a section of Pyrex tubing that forms the walls of the chamber, allowing observation of the process inside of the chamber. The top section contains a swivel-ball assembly that permits free movement of the top (negative) electrode or stinger. The bottom section contains an opening that allows insertion of the hearth (typically copper or graphite). The bottom-loading hearth design allows for the use of different hearth types. The atmosphere inside the chamber is purged with inert gas. A check valve prevents any over pressuring of the melting chamber. The arc-casting performance of this unit was improved by replacing the 0.094-inch top electrode with a 0.152-inch electrode.

Slug casting has previously been performed at ANL-W for the Reduced Enrichment for Research and Test Reactors (RERTR) program using a split-copper insert in a standard hearth. In that process, the constituents were first melted and blended to form a homogenous alloy button. The button was placed on the split-copper hearth and melted so as to run down into the copper hearth cavity. The slugs cast by this method were 0.25 inches in diameter and slightly greater than one inch in length.

The requirements for the ATW-1 irradiation test program called for a thinner and longer slug (0.157 inches or 4 mm in diameter and 2 inches or 50.8 mm in length). Because premature cooling of the molten metal during the initial pour into the slug mold was considered to be problematic for the required geometry of the AAA fuel slugs, the split copper hearth design was abandoned. In its place a quartz tube of the required internal diameter was inserted into the hearth. The quartz tube acts as both a mold for the fuel slug and as an insulator between the flowing molten metal and the water-cooled copper hearth that allows the metal to flow the required length prior to solidification. Fig. 2 illustrates a blank Centorr hearth and the modified design. The modifications consist of a slanted hearth cavity to allow the melt to flow downward into the quartz tube. The quartz tube enters the hearth cavity from the bottom at its lowest region. The quartz tube is held in place by an outer tube that attaches to the bottom hearth by a threaded fitting.

The quartz tube used for testing is a commercially procured, 6-mm outside diameter tube with a 4-mm inside diameter (0.232-inches OD x 0.157-inches ID). A TIG-welding power supply was used to power the arc-melting furnace. It was run at 375 amps, in the straight DC mode. An adjustable foot pedal was employed for fine control during the melting runs. A high frequency arc starter was used to aid in establishment of the arc, but is not essential.

¹ Ellinger, et. al., *J. Nuc. Mat.* 20 (1966) 83-86

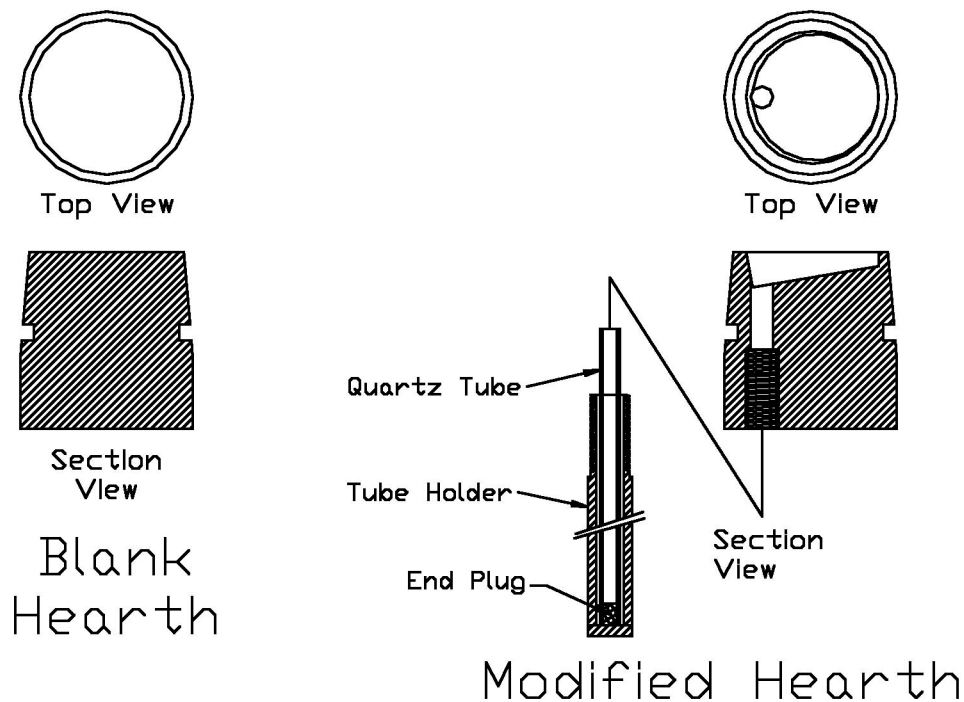


Fig. 2. Hearth Modifications

Approximately 35 pins were cast from stainless and carbon steels. Iterations of hearth design and operational methods that are not described here resulted in the design described above. Using this design, slug lengths of up to 13 inches have been attained, and lengths of 10–11 inches are routine. The total mass of the feedstock ingot must be greater than the desired slug length or a hollow cored slug will be cast. The excess charge mass forms a header on top of the cast slug that can be removed by trimming. Typically, upon cooling, the arc-cast slug was easily removed from the quartz tube with little or no difficulty. In nearly all test runs, the quartz tube was recovered intact and could be reused in subsequent casting. The quartz tube was used as-is with no applied coating as is typically required for injection casting of U-Zr or U-Pu-Zr fuel slugs, although such a coating is not anticipated to be detrimental to the casting process.

Nitride Fuel Fabrication

Glove box operations intended to avoid oxygen contamination have been established for synthesis of zirconium nitride powders. Similar procedures have also been established for pellet pressing and sintering operations. Sintering experiments have been conducted at various temperatures between 1400°C and 1700°C. While sintering is observed at lower temperatures, little densification occurs below 1700°C. Low-temperature processing is anticipated to be necessary to minimize Am volatilization, which will in turn yield a fuel pellet with significant residual porosity. This is consistent with the current nitride fuel pellet design to permit accommodation and release of helium and fission product gases.

A furnace for the conversion of plutonium hydride has been identified. This had been seen as a major impediment to the synthesis of actinide nitrides. It is in the process

of having its standard operating procedure converted to a work instruction. The short-duration hazard control plan to make hydride in one part of the LANL plutonium facility (PF-4), transport it to the fuels rooms, and convert it to nitride is also being written. This will enable the synthesis of nitride feed powder for development tests.

Irradiation Testing

ATW-1

The ATW-1 Experiment Description is nearing completion and will be issued to the Program during the month of July as an expected deliverable. However, several aspects of the experiment as presently conceived will likely be changed before the design is finalized and the experiment inserted into the reactor—specifically, the test matrix of fuel types and the elemental mix of the TRU component in the fuels. The need to modify the test is being driven in large measure by the dual-strata approach now under consideration and the changing TRU fuel compositions associated with the new transmutation strategy. We anticipate a series of ATW-1 irradiation experiments, to be designated ATW-1A, ATW-1B, ATW-1C, etc., in order to accommodate the variety of fuel designs and compositions to be tested and the different target discharge burnups desired. ATW-1A, as presently conceived, is designed to test metallic and nitride fuel forms and will be summarized here. Efforts are now underway to incorporate the proposed oxide fuel designs into the test matrix.

The design of the generic ATW-1 irradiation vehicle accommodates six miniature fuel rods (termed “rodlets”), which are located inside a secondary containment vessel. The containment vessel is required to guard against the release of bond sodium inside the rodlets to the water coolant, provide an additional gas gap to elevate fuel and cladding temperatures into the target ranges, and provide additional plenum volume for fission gas and helium expansion should any fuel rodlet be breached during irradiation. This containment vessel is exposed to the primary reactor coolant, which flows downward. Surrounding the containment vessel is a hafnium (Hf) shroud designed to reduce the incident flux on the experimental fuel rodlets, achieving a target of approximately 400 W/cm linear power at the reactor axial mid-plane. The containment vessel and Hf shroud are contained within a structure termed by the Advanced Test Reactor (ATR) as the “basket”, which is inserted into the desired reactor position. A schematic diagram of the configuration described is shown in Fig. 3. The ATW-1 irradiation vehicle is designed to be irradiated in one of four possible outboard-A positions associated with the two northern lobes of the reactor, which are operated at consistent lobe powers of 17-19 MW.

The experiment, as designed, receives a downward coolant flow velocity of 657 cm/sec and a volumetric flow rate of 172 cm³/sec between the containment vessel and the Hf shroud. The Hf shroud is nominally 0.050 inches in thickness, but may vary as the elemental mix of the TRU component of test fuel is established. This thickness is based on a fuel TRU composition of 86% Pu, 9% ²⁴¹Am and 5% ²³⁷Np; if the Pu fraction of the test fuel is reduced, as anticipated, the thickness of the Hf shroud would be expected to be reduced as well.

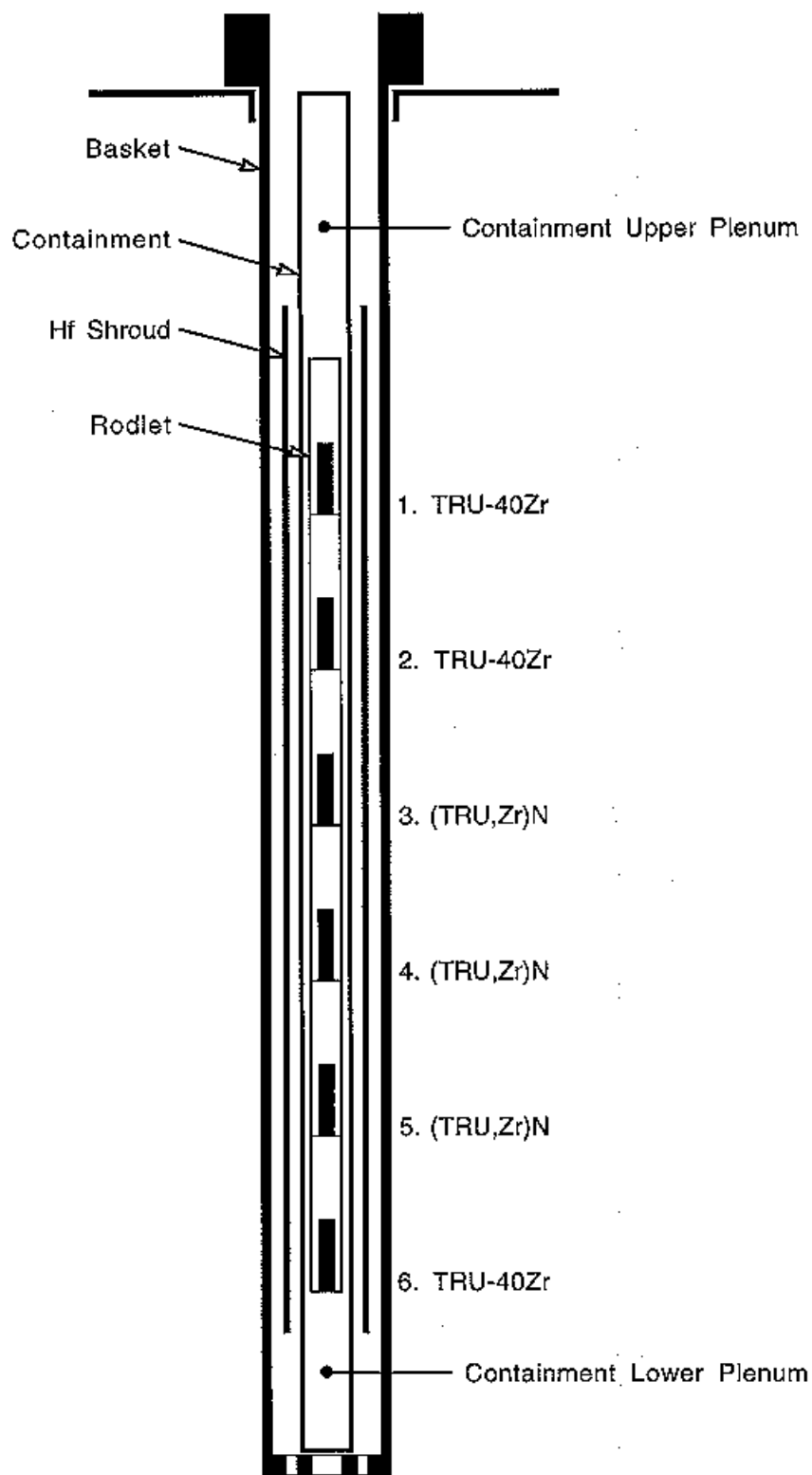


Fig. 3. Schematic diagram of the ATW-1 irradiation vehicle.

The rodlets are 6.0 inches in total length, have a fuel column height of 2.0 inches, and have a plenum-to-fuel height ratio of 1.625; this ratio may need to be increased if the Am fraction in the TRU increases, and would be accomplished by reducing the fuel column height. The rodlets will be fabricated using HT-9 cladding having a nominal OD of 0.230 inches and a wall thickness of 0.018 inches. Because these actinide transmutation fuels are expected to exhibit considerable fuel swelling, the fuel smeared densities are to be kept low: 70% for metallic fuels and 80% for nitride fuels. Both of these fuel types will therefore require sodium bonding. The temperature target is a 500°C peak cladding temperature.

Appropriate sizing of the fuel-pin plenum volumes is still being considered. Of concern is the substantial He production during the thermal irradiation of ^{241}Am , which is expected to produce up to 6 times as much He as fission gasses. It has been currently assumed that the TRU content of the experimental fuel pins will contain 9 wt.% ^{241}Am . Assuming such a fuel pin is irradiated to 20 at.% burnup, 80% of all fission gases are released, and 100% of all He is released, the amount of gas to be accommodated by the plenum is $3.04 \cdot 10^{-4}$ moles/g-TRU. For a fuel column height of 2.0 inches and a fuel-to-plenum height ratio of 1.5, this would mean a fuel-pin pressure at end of life of 573 psi. The ATR technical specifications normally restrict experiment pressures on the outermost boundary to below the primary coolant pressure of 235 psi. Thus, the secondary container must be sized with an adequate free volume to reduce the gas pressure to this value assuming all experimental fuel pins fail. Alternatively, the fuel-to-plenum height ratio can be increased.

The schedule for the insertion of the first of the ATW-1 series of fuels tests in the ATR is June 2002. Meeting a June 2002 insertion date will require completion of the fabrication of the irradiation vehicle, including rodlets, by May 2002. This is a very aggressive schedule, which is being driven by two factors. The first is simply the need to obtain initial irradiation performance data on a variety of Am-rich, non-fertile fuel forms as quickly as possible so that the field of candidate fuel forms can be narrowed. The second is an upcoming ATR outage for a core-internals change-out planned for the summer of 2003, which will result in the ATR being shutdown for 8-10 months.

ATW-3

An AAA Fuels Working Group meeting was held in Chicago during the last week of June, with a representative from the CEA (France). Fuel testing requirements in the PHENIX fast reactor in France were discussed at length. CEA presented the framework for a proposed actinide transmutation fuels irradiation in PHENIX, which would be a collaboration between CEA, DOE, and possibly the Transuranic Institute (ITU) in Germany. The proposal was well received by the Working Group and the Program management personnel in attendance. It is anticipated that this irradiation will become the fast spectrum irradiation test designated ATW-3 in the Fuel Development Program Plan.

During the month of May, John Lambert (ANL), representing the US ATW program, visited the Russian Institute of Atomic Reactors (RIAR) in the Russian Federation (RF). Lambert was joined by Dr. Janne Wallenius of the Royal Institute of Technology (Sweden) representing the European Union's CONFIRM program. Both programs visited RIAR for the purpose of opening discussions related to the possibility of testing actinide transmutation fuels in the BOR-60 fast reactor and

subsequent examinations of such test fuels in local hot cells. The RIAR management extended a warm reception and was very enthusiastic about the long-term scientific interest of the ATW program to their Institute.

Mr. Lambert presented information related to the US ATW fuel development program and its requirements for fast flux irradiation tests. RIAR staff made numerous presentations on the ability of the BOR-60 reactor facility to accommodate fuels tests and the capability of RIAR hot cells to perform post-irradiation examinations of test specimens. At present, the major focus of the BOR-60 reactor is the installation of a Pb-Bi loop, which should be operational in late 2001, to test fuels designed for the Russian BREST reactor. This would not interfere with an ATW test program that begins in 2004 (both the US and European Union programs call for tests of fast-flux fuels to begin in approximately 2004).

The BOR-60 reactor can easily accommodate experimental fuel pins for irradiation through use of "dismountable" assemblies that allow certain numbers of experimental pins to be mixed among driver fuel pins in a standard assembly. Although not explicitly stated, the impression gained in discussions was that RIAR would prefer to sub-contract as the fuels experimenter for ATW in BOR-60. This approach would be more costly, but has the advantage of being more efficient than if the US or a Western consortium assumed that role. This discussion naturally raised the question of whether fuel and fuel pins would best be fabricated in the country of origin, in the RF, or in some combination of the two. It was agreed by all that the test fuels are best fabricated in the country of origin but assembled into pins, and subsequently into test assemblies at RIAR to simplify QA requirements.

Post-irradiation examination capability at the RIAR hot cells is virtually exhaustive, especially with regard to shielded electron instruments (EPMA, SEM/TEM, SIMS, etc); the only capability lacking is neutron radiography. One potential drawback to the RIAR hot cells is that they employ an air atmosphere. When questioned about dealing with sodium-bonded and metallic-alloy fuels, answers provided were vague and it was not clear what procedures are used in the examination of such fuels. Similarly, the use of water as a lubricant in specimen preparation needs evaluation.

Assessment of Radiation Tolerance

Xe-ion implantations of ZrN reveal that this material resists amorphization to high doses of irradiation. ZrN is of interest as a candidate diluent and as a surrogate because it is isostructural with the (TRU)N's. 300 keV Xe⁺⁺ irradiations of ZrN were performed to a fluence of $1 \cdot 10^{16}$ Xe/cm² at a temperature of 70 K (flux = $6 \cdot 10^{12}$ Xe⁺⁺/cm²·s). The ions penetrate about 100 nm into the ZrN and produce a peak nuclear displacement damage equivalent to about 60 dpa. The irradiated material exhibited defect accumulation, but remained crystalline and exhibited the same structure as the substrate (Fig. 4). No amorphization of ZrN was observed to a dose of 60 dpa. This is an important benchmark-irradiation experiment because it demonstrates that ZrN behaves as well as certain ceramics that are classified as radiation tolerant based on their performance under similar radiation conditions. For instance, magnesium aluminate spinel (MgAl₂O₄) is considered to be a radiation resistant material, yet it amorphizes under similar irradiation conditions at ~25 dpa².

² N. Yu, K. E. Sickafus and M. Nastasi, *First Observation of Amorphization in Single-Crystal MgAl₂O₄ Spinel*, Philosophical Magazine Letters **70**[4], 235 [1994]

Cubic-stabilized zirconia ($\text{ZrO}_2 + \text{Y}_2\text{O}_3$) remains crystalline to well over 100 dpa and seems to behave very similarly to ZrN.³ These preliminary experiments indicate that ZrN exhibits radiation tolerance behavior similar to some of the best ceramic oxides.

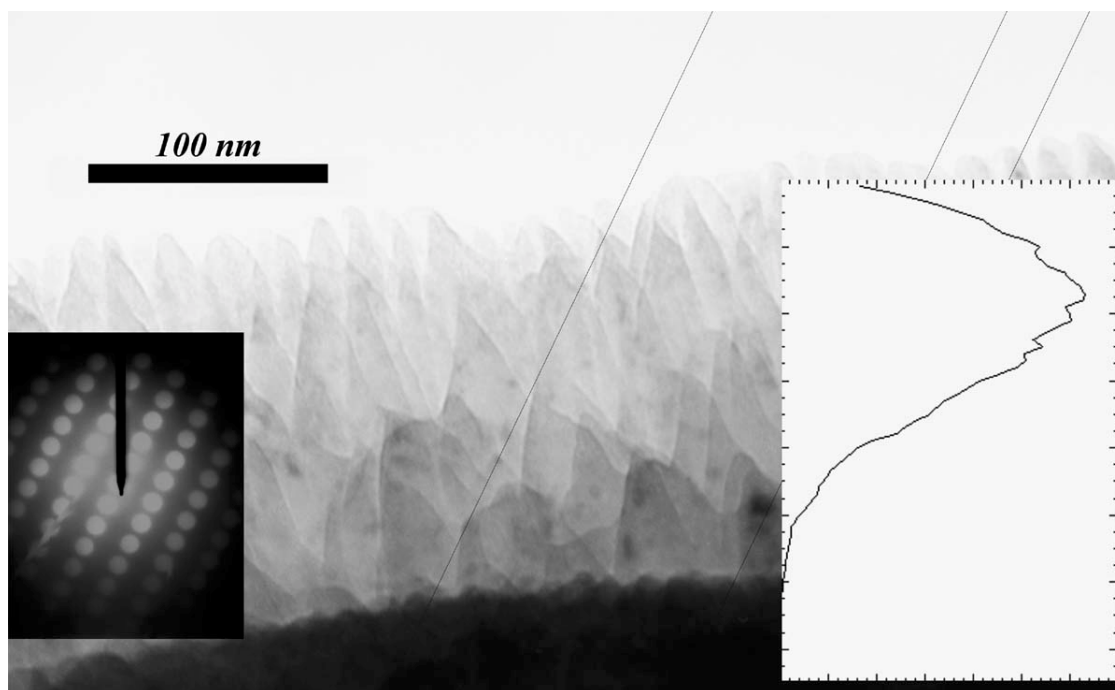


Fig. 4. Transmission electron micrograph of the irradiation damaged layer in ZrN with a corresponding diffraction pattern (inset on left) and the anticipated Xe implantation depth profile (inset, right). The maximum damage is approximately 60 dpa. The diffraction pattern shows damage to the lattice but the basic face-centered cubic structure is still evident, indicating that the lattice is able to accommodate this level of damage.

Fuel Design

Personnel continued to review information from previous work with fuels of high actinide content. Much of this work was performed in the late 1980s and early 1990s, and was specific to breeder-reactor fuel cycles. Therefore, the fuel compositions considered in those programs contained uranium and modest-to-small amounts of minor actinides. However, the irradiation performance of fuels with increased amounts of minor actinides is quite relevant to the current work with non-fertile fuels. By assessing the impact that modest-to-small amounts of minor actinides have on performance of U-Pu-based fuel forms, the performance of which is fairly well known, some indication of performance issues with TRU fuels can be obtained.

There are four known experiments involving transmutation of ^{241}Am . Results from two, the EFTTRA-T4 test and the SUPERFACT-1 experiment have been published. Results from two additional experiments, the ANL X501 experiment and a BNFL oxide experiment have not been published and are discussed in the subsequent

³ N. Yu, K. E. Sickafus, P. Kodali and M. Nastasi, *In Situ Observation of Defect Growth Beyond the Irradiated Region in Yttria-Stabilized Zirconia Induced by 400 keV Xenon Ion-Beam at -90°C and 30°C* , J. Nucl. Mater. **244**, 266 (1997).

section. The helium generation and release results of all four experiments are evaluated in the subsequent section. The summary in this section on Fuel Design discusses the implications of apparent He generation and release tendencies on design of AAA transmutation fuels.

General Discussion of Unpublished, Relevant Fuel Performance Results

US/UK Oxide Experiment - Post-irradiation data from a joint US/UK actinide-burning experiment irradiated in the Prototype Fast Reactor (PFR) at Dounreay, Scotland, was obtained from BNFL (British Nuclear Fuels, plc). The information has not been published in the open literature, although efforts are underway at BNFL to secure a release to allow for publication. The results of discussions with BNFL staff are summarized here.

Three types of oxide fuel pellets were fabricated at ORNL.⁴ The pellets were assembled into small fuel pinlets at Hanford⁵ and shipped to Dounreay for assembly into the irradiation test vehicle and for irradiation in the PFR. Pellet, fuel pinlet, and irradiation parameters are provided in Table 1.

Table 1. Fuel Parameters for Joint DOE/UKAEA Actinide-Burning Test

Fuel Compositions	Am ₂ O ₃ , Cm ₂ O ₃ , (Am ₆ Lan ₇ Cm) ₂ O ₃ Lan=La:2Ce:3Nd:Sm
Isotopes	²⁴¹ Am, ²⁴⁴ Cm
Pellet Diameter	0.150 inches (3.8 mm)
Smeared Density	80%-86%
Cladding	D9, 0.230 inches OD, 0.030 inches wall (5.83/0.76 mm)
Fuel Column Length (approx.)	1.5-2.0 inches (40-50 mm)
Plenum:Fuel Length Ratio (approx.)	~1:1
Linear Power	9–10.5 kW/m
Irradiation Time	63.4 EFPDs (effective full-power days)
Burnup	1.6 at% (assumed, based on initial inventory)
Peak Temperature	T _{CL} < 800°C

PFR had a 600-MW_t rating, but was operated at only 166–180 MW_t during this experiment (due to reasons unrelated to the experiment), resulting in lower-than-anticipated fuel temperatures. After one cycle of 63 EFPDs (effective full-power days), the experiment was withdrawn from the reactor for an interim examination. Gamma radiography showed that the fuel column in the Cm₂O₃ sample had grown approximately 80% in length. The experiment was not reinserted in the reactor, and further examination commenced on all MA-bearing fuel samples. PIE (post-irradiation examination) results are summarized in Table 2.

Table 2. Summary of PIE Results for (MA)₂O₃ Specimens.

	Am ₂ O ₃	Cm ₂ O ₃	(Am ₆ Lan ₇ Cm) ₂ O ₃
Fuel Column Elongation	~6%	~80%	~0%
Cladding Diameter Increase	~0.3%	~0.3%	~0.15%
Evidence for Plastic Flow	Yes	Extreme	No
Gas Release from Fuel	~0%	~0%	~0%

⁴ ORNL Report, ORNL-TM-5858

⁵ Hanford Report HEDL-7057

In general, all fuels swelled to contact the cladding wall. In the case of the Am_2O_3 and Cm_2O_3 pellets, there was evidence for a large amount of plastic flow, as the fuel crept into the space between the insulator pellets and the cladding wall and formed essentially a single mass. The Cm_2O_3 microstructure resembled that of a sponge; the other two fuels had the same microstructural features seen in Cm_2O_3 , although to a lesser degree. In all three fuels, there was a gradient in bubble size from larger at the fuel centerline to smaller near the cladding, presumably related to the fuel temperature gradient and the effects of restraint at the cladding wall. There were some anomalies in gas sampling, but the conclusion reached is that there was no gas release from the fuel pellets.

There are only two other known data points for MA-oxide irradiation behavior. The EFTTRA-T4 test⁶ (americium oxide in magnesium aluminate spinel, irradiated at HFR, Petten) also showed high swelling behavior. Helium gas release was about 20% in this experiment. A similar test of uranium oxide (i.e., rather than minor actinides) in the same spinel matrix (Efttra-T3) showed good swelling behavior, so that the effects of helium gas generation appear to dominate fuel behavior in the case of EFTTRA-T4. The same is obviously true of the Am_2O_3 and Cm_2O_3 results discussed above. This contrasts with the SUPERFACT experiment,⁷ where acceptable results were obtained on irradiation of americium and neptunium oxides in a UO_2 matrix in the fast-spectrum PHENIX reactor. Gas release in the SUPERFACT test was 57%–65%, typical of oxide fuel operating under fast reactor conditions. The general conclusions that can be drawn from the three known MA-oxide irradiation tests are that (1) the effect of helium gas generation (due to alpha-decay) tends to dominate fuel behavior if the gas is not released from the fuel, (2) the behavior of uranium-bearing analogues in the presence of uranium (and plutonium) fission is not necessarily an indicator of the performance of similar MA-bearing fuels, and (3) the existing database on commercial UO_2 and MOX is probably not directly applicable to MA-burning fuels.

IFR X501 Experiment - Further metallographic analysis was performed on an HT-9 clad fuel pin from the Integral Fast Reactor (IFR) X501 actinide-burning experiment. HT-9 is the reference cladding for transmuter fuel. X501 fuel parameters and operating conditions are shown in Table 3. Operating conditions are typical of those for metal fuel in a fast reactor. High-magnification optical micrographs at four elevations in the fueled region of the pin show no evidence of HT-9 cladding attack at 6.5% estimated heavy metal (HM) burnup. Typical results for mid-plane and top-of-fuel cross-sections are shown in Fig. 5. These results indicate that under typical operating conditions, FCCI (fuel-cladding-chemical-interaction) in metal fuel is not accelerated by small amounts of americium or neptunium.

Review of Experimental Data on He Generation in Am-Bearing Fuels

The generation of helium gas during transmutation of ^{241}Am is a significant issue that must be accounted for in the design of transmuter fuel. Helium generation principally arises from a sequence involving neutron capture to ^{242}Cm with subsequent decay by alpha particle emission to ^{238}Pu . Four irradiation tests of high-minor actinide fuels have been performed. Some data on helium generation is available for each

⁶ R.J.M. Konings, et. al, J. Nuc. Mat. 282 (2000) 159-170

⁷ C.T. Walker, G. Nicolaou, J. Nuc. Mat. 218 (1995) 129-138

experiment, and the results are analyzed here and presented in a uniform set of units for comparison. The quality and completeness of data vary for each experiment; therefore, the results of this analysis contain a good deal of uncertainty, and do not provide a good basis for extrapolation. The data does show, however, that helium generation is an important consideration in fuel selection and design.

Table 3. Attributes of X501 Actinide-Bearing Fuel Elements

Composition (average wt%)	U-20.2Pu-9.1Zr-1.2Am-1.3Np
Major impurities (average wt%)	Si:0.26, Al:0.089, Ca:0.067, Cr:0.0025, Mg:0.009, Fe:0.001, Mn:0.001
Element length (nominal)	74.9 cm (29.5 inches)
Cladding OD	5.84 mm (0.230 inches)
Cladding wall	0.457 mm (0.018 inches)
Plenum gas	Ar-He
Smeared density	75%
Estimated peak linear heat generation rate	45 kW/m (13.7 kW/ft)
Estimated fuel peak centerline temperature	700°C
Estimated cladding inner surface temperature	540°C

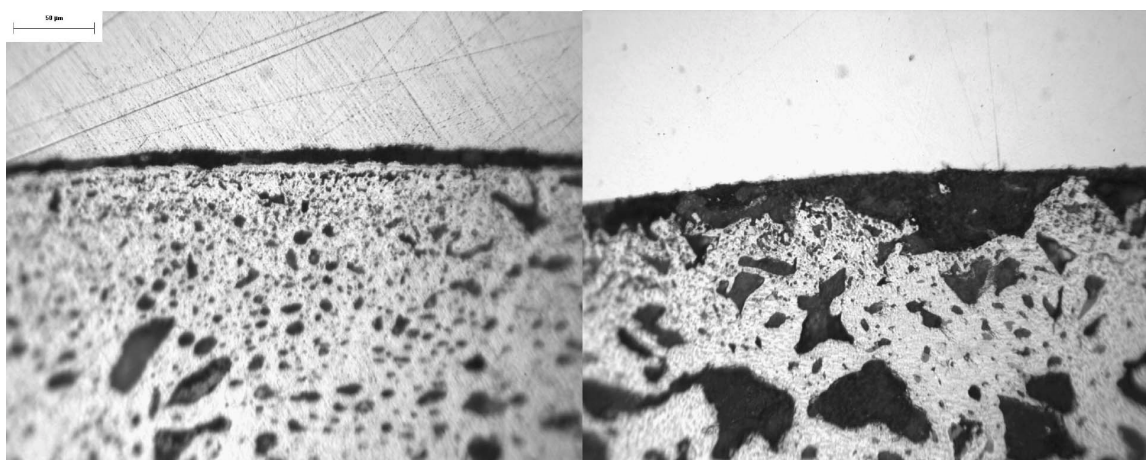


Fig. 5. Optical micrographs from (a) mid-plane and (b) top sections of an X501 fuel pin showing the absence of cladding attack by the fuel

EBR-II X501 Experiment - The X501 experiment was conducted in EBR-II as part of the Integral Fast Reactor Program to demonstrate minor actinide burning through the use of a homogeneous recycle scheme. The X501 subassembly contained two metallic fuel elements loaded with relatively small quantities of americium and neptunium. The attributes of these elements are given in Table 4. X501 was inserted into EBR-II for run 163, beginning in February 1993, and withdrawn just prior to shutdown in August 1994. Total irradiation time was approximately 339 EFPDs. Burnup, calculated on the basis of REBUS/RCT/ORIGEN data supplied by ANL

reactor analysis personnel was 7.6% HM (heavy metal) with transmutation of 9.1% of ^{241}Am . Plenum helium volume was measured by gas sampling, and agrees reasonably well with the calculated data. Because the fill gas was Ar-25He (Argon gas + 25 vol.% He), and the fill volume is not known, the assumption was made that all argon fill gas was recovered on post-irradiation gas sampling. The initial helium fill-gas volume was then calculated by using the Ar:He ratio. Data relevant to the calculation of specific helium gas generation are given in Table 5. The helium generation rate is presented in units of cubic centimeters of helium at STP (standard temperature and pressure) per gram of ^{241}Am transmuted, for comparison with other data. Helium generation rate is calculated to be in the range of 38.6–44.8 $\text{cm}^3 \text{He/g}$ Am transmuted, depending on the value used for post-irradiation helium inventory.

Table 4. Attributes of X501 Minor Actinide-Bearing Fuel Elements.

Composition (average wt%)	U-20.2Pu-9.1Zr-1.2Am-1.3Np
Major impurities (average wt%)	Si:0.26, Al:0.089, Ca:0.067, Cr:0.0025, Mg:0.009, Fe:0.001, Mn:0.001
U-235 enrichment (nominal)	60%
Fuel mass	77.5 g
Fuel length	34.3 cm (13.5 inches)
Element length (nominal)	74.9 cm (29.5 inches)
Cladding OD	5.84 mm (0.230 inches)
Cladding wall	0.457 mm (0.018 inches)
Slug diameter	4.27 mm (0.168 inches)
Plenum volume	7.1 cm^3
Plenum gas	Ar-25He
Smeared density	75%
Fuel slug density, % theoretical	99.5%
Estimated peak linear heat generation rate	45 kW/m (13.7 kW/ft)
Estimated fuel peak centerline temperature	700°C
Estimated cladding inner surface temperature	540°C

Table 5. Parameters Used in Calculating He Gas Generation Rate for X501 Pin G582.

Parameter	Value	Data source
BOL (beginning of life) ^{241}Am content	0.972 g	ANL chemical analysis samples 92-2087-01 to -06
EOL (end of life) ^{241}Am content	0.884 g	R. D. McKnight, ANL, REBUS/RCT/ORIGEN analysis
^{241}Am transmutation	0.088 g (9.1 %)	
Measured He in plenum	3.94 cm^3	Based on AGHCF gas sampling (sample 505A1A, 12/15/95) with assumptions about He volume in initial fill gas
Calculated He inventory	3.4 cm^3	R. D. McKnight, ANL, REBUS/RCT/ORIGEN analysis decayed to 6/01/96
Specific He gas generation	38.6-44.8 cm^3/g	He gas volume at STP per gram of ^{241}Am transmuted

PHENIX SUPERFACT-1 Experiment - SUPERFACT-1 was irradiated in PHENIX from October 1986 to January 1988. Attributes of the high-ameridium SUPERFACT-1 pins are given in Table 6. In addition to two high-ameridium elements, (U-45Np)O₂, elements of (U-24Pu-1.8Am)O₂, and (U-24Pu-1.5Np)O₂ were also irradiated. Gas inventories were measured by vacuum evaporation, and are given in Table 7. The helium-to-fission gas (He:FG) ratio of 4.7 is somewhat lower than the value of 6.0 calculated for the thermal spectrum EFTTRA-T4 test (Table 10).

Table 6. Attributes of SUPERFACT-1 Am-Bearing Fuel Elements.

Composition	(DU-19.2Am-21.2Np)O ₂
Fuel column length	39.9 cm (15.7 inches)
Element length (nominal)	179.3 cm (70.6 inches)
Cladding OD	6.55 mm (0.258 inches)
Cladding wall	0.45 mm (0.018 inches)
O/M ratio	1.927
Plenum volume	7.1 cm ³
Plenum gas	He
Smeared density	89%
Estimated peak linear heat generation rate	17.4 –27.3 kW/m (13.7 kW/ft)

Table 7. Gas Sampling Data for SUPERFACT-1.

Composition (wt%) (nominally MO ₂)	%HM burnup	Kr + Xe (cm ³)	He (cm ³)	He:FG
(U-28Pu)O ₂	8.5	235	10.3	0.04
(U-24Pu-1.8Am)O ₂	6.8	153	39.9	0.26
(U-45Np)O ₂	4.6	141	22.9	0.16
(U-19.2Am-21.2Np)O ₂	4.3	134	631	4.7
(U-24Pu-1.5Np)O ₂	6.8	153	14.4	0.09

The data presentation is difficult to interpret in terms of specific helium release, due to the lack of data on fuel mass in the published SUPERFACT literature. Instead, data from Table 7.1 of the EFTTRA-T4 report⁸ was used to estimate specific helium release; these data are shown in Table 8. These numbers are calculated for EOI (end-of-irradiation) and after one year of cooling. The helium gas inventory increases with cooling time due to decay of ²⁴²Cm, which has a 163-day half-life. This causes the specific helium gas generation rate to increase from 33.3 cm³/g ²⁴¹Am transmuted at EOI to 63.4 cm³/g ²⁴¹Am after cooling. The latter number should be compared to the specific generation rate of 38.6–44.8 cm³/g for X501.

Thermal Spectrum EFTTRA-T4 Experiment - The EFTTRA-T4 experiment⁹ was irradiated in hafnium-filtered thermal flux at the High Flux Reactor (HFR). The EFTTRA-T4 experiment consisted of ²⁴¹Am-bearing oxide particles incorporated in an inert oxide matrix (MgO·Al₂O₃ spinel). Test parameters and some test results from EFTTRA-T4 are given in Table 9

⁸ EUR 19138 EN

⁹ R.J.M. Konings, et al., *J. Nuc. Mat.* 282 (2000) 159-170

Table 8. Parameters Used in Calculating He Gas Generation Rate for SUPERFACT-1 Am-Bearing Pins.

Parameter	Value	Data source
Calculated He inventory, EOI	7.12×10^{-4} mol He/cm ³ fuel (16.0 cm ³ He/cm ³ fuel)	Table 7.1 of Euratom report EUR 19138 EN compares SUPERFACT-1 to EFFTRA-T4
Calculated He inventory, 1 year cooling	1.36×10^{-3} mol He/cm ³ fuel (30.5 cm ³ He/cm ³ fuel)	
BOL ²⁴¹ Am content	1.89 g Am/cm ³ fuel	Calculations based on information in Walker, JNM 218 (1995) 129-138 and Prunier, Proc. FR'91 Vol. II.
²⁴¹ Am transmutation	0.481 g Am/cm ³ fuel (25.4%)	
Specific He gas generation at EOI	33.3 cm ³ /g	He gas volume at STP per gram of ²⁴¹ Am transmuted
Specific He gas generation at 1 year cooling	63.4 cm ³ /g	

Table 9. Parameters and Some Results of the EFFTRA-T4 ²⁴¹Am Transmutation Test.

Temperature (aluminum carrier near cladding)	400°–450°C
Fuel phases (some uncertainty)	MgO·Al ₂ O ₃ spinel + ~3 μm dia. (Am,Al)O ₃
²⁴¹ Am loading	9.7-11.9 wt%
Duration of irradiation	358.4 EFPDs
²⁴¹ Am transmutation	96%
Total actinide burnup	28%
Total fluence (calculated)	3.5×10^{26} m ⁻²
Fluence >0.1 MeV (calculated)	1.7×10^{26} m ⁻²
Volumetric pellet swelling	~18%

Generation of helium during irradiation caused high fuel swelling and significant fuel-cladding mechanical interaction (FCMI). The helium release rate from the fuel was much higher than the fission gas release rate. Gas pressure after one year of cooling was 0.5 MPa, of which 94.9 vol% was helium. As seen in Table 10, the inventory of helium was nearly six-fold that of fission gas, and the volume release of helium from the fuel was twenty-two times that of fission gas.

Table 10. Gas Inventories and Release at End Of Life in EFFTRA-T4 (One Pin).

Gas species	Inventory, moles	Release, moles	%Release
He	1.37E-03	2.66E-04	22.3
Kr	8.92E-06	1.07E-06	11.9*
Xe	2.20E-04	1.08E-05	4.9
He:fission gas ratio	5.98	22.3	-

* The authors of reference EUR 19138 EN consider this value suspect, since the measured quantity of Kr was near the detection limits of the apparatus.

Parameters used to calculate the helium gas generation rate are given in Table 11. No experimental verification of calculated helium inventory was conducted. Helium generation rate was calculated to be 44.8 cm³/g Am transmuted at EOI and 59.9 cm³/g Am transmuted after one year cooling.

Table 11. Parameters Used in Calculating He Gas Generation Rate for EFTTRA-T4.

Parameter	Value	Data source
Calculated He inventory, EOI	1.37×10^{-3} mol He (30.7 cm ³)	Table 6.2 of Euratom report EUR 19138 EN, MCNP-FISPACT calculations at EOI (end-of-irradiation) and after 1 year cooling.
Calculated He inventory, 1 year cooling	1.73×10^{-3} mol He (38.7 cm ³)	
BOL ²⁴¹ Am content	0.685 g	
²⁴¹ Am transmutation	0.646 g (94.9 %)	
Specific He gas generation at EOI	44.8 cm ³ /g	He gas volume at STP per gram of ²⁴¹ Am transmuted
Specific He gas generation at 1 year cooling	59.9 cm ³ /g	He gas volume at STP per gram of ²⁴¹ Am transmuted

PFR Sesquioxide Experiment - Three types of oxide fuel pellets were fabricated at ORNL⁴ and assembled into small fuel pinlets at Hanford.⁵ The pinlets were shipped to Dounreay for assembly into an irradiation test vehicle and for insertion in the PFR (Prototype Fast Reactor) by BNFL. Information on this experiment has not been published in the open literature. Pellet, fuel pinlet, and irradiation parameters were given earlier in Table 1. As mentioned earlier, after one cycle of 63 EFPDs, the experiment was withdrawn from the reactor for an interim examination at approximately 1.6% HM burnup. Gamma radiography showed that the fuel column in the Cm₂O₃ sample had grown approximately 80% in length. The experiment was not reinserted in the reactor, and further examination commenced on all MA-bearing fuel samples. The FISPIN code was used to calculate gas production; data are summarized in Table 12. The calculated value of 68.8 cm³ He/g transmuted Am (EOI) appears high relative to other data presented here. This is likely due to uncertainty in calculation of the small amount of americium transmutation.

Table 12. Data Relevant to Calculation of Specific He Gas Generation for Am₂O₃ Pin

Parameter	Value
Calculated He inventory	1 cm ³ /g
BOL ²⁴¹ Am content	0.909 g/g fuel
²⁴¹ Am transmutation	0.015 g (1.6 %)
Specific He gas generation (EOI)	68.8 cm ³ /g

Comparison to the ANL Sodium Point Design - ORIGEN output for sodium-cooled transmuter fuel to 30 at% burnup was supplied by ANL reactor analysis personnel.¹⁰ The data was calculated for seven 135-day irradiation cycles followed by a 45-day cooling period, an eighth 220-day cycle, and a five-year cooling at end of life. The fuel feed actinide composition is given in Table 13. The ORIGEN output data was used to determine the rate of ²⁴²Cm buildup and decay during irradiation and cooling (reported in the ANL February 2001 monthly report). Based on the beginning- and end-of-cycle activities, a linear ²⁴²Cm generation rate was calculated for each cycle. The number of decay events was then calculated by determining the difference in the initial and generated activity with the end of cycle activity. All ²⁴²Cm was assumed to decay by alpha emission, producing ⁴He. The ORIGEN output was also used to determine specific helium generation and the relative ratio of helium and fission gas.

¹⁰ K.N. Grimm, *Decay Isotopics and Decay Powers for the Sodium-Cooled ATW Fuel*, ANL Reactor Analysis and Engineering Division memorandum, January 16, 2001

This data is shown in Table 14. The helium-to-fission gas molar ratio is 0.32 for an ^{241}Am content of 6.78 wt%. The specific helium generation rate of $58.1 \text{ cm}^3 \text{ He/g}$ transmuted ^{241}Am at EOI is at the high end of the experimental data.

Table 13. ATW Equilibrium Fuel Feed Composition.¹²

Isotope	Mass %	Isotope	Mass %	Isotope	Mass %	Isotope	Mass %
U-234	0.431	Pu-236	1.1×10^{-5}	Pu-242	10.1	Cm-243	0.036
U-235	0.101	Pu-238	4.74	Am-241	6.78	Cm-244	2.28
U-236	0.137	Pu-239	30.7	Am-242	0.314	Cm-245	0.655
U-238	0.978	Pu-240	30.7	Am-243	3.20	Cm-246	0.407
Np-237	3.07	Pu-241	5.38	Cm-242	0.028		

Table 14. Fission Gas Production and Helium Generation in Sodium-Cooled Transmuter Using Fuel Composition in Table 13 (EOI Cycle 8).

Parameter (per pin)	Value
^4He inventory due to ^{242}Cm decay	167.9 cm^3
Total fission gas	490.5 cm^3
He:fission gas ratio	0.34
BOL ^{241}Am inventory	6.06 g
EOL ^{241}Am inventory	3.17 g
^{241}Am transmutation	2.89 g
Specific helium generation (EOI)	$58.1 \text{ cm}^3 \text{ He/g } ^{241}\text{Am}$

Summary

A summary of the estimates for specific helium gas generation is given in Table 15. Values range from $33.3\text{--}68.8 \text{ cm}^3 \text{ He/g } ^{241}\text{Am}$ transmuted. Variations may be due to differences in data quality, core neutron spectra, the arrangement of irradiation and cooling cycles, uncertainties in cross sections for ^{242}Cm formation, and the method used for estimating helium generation for the point design. The data in Table 15 are not amenable to extrapolation, but provide an indication of the volumes of gas that must be taken into account during fuel design. Based on the limited irradiation data available, release of helium gas from the fuel appears to be a desirable attribute of Am-bearing fuel.

The impact of helium production on fuel design is significant for pins containing less than 10 wt% ^{241}Am , and becomes overwhelming for fuel with high americium content. A simple example showing relative plenum sizes required for 100% helium gas release is given in Table 16, which lists the plenum-to-fuel volume ratio required to maintain plenum pressure below 1200 psi as a function of americium content. These estimates are based on a helium-to-fission gas generation ratio of 4.7 for americium.

Table 15. Summary of Helium Gas Generation.

Test	Specific He generation ($\text{cm}^3 \text{ He at STP/gram of } ^{241}\text{Am}$ transmuted)	Notes
X501	38.6-44.8	14-21 months cooling
SUPERFACT-1	33.3-63.4	EOI - 1 year cooling
EFTTRA-T4	44.8-59.9	EOI - 1 year cooling
PFR 0402AE	68.8	EOI
Na point design	58.1	EOI

Table 16. Example of Plenum Sizing as a Function of Americium Content (500°C)

Americium content, wt%	Required plenum-to-fuel volume ratio	Volume relative to 0% Am case
0	1.2	-
6.0	1.5	125%
12.0	1.9	184%
30.0	3.1	258%
60.0	5.1	425%

Evaluation of Potential He Generation Effects on Transmutation Fuel Performance

The generation of helium gas during transmutation of ^{241}Am is an important fuel design consideration. Increased gas inventory leads to a higher pressure loading on the cladding tube, and can significantly affect in-reactor creep rates. This section provides a rough estimate of the changes in cladding creep rate and operating temperature limitations that can be expected for a fixed fuel configuration. Fuel parameters are those used for the draft sodium-cooled point design¹¹ and are listed in Table 17. Cladding wall thickness was decreased from 0.56 mm to 0.48 mm to account for wastage. The fuel type considered here is a generic metal alloy containing plutonium, americium, and zirconium. The present results may also be applicable to ceramic fuels, since a high gas release rate may be necessary to maintain fuel swelling at acceptable levels. The plenum-to-fuel volume ratio was calculated assuming a sodium bond and attached end plugs.

Table 17. Fuel Pin Parameters

Fuel type	Pu-xAm-40Zr alloy
Composition range	0-40 wt.% ^{241}Am
Cladding type	HT-9 steel
Cladding O.D.	0.744 cm (0.293 inches)
Cladding wall thickness	0.48 mm (0.19 inches)
Fuel active length	1.07 m (42.1 inches)
Fuel smeared density	0.75
Total fuel pin length	2.31 m (91 inches)
Plenum:Fuel volume ratio	1.51
Fission gas release fraction	0.8
Helium release fraction	1.0

ORIGEN calculations performed at ANL were used to select linear helium production rates, fission gas yields, and Am:HM (Heavy Metal) burnup ratios for compositions containing 6%-40% ^{241}Am for use in modeling cladding creep. The values of these parameters, given in Table 18, match the burnup and gas inventories generated by ORIGEN for the 1480-day fuel lifetime assumed for the sodium point design. Note that there are significant variations in fission gas yield due to a decreasing fission to

¹¹ R. Hill and H. Khalil, Draft Report on Sodium Cooled ATW Blanket Development, ANL memorandum July 21, 2000

capture ratio with increasing americium. The helium generation rate stays nearly constant at 46.6–47.2 ml of He/g ^{241}Am transmuted.

For the examples provided here, it was assumed that cycle length was constant at 1480 days, burnup was 30% HM for all cases, and peak cladding fluence was $4.0 \times 10^{23} \text{ n/cm}^2$. These assumptions provide a basis for direct comparison of the effects of helium production on cladding thermal creep strain, although they may be difficult to achieve in a transmuter core.

A key result is that the gas inventory increases by ~3.6 times (at EOI) as the ^{241}Am content is increased from zero to 40 wt.%. The helium gas inventory will continue to increase on cooling due to continuing ^{242}Cm decay in the americium-containing fuels.

Table 18. Parameters and Results of Gas Generation Calculations.

Fuel composition	Pu-40Zr	Pu-6Am-40Zr	Pu-20Am-40Zr	Am-20Pu-40Zr
Cycle length	1480 days			
Peak cladding fluence	$4.0 \times 10^{23} \text{ n/cm}^2$			
Am:HM burnup ratio	-	1.185	1.39	1.87
Fission gas yield	0.246	0.235	0.207	0.141
He generation (ml He/g ^{241}Am transmuted)	-	47.2	46.8	46.6
Total gas inventory @EOI (liters at STP)	0.85	1.1	1.72	3.08
He fraction in gas inventory	-	0.24	0.58	0.85
Plenum pressure @550°C (ksi)	0.95	1.2	1.9	3.4
Hoop stress at 550°C (ksi)	6.4	8.2	12.8	22.9

The calculated gas inventory was used to determine fuel pin plenum pressure, given the gas release rates in Table 17. Plenum pressure was in turn used to calculate hoop and effective stresses in the cladding. Plenum pressure and hoop stresses calculated at 550°C for each fuel type are given in Table 18. The creep correlation developed for HT-9 during the IFR program was used to model the thermal creep strain expected due to internal pressurization; results are shown in Fig. 6.

Based on the HT-9 thermal creep model, the effects of increasing americium content are twofold. First, the fuel operating temperature that can be attained for a given thermal creep limit is less for the higher plenum pressure. Second, the thermal creep rate is more sensitive to changes in cladding temperature due to higher internal fuel pin pressures. The plenum pressure calculated for the 40 wt.% Am case is greater than that typically encountered in fast reactor fuel testing and may require measures to decrease plenum pressure.

A conservative fuel-operating criterion would be the limiting of thermal creep strain to 1%. Based on this criterion the allowable peak cladding temperature for Am-20Pu-40Zr is estimated to be ~540°C; increased temperature sensitivity at high pressure and a large amount of irradiation enhanced creep may warrant a more conservative temperature limit or a larger plenum if irradiated to 30% HM burnup. On the other hand, 30% burnup may be difficult to achieve for high Am compositions under the HT-9 fluence limit. Other fuel compositions considered here operate at pressures and temperatures more typical of fast reactor fuel tests.

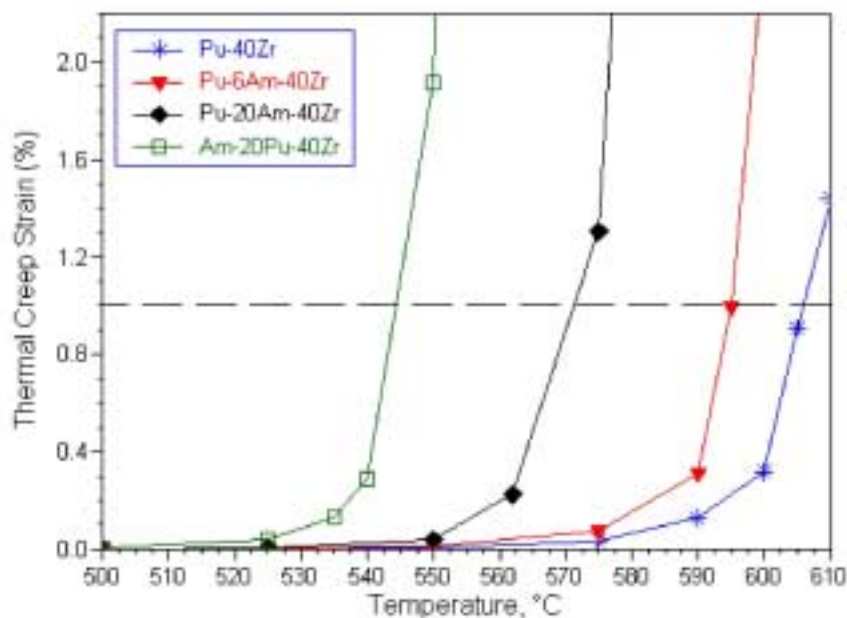


Fig. 6. Cladding thermal creep strain for HT-9. Shown as a function of cladding temperature for varying ^{241}Am content at EOI.

Modeling

In anticipation of the nuclear-fuels modeling effort, which will begin in October 2001, the approach for atomic-scale and thermodynamic modeling of properties and processes is being refined. Literature searches for thermodynamic data, for chemical reaction kinetics data and for nitrogen-nitrogen (N-N) potential forms are underway.

A critical issue in developing a reliable effective potential model for nitrides is the quality and functional form of the N-N interaction. The initial review of existing literature has identified two papers with pertinent information: one that models Si_3N_4 ,¹² and a second that models AlN (aluminum nitride)¹³. In both cases, the N-N potential form is based on the Buckingham function that describes the short-range contribution to the interaction energy. For Si_3N_4 , the model was able to reproduce lattice parameters, elastic constants, phonon spectra and specific heats to a high degree of reliability. This is an impressive array of properties for such a simple functional form. For AlN , the model was able to predict structures exhibited by oxygen ions associated with planar defects within the lattice, which agreed very well with experimental observations using TEM. In both studies, inclusion of angular or anisotropic bond bending or torsional terms in the potential description was determined to be unnecessary. These studies will provide an initial basis for the modeling of (TRU)N and ZrN materials beginning in the next fiscal year.

¹² W-Y. Ching, Y-N. Xu, J. D. Gale, M. Rühle, *Ab-Initio Total Energy Calculations of α - and β -Silicon Nitride and the Derivation of Effective Pair Potentials with Application to Lattice Dynamics*, J. Am. Ceram. Soc., **81**, 3189 (1998).]

¹³ A. D. Westwood, R. A. Youngman, M. R. McCartney, A. N. Cormack, M. R. Notis, *Oxygen Incorporation in Aluminum Nitride via Extended Defects .1. Refinement of the Structural Model for the Planar Inversion Domain Boundary*, J. Mat. Res., **10**,1270 (1995).

2. Separations Technology

Scope

The AAA Separations Technology activity consists of three tasks addressing the various stages in the process of partitioning irradiated fuels for subsequent fissioning of transuranic elements and transmutation of long-lived fission products. The tasks are as follows:

- **Light Water Reactor Spent Fuel Treatment** – This task involves the development and demonstration of efficient and economic means for the separation of uranium, transuranic elements, specific long-lived fission products, and other fission products from LWR spent fuel. An aqueous partitioning process (UREX) is envisioned for the initial treatment of LWR fuel, which involves the extraction of uranium for disposal as a low-level waste. This will be followed by a pyrochemical process (PYRO-A) to separate the transuranic elements from fission products.
- **Transmuter Blanket Fuel Treatment** – Non-fertile blanket fuel that has been irradiated in the AAA transmuter to fission transuranic elements must be processed to recover and recycle the unburned transuranics and to extract newly generated long-lived fission products for transmutation. This task accomplishes the development and demonstration of the means for processing that blanket fuel. A pyrochemical process (PYRO-B) is planned for the separation of unburned transuranics and long-lived fission products. Such processes are favored because the reagents are stable under high radiation fields and because the processes are normally operated at elevated temperatures with the use of molten salts, and can thus accommodate high levels of decay heating.
- **Waste Form Production** – One of the overarching criteria for AAA separations technology development is the minimization of high-level waste generation. Design of the LWR fuel-treatment process has been oriented toward the elimination of liquid high-level waste streams, and the pyrochemical processes are similarly being designed to minimize high-level waste volumes. This task involves the development and qualification of durable high-level waste forms to accommodate the two principal waste streams (salt and metal) that emanate from the separations process as well as the waste form for the disposal of the pure uranium extracted from the spent LWR fuel.

Highlights

- **Optimization of Solvent Extraction Process** - The AMUSE code for modeling AAA solvent extraction processes is nearly complete. This code can now be used to good effect in optimization of the demonstration of the complete UREX flowsheet with simulated LWR spent fuel dissolver solution, to be conducted in September.
- **UREX Process Reductant/Complexant** - The stability of acetohydroxamic acid (AHA, the reagent that suppresses plutonium and neptunium extraction in

the UREX process) in nitric acid was determined and found to be more than adequate for AAA applications.

- **PYRO-A Process Development** - Direct electrochemical reduction experiments using CaO-CaCl₂ salt showed that the process is capable of reducing rare earth oxides. This makes the process practical for the treatment of the oxide product of the UREX process.
- **PYRO-B Process Development** - Conceptual process flowsheets, similar to the PYRO-A process for LWR spent fuel treatment, have been developed for the treatment of transmuter oxide (cercer and cermet) fuels. A commonality of process design could result in significant reductions in costs for chemical separations.
- **Recovery of Technetium** - Studies of the extraction of Tc in the UREX process confirmed the expectation that Tc will extract with uranium and can be subsequently stripped with high efficiency. This should make it feasible to achieve the goal of >95% Tc recovery from LWR spent fuel.

Development of the AMUSE Code

The code portion of the Generic TRUEX Model is being revised for the Argonne Model for Universal Solvent Extraction (AMUSE). It will use the Microsoft Excel Visual Basic for Applications programming language. The Generic TRUEX Model is written in Microsoft Excel 4 Macro Language. Initial work has been done on converting the user-input portion of the model. The user-input section will now be done using Excel forms, a part of Visual Basic for Applications, instead of designing the input using portions of worksheets. This change to Visual Basic for Applications provides greater flexibility and functionality in designing the user interface. It is simple to add drop down menus, buttons, and option groups to the forms and then add code that executes when one is selected. Models have been developed for the extraction of U(VI), Np(IV), Np(V), Np(VI), Pu(III), Pu(IV), and TcO₄⁻ by TriButylPhosphate (TBP) for inclusion in the AMUSE code. Most of the models contain the ability to calculate the effects of process temperature, and TBP and AHA concentrations.

Evaluation of the Stability of AHA

The stability of AHA was determined as a function of time (up to three weeks), nitric acid concentration (high purity water to 5.5 M nitric acid), and the presence of Fe³⁺ to better establish the time window for the process/redox chemistry. When only nitric acid is present in solution, the stability of AHA decreases with decreasing pH. Similar AHA stability was obtained when AHA was dissolved in perchloric acid showing that the acid-catalyzed hydrolysis, not oxidation by nitrate, was the key factor. Below 0.1 M nitric acid concentrations, AHA (pH ~4-5) is very stable (order of weeks). Between 0.1 M and 0.5 M, the instability of AHA is significantly increased. At the highest acid concentrations, the lifetime of the AHA was ~3 hours (2.8 hours at 5.6 M nitric and 2.9 hours at 2.7 M nitric acid).

Effect of Dissolved Iron on AHA Stability

The predominant aqueous iron species in the AHA/nitric acid system is expected to be Fe^{3+} . When the concentration of iron is in excess, essentially all the AHA in solution is tied up as a complex that has a much longer lifetime than the AHA itself. When the AHA is present in excess, the effective rate of AHA decomposition decreases as the iron concentration is increased. This is presumably due to the lowered effective free AHA concentration (due to the formation of the Fe-AHA complex). The important result here is that under process-relevant conditions (e.g., ~1 M nitric acid), the presence of dissolved iron increases the effective lifetime of the AHA in solution.

Development of Processes for Treatment of Oxide Transmuter Fuels

Conceptual flowsheets have been developed for the treatment of ATW transmuter oxide dispersion fuels (ceramic-ceramic, or cercer, and ceramic-metal, or cermet). The proposed flowsheet for cercer fuel mirrors the PYRO-A treatment process, incorporating two major processing steps: (1) direct electrolytic reduction to convert oxides to metals; and (2) electro-refining to separate and recover TRU metals. The primary difference in application of these steps to transmuter-fuel treatment versus the PYRO-A process for UREX-oxide-product treatment is the presence of the matrix material. Experimental work underway for PYRO-A process development will be directly applicable to the development of this process proposed to treat ATW ceramic-ceramic oxide dispersion fuels.

Ceramic-Ceramic Oxide Dispersion Fuels

In the proposed process to treat ceramic-ceramic dispersion fuels, the spent fuel is chopped or crushed and loaded into baskets. The baskets are transferred to the direct electrolytic reduction reactor where the fuel and matrix oxides are converted to metals in an electrolyte yet to be selected (perhaps $\text{CaCl}_2\text{-CaO}$). Oxygen gas is evolved at the anode during the electrochemical reaction. Active metal fission products (Cs, Sr, Ba) partition to the molten salt in this process step. When their concentration in the molten salt reaches an upper limit (defined either by the heat load or by reduction performance), the salt is removed and disposed of in a ceramic waste form.

At the completion of the oxide reduction reactions, the basket containing TRU, fission product, cladding, and matrix metals is removed and treated to vaporize residual salts. The condensed salts are returned to the reduction reactor. The metals in the basket are transferred to the electro-refiner where the TRU metals are electro-deposited at a liquid product cathode after the addition of an oxidant (dependent upon the nature of the matrix metal, possibly zirconium chloride) to form TRU chlorides and promote electro-transport. The objective of the electro-refining step is to separate the TRU product from the noble metal fission products, cladding, and matrix metals that are retained in the anode basket, and from most of the rare earth metals that partition to the salt. The capability to separate TRUs from the matrix metals by electro-refining is dependent on the matrix composition. Thermodynamic calculations suggest that TRUs can be separated from Zr and Al, but not Mg (a component of common spinels).

The metals remaining in the anode basket after electro-refining (matrix metal, cladding, and noble metal fission products including technetium) are treated to remove residual salts by vaporization of the salts, which are then condensed and returned to the electro-refiner. The remaining metals are treated by a process yet to be defined to extract the technetium for transmutation. The residual metals are then stabilized for disposal in a metal waste form. When the concentration of fission products in the electro-refining salt reaches an upper operating limit (defined either by the heat load or by electro-refining performance), the salt is removed and processed for disposal. The TRUs in the salt are recovered by electrolysis and collected at a liquid product cathode. Once the extraction of TRUs from the waste salt has reached a sufficiently high level such that the target system values for TRU recovery are met, the salt is transferred to ceramic waste form production.

Ceramic-Metal Oxide Dispersion Fuels

The processes envisioned for the treatment of ceramic-metal dispersion fuels incorporate the same two major steps as the process just described for ceramic-ceramic dispersion fuels: direct electrolytic reduction and electro-refining. The metal matrix, however, must be removed or partially digested to allow access of the reductant or oxygen carrier to the oxide fuel particles. Technologies for separating the metal matrix from the oxide fuel will be specific to the matrix material and will add complexity to the process. For example, a Zr matrix may be removed by chloride volatility or electro-refining.

Extraction of Technetium in the UREX Process

The tributyl phosphate extraction of technetium was studied under many different conditions in the presence of acetohydroxamic acid (AHA) to determine if this reductant has any effect on technetium distribution coefficients. The distribution coefficients for the AHA systems, when compared to non-AHA systems, were not significantly different and are consistent with literature values. Based on these results it is concluded that AHA does not reduce pertechnetate. The uranium distribution coefficients that were measured were also consistent with the literature, indicating that AHA had no effect on its extraction.

PYRO-A Process Development

A series of oxide reduction experiments using CaCl_2 -CaO salts at 800°C were completed during this quarter to evaluate the calcium-based option for the reduction of rare-earth oxides in the PYRO-A process. Calcium is a much stronger reductant than lithium, thus the process conditions are more favorable for reduction of rare-earth oxides such as Nd_2O_3 . Electrochemical reduction experiments were performed with CaCl_2 -CaO salt and Nd_2O_3 powder at 800°C. The cathode product contained a gray layer that was clearly distinguishable from the unreacted Nd_2O_3 (blue layer). The gray material was contacted with molten tin to extract any neodymium metal that may be present. The tin alloy was then analyzed by inductively coupled plasma atomic-emission spectroscopy (ICP-AES) for neodymium metal. The results of the analysis revealed the presence of neodymium metal in the tin-alloy samples. Based on these analytical results, it is clear that the direct electrochemical reduction of Nd_2O_3 , and, by a logical extension, other rare-earth oxides, is feasible using the calcium-based PYRO-A option.

3. Accelerator Development

3.1 Low Energy Demonstration Accelerator

Scope

Construction and operation of the Low-Energy Demonstration Accelerator (ED&D) will confirm the design and demonstrate the viability (at full power) of the technically challenging initial stages of the accelerator. It will provide the first opportunity to look for possible beam halo at low energies (<8 MeV), develop a commissioning and operating plan for a cw system, and prototype the entire low-energy accelerator.

The LEDA beam activities are being conducted in three distinct stages (listed below). LEDA operates predominantly in continuous mode (cw), but short periods of pulsed operation are used during commissioning to permit use of interceptive diagnostics.

- **Stage I** - Install and test a 75-keV, 110-mA proton injector (completed).
- **Stage II** - Add a 350-MHz radiofrequency quadrupole (RFQ) accelerator to accelerate a 100-mA proton beam to 6.7 MeV (completed). Measure the formation and development of beam halo in a magnet lattice after the RFQ, including detailed beam profiles at multiple points along the transport line, perform analysis and compare with profiles predicted by the beam-simulation codes, using the results to make corrections (if needed) to beam codes.
- **Stage III** - Add a 700-MHz coupled-cavity drift-tube linac (CCDTL) section to accelerate 6.7-MeV beam to ~ 8 MeV to confirm beam matching from the 350-MHz RFQ into the 700-MHz CCDTL. Complete CCDTL structure fabrication, assembly, and tuning.

Major Highlights

- **Beam-Halo Experiment** - We matched 16-mA, 50-mA, and 75-mA RFQ output beams to the beam transport (halo) channel. We then intentionally introduced mismatches into these beams as they entered the halo channel and measured the effects of those mismatches. We used the wire-scanner/halo-scraper (WS/HS) devices located at the center and at the end of the beam channel to complete these measurements.
- **CCDTL Section 2** - Section 2 of the coupled-cavity drift-tube linac (CCDTL) was tuned and installed on the hot-model test stand. We are presently testing that structure with RF power.

Layout of the Quadrupole Magnet FODO Lattice

A schematic of the beam-transport (halo) channel is shown in Fig. 7. This 11-m-long FODO¹⁴ lattice consists of 52 quadrupole singlet magnets and several beam diagnostic devices. The wire scanner/halo scraper (WS/HS) devices have one wire

¹⁴ focus-drift-defocus-drift

and two halo scrapers per unit. The central profile of the beam was measured with the wire scanner, and the profile in the periphery of the beam was obtained by using the halo scrapers, one on each side of the beam in each plane (+x, -x, +y, -y). The wire scanner data and the halo scraper data were acquired with overlapping position intervals and then joined to form one data file, giving about five orders of magnitude peak-signal-to-noise ratio for the beam profile measurements (Figs. 8 and 9). The beam current and transmission through the halo channel was measured with the A/C current toroids. The steering magnets were used to center the beam in the halo channel, the location of which was determined with the beam position monitors (BPMs). Beam loss was detected with the photo-multiplier-tube beam loss monitors (BLMs). The location of the various diagnostics devices in the halo channel is given in Table 19.

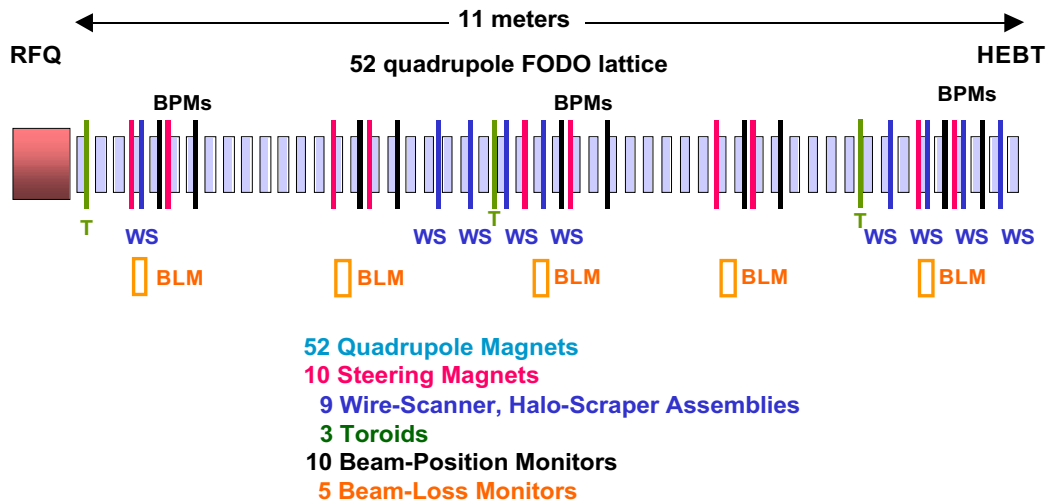


Fig. 7. Schematic of the beam-halo channel that includes the location of the diagnostic devices. The 6.7-MeV RFQ output H^+ beam enters from the left and exits to the right.

Table 19. Halo Lattice Beamline Component Locations

Device	Locations (Quadrupole Magnet No.)
WS/HS	4, 20, 22, 24, 26, 45, 47, 49, 51
BPM	5, 7, 16, 18, 27, 29, 37, 39, 48, 50
Steerers	3, 5, 14, 16, 25, 27, 35, 37, 46, 48
BLM	4, 15, 26, 36, 47
Transformer	1, 23, 43

Measurements of Beam Halo in the Quadrupole Magnet Lattice

At each current level, the WS/HS devices were used to measure the profiles of the beam as injected into the magnet lattice with initial matching quadrupole settings (quads 1-4) determined from beam simulations. Based on these measurements, the matching quadrupoles were then adjusted to obtain a better match. Typically after two iterations, the beam size was uniform, about $1.1 \text{ mm} \pm 0.05 \text{ mm}$, as measured with each wire scanner in the two groupings of four WS/HS assemblies. A full beam profile for a 75-mA beam during the mismatch scan, obtained with both the wire scanner and halo scrapers just after quadrupole magnet #26, is shown in Fig. 9. After verifying that the beam was matched to the halo channel, we then intentionally

introduced either a breathing-mode or a quadrupole-mode mismatch into the beam and measured the effects of these mismatches. The amount of mismatch is characterized by the mismatch parameter “ μ ”, that ranges from 1.00 for a matched beam to greater than 1.75 for a significantly mismatched beam.

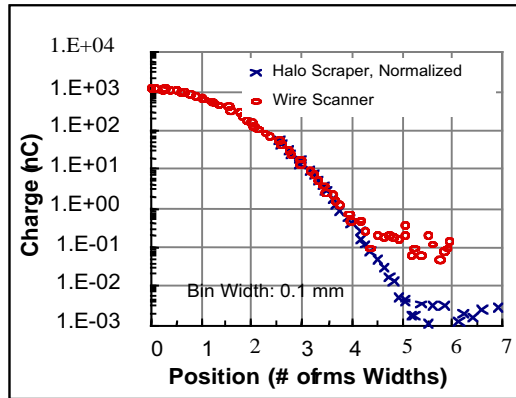


Fig. 8. Simulated beam profile distribution measurement. Wire placement, electronics noise, and beam current and position errors are included in this simulation. The wire scanner can detect to 4 rms widths: the halo scraper acquires another rms width.

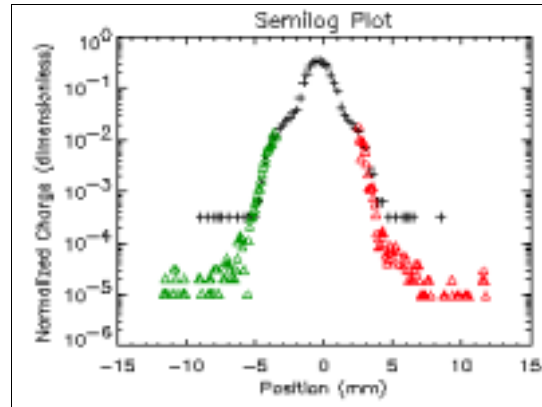


Fig. 9. Measured beam profile in y-plane mid-way down the transport channel for a mismatched beam. The black crosses are the wire scanner measurements: the red and green triangles are the +y and -y halo scraper measurements, respectively.

The data obtained during the mismatch scans were also used to determine the emittance of the 6.7-MeV proton beam exiting the RFQ. Measurement results for 16-mA, 50-mA, and 75-mA beams are shown in Figs. 10 and 11.

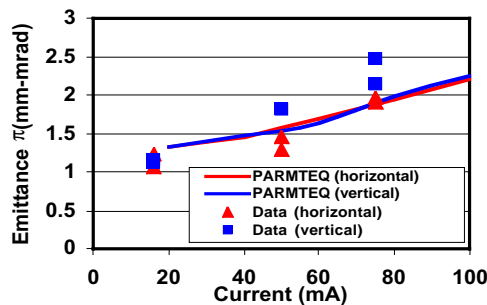


Fig. 10. Measured transverse emittances and PARMTEQM predictions.

Current	16 mA		50 mA		75 mA	
Code	Linac	Trace	Linac	Trace	Linac	Trace
ϵ_x (mm-mrad)	1.23	1.06	1.45	1.28	1.89	1.96
α_x	1.69	1.53	1.43	1.46	1.20	1.26
β_x (cm)	20.4	19.5	20.1	25.5	19.4	24.3
ϵ_y (mm-mrad)	1.17	1.12	1.81	1.82	2.46	2.14
α_y	-1.89	-1.98	-1.09	-1.68	-1.56	-1.68
β_y (cm)	55.7	59.1	35.7	52.2	48.2	55.5

Fig. 11. Transverse Courant-Snyder parameters as predicted using TRACE3D and LINAC.

Although measurements were made at the three beam currents, results are presented mainly for the 75-mA case. The mismatch strength, measured by a parameter μ , equals the ratio of the rms size of the mismatched beam to that of the matched beam. First, the measured transverse profiles (Fig. 12) show unexpected structure in the form of shoulders in the semi-log plots and some asymmetric profiles. The shoulders and asymmetries are most prominent for the mismatched beams. Figs. 13 and 14 show the x- and y-rms sizes at the different scanners for a matched and mismatched case, respectively.

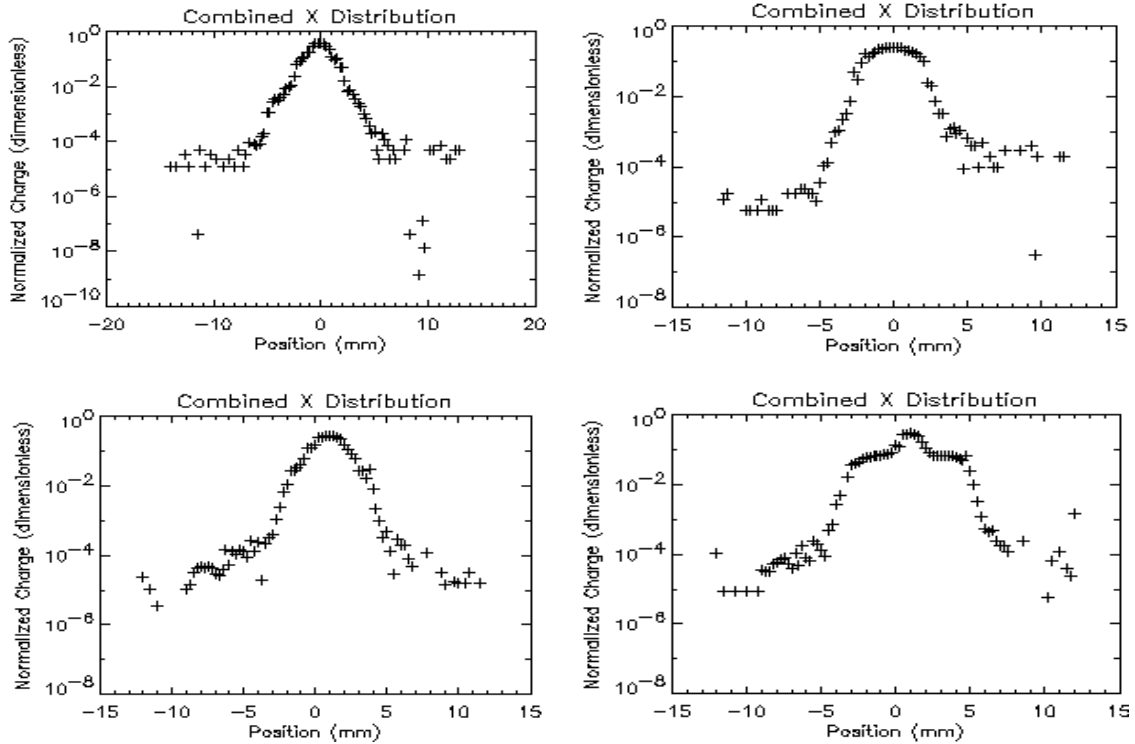


Fig. 12. Measured beam profiles in x at 75 mA: scanner 22, (upper left) $\mu=1.0$ matched, (upper right) $\mu=1.5$ mismatched; scanner 51, (lower left) $\mu=1.0$ matched, (lower right) $\mu=1.5$ mismatched.

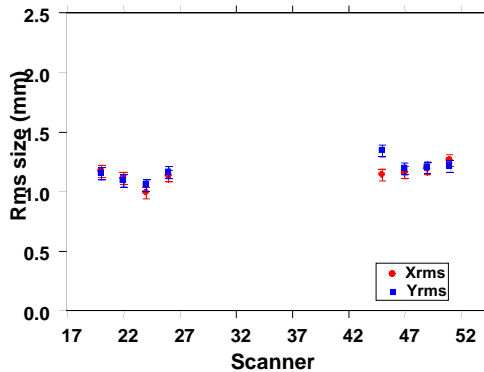


Fig. 13. Rms displacements at the 8 profile scanners for matched beam case at 75 mA.

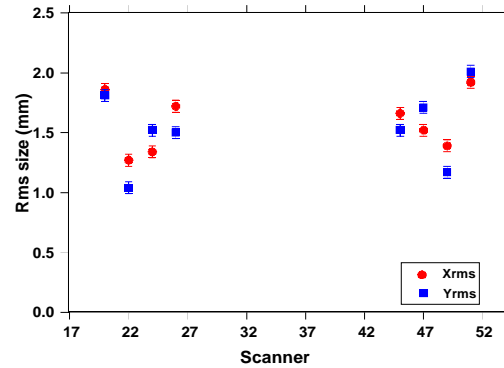


Fig. 14. Rms displacements at the 8 profile scanners for the breathing-mode mismatch case ($\mu=1.5$) at 75 mA.

As expected, we observed beam emittance growth as the mismatch increased. This effect is illustrated in Fig. 15 for a 75-mA beam with breathing-mode mismatches of $\mu=1.00$, 1.25, 1.50, and 1.75. Note that the rms normalized beam emittance also grows as the beam traverses the halo channel. When the beam current was reduced to 16 mA (and matched at that current), the result was quite different (Fig. 16). The reduced space-charge forces resulted in little, if any, emittance growth as the beam traversed the halo channel. There may be a slight increase in emittance as the mismatch is increased from $\mu=1.00$ (matched) to 1.75, but this increase is considerably smaller than what is measured at 75 mA.

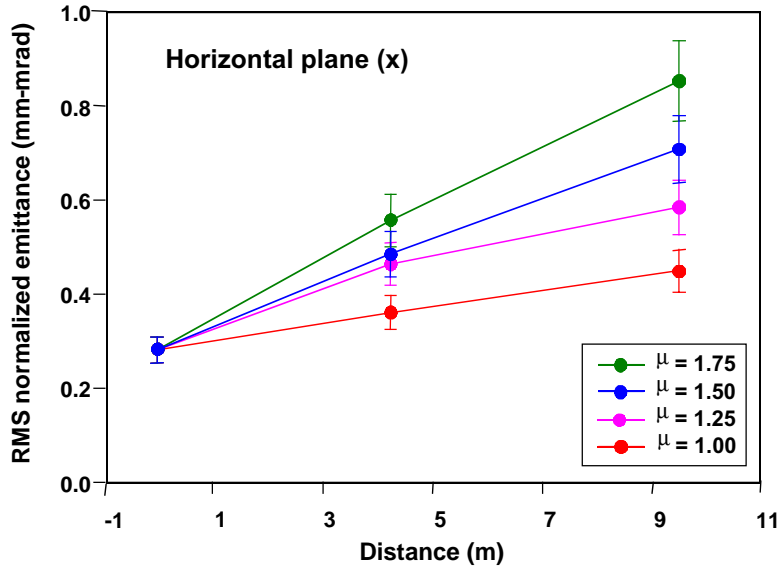


Fig. 15. RMS normalized emittance in the halo channel for a 75-mA proton beam having breathing-mode mismatches 1.00–1.75.

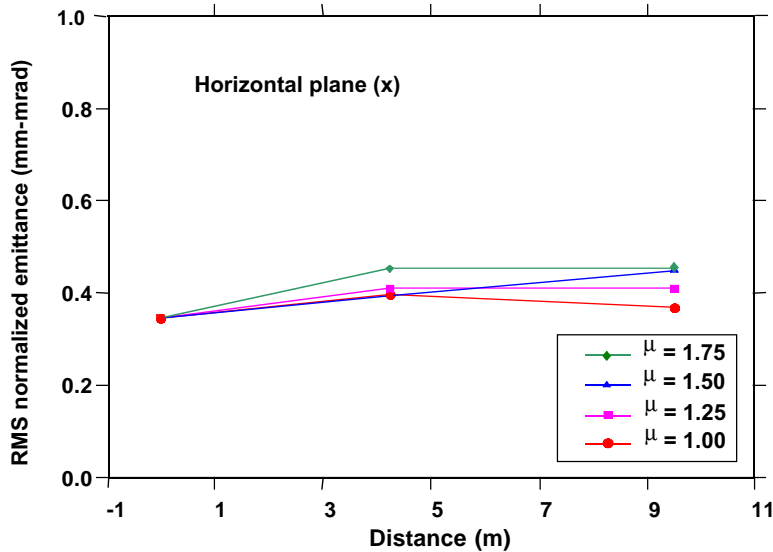


Fig. 16. RMS normalized emittance in the halo channel for a 16-mA proton beam having breathing-mode mismatches 1.00–1.75.

Measurement of the Bunched-Beam Current

The bunched-beam current is a measure of the strength of the 350-MHz signal in the beam pulse and can be determined from the phase spread of the beam distribution. The phase spread of the beam increases as the beam traverses the beam-halo lattice. In the absence of space charge forces, the increase in the phase spread can be determined directly from the energy spread of the beam. For high-current beams, space charge forces contribute significantly to increasing the phase- and energy-spread of the beam.

The beam-position monitors (BPMs) were used to measure the bunched-beam current at ten locations in the beam-halo lattice. The data were obtained by averaging the measured bunched-beam current over many pulses to reduce pulse-to-pulse jitter. Measurements were made at many values of the beam current ranging from 5–95 mA. The data show that the location of the first null in the distribution is observed to appear further upstream as the beam current is increased. At the higher currents (>50 mA), a second null is observed in the 11-meter transport channel.

The amplitude of the bunched-beam current can be expressed as a function of the phase spread of the beam as shown in Equation 1 for a parabolic longitudinal phase distribution.

$$A = 3 \left(\left(\frac{\sin(a)}{a^3} \right) - \left(\frac{\cos(a)}{a^2} \right) \right) \quad (1)$$

Here, $a = \pi W/T$, where W is the full phase width at the base of the bunch and T is the bunch spacing ($T=1/f$).

The rms phase spread of the beam is calculated at many locations along the beam-halo lattice using the LINAC code. A 6-D waterbag distribution has been assumed for the initial distribution at the end of the RFQ. This distribution gives the same result as the beam distributions from PARMTEQM simulations of the RFQ. The full phase spread at the base of a parabolic distribution is 4.472 times the rms phase spread. The beam phase distributions from LINAC are consistent with parabolic distributions, although due to the finite number of particles, the full width at the base of the phase distribution is typically 4.25 rms. This value is used in the calculations of the bunched-beam current. Beam phase distributions other than parabolic have been studied and these do not appear to predict either the locations or successive nulls of relative heights of the lobes.

The LINAC code is used to determine the values of ϵ_z and β_z that provide the best fit to the bunched-beam current data. Fig. 17 shows a typical fit to the data at 79 mA.

CCDTL Post-Braze Tuning and Installation on the Hot Model Test Stand

At the time of the last report, Section 2 of the Coupled-Cavity Drift-Tube Linac (CCDTL) had been brazed and preparations were underway for post-braze tuning of that structure to tune the cavities to the desired operating frequency and stopband and to tune the bridge-coupling (BC) cavity and waveguide coupling iris. Post-braze tuning of the LEDA CCDTL Section 2 was completed. It is presently installed on the test stand in the LEDA building (see Fig. 18). High-power RF testing will begin in July. Several measurements are scheduled for this test. After the initial conditioning phase has been completed, an x-ray endpoint measurement will be made to calibrate the cavity power, low-level RF amplitude set point with CCDTL gap voltage. Measurements to determine the adequacy of cooling on the transverse-coupling cells will also be made. High power stopband measurements are also scheduled for this time.

In view of the proposed change from a CCDTL to a superconducting spoke-resonator structure immediately following the RFQ, fabrication of CCDTL Section 1 is on hold.

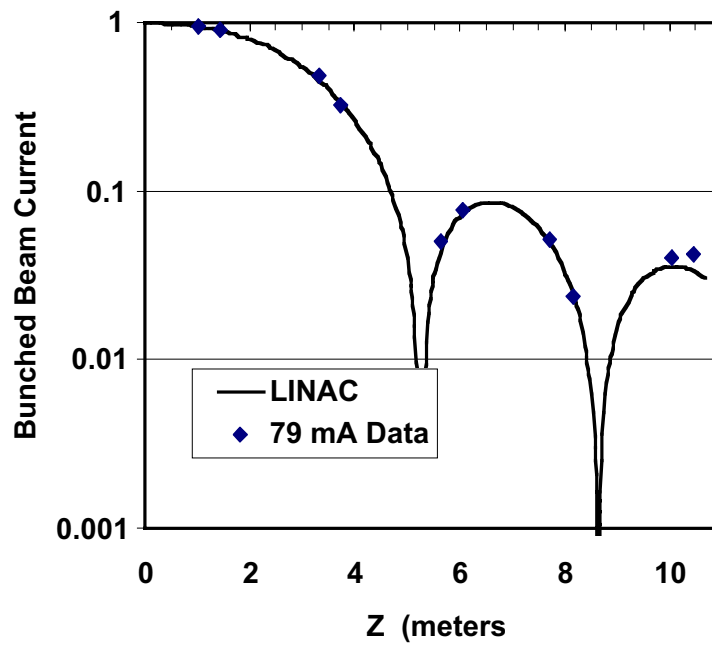


Fig. 17. Normalized bunched beam current at 79 mA compared to typical LINAC fit.

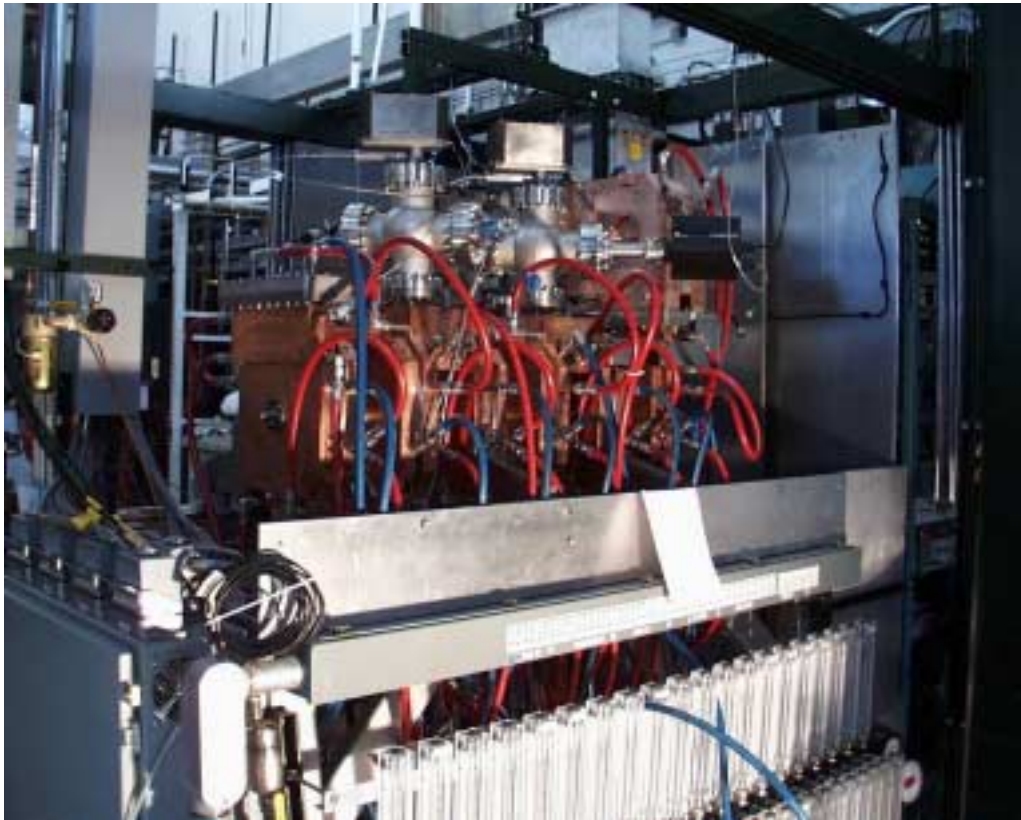


Fig. 18. Section 2 of the CCDTL (the copper structure located at the center of the photo) installed on the hot model test stand in the LEDA building. Two ion pumps are located on top of this structure. Some of the cooling lines are clearly visible.

Milestone and DDN Documentation Progress

The LEDA Level-1 milestone “End of Data Acquisition (Beam Halo)” was met as scheduled in June.

Design Data Need, DDN PPO-A21-G-DDN-X-59, *LLRF Response to Amplitude Variations*, was deferred until 08/01. The first experimental work on this DDN was deferred until after the 06/08/01 beam-halo completion date so the beam-halo experiment would not be impeded. The DDN experimental work will be completed in July, and the report is scheduled to be finished by the end of August.

Another DDN, PPO-A12-G-DDN-X-49, *RFQ Construction/Performance Documentation*, was split into two parts, *Summary of LEDA RFQ Constructability* (TPO Report TPO-E18-R-X-00247) and *Summary of LEDA RFQ Performance* (TPO Report TPO-E18-R-X-00246). The report *Summary of LEDA RFQ Constructability* was submitted to the Information Management System (IMS) in May. The report *Summary of RFQ Performance* has been written and is in the final stages (resolution of PPO comments) before it can be submitted to the IMS.

3.2 High Energy Linac

Scope

Develop and demonstrate superconducting RF linac technology required to build the Accelerator-Driven Test Facility (ADTF) linac for the AAA Program. Work in FY01 includes:

- **Spoke Cavity Development** – The spoke cavity is a superconducting accelerating structure that may be used at low energies, as low as 6.7 MeV (RFQ exit energy) to ~100 MeV. Development work will lead to the design and fabrication of spoke cavities that will be beam tested on LEDA.
- **Cavity Testing / SC Laboratory Operation** – Testing of superconducting cavities and related components (e.g., power couplers) is being performed in the LANL Superconducting Laboratory. In FY01, spoke cavities are being tested in support of spoke-cavity development. Elliptical cavities are also being tested to improve their performance. General-purpose instrumentation for cavity testing and the bench testing of other components related to SCRF linacs are being developed.
- **Completion of SCRF APT DDN Work** - Work related to the development of the APT SCRF high-energy linac will be completed and documented.

Highlights

- **ADTF Linac Review** – A review of the Accelerator-Driven Test Facility (ADTF) Linac was held in mid-April. Comparisons of cost and performance of normal-conducting and superconducting low energy linacs (6.7–211 MeV) were presented to a subgroup of the AAA External Review Committee. The committee recommended replacing the CCDTL and CCL of the ADTF design with superconducting spoke cavities and $\beta=0.48$ elliptical cavities,

respectively. This recommendation results in an ADTF linac that is totally superconducting except for the RFQ.

- **Superconducting Laboratory Operation** – We completed the fabrication of a diagnostic system that can map cavity-wall temperatures and x-ray intensities in an elliptical cavity to help identify problem areas. Commissioning of this system is underway.
- **Completion of SCRF APT DDN Work** – We successfully completed Design Data Need (DDN) “Medium-Beta Superconducting Cavity for the HE Linac.”

Spoke Cavity Development

ADTF Linac Review - A review of the ADTF linac was held at LANL April 10-12, 2001. The review committee consisted of a subgroup of the AAA External Review Committee. The committee recommended replacing the CCDTL and CCL of the ADTF design with superconducting spoke cavities and $\beta=0.48$ elliptical cavities, respectively. After the review, and in conjunction with preparation for the APS Particle Accelerator Conference (Chicago, June 2001), we fully documented the spoke cavity study with a total of 14 reports.

Spoke Cavity Procurement - The final physics and engineering requirements for the $\beta=0.175$, 2-gap, 350-MHz spoke cavity were established. Preparation of detail drawings, statement of work, and request for quotation are underway. It is planned that the request for quotation for the fabrication of two cavities will be sent out to US and foreign vendors at the end of July 2001. These cavities have been designed without a helium vessel (Fig. 19). They will be used on the LEDA beamline with a simple immersion-type cryomodule. The intention is to utilize a commercially available vertical cryostat with suitable modifications. However, a concept for a helium vessel for a beamline cryostat for the ADTF has been developed. The cavities can be retrofit with a helium vessel for ADTF-linac beamline use.

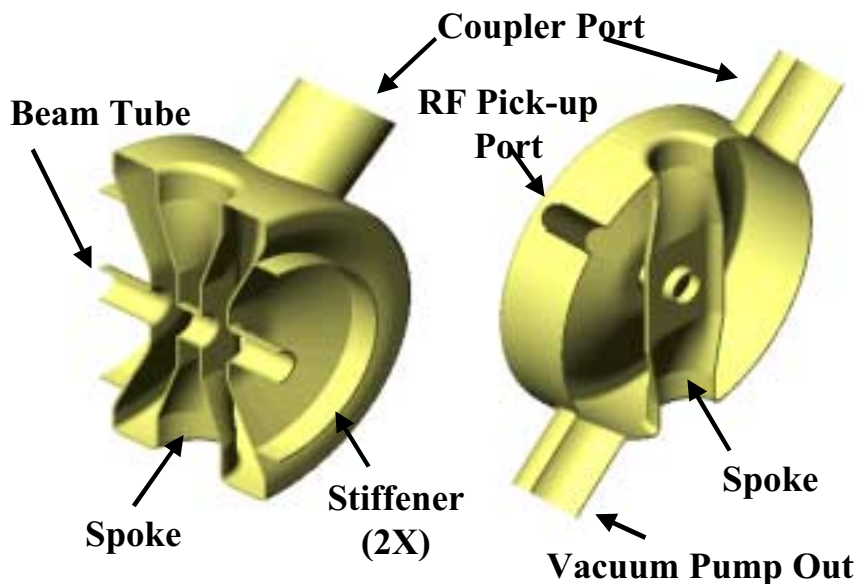


Fig. 19. $\beta=0.175$, 2-gap, 350-MHz spoke cavity

A concept for a tuner for the ADTF linac spoke cavities has also been developed, utilizing the frictionless Ledford/Wood tuner developed for the PILAC¹⁵ cavity with the addition of a piezoelectric element. The piezoelectric element will provide the necessary rapid small motion to take the cavity off-frequency in under 300 ms. The concept of the complete cavity/tuner/helium vessel assembly is shown in Fig. 20.

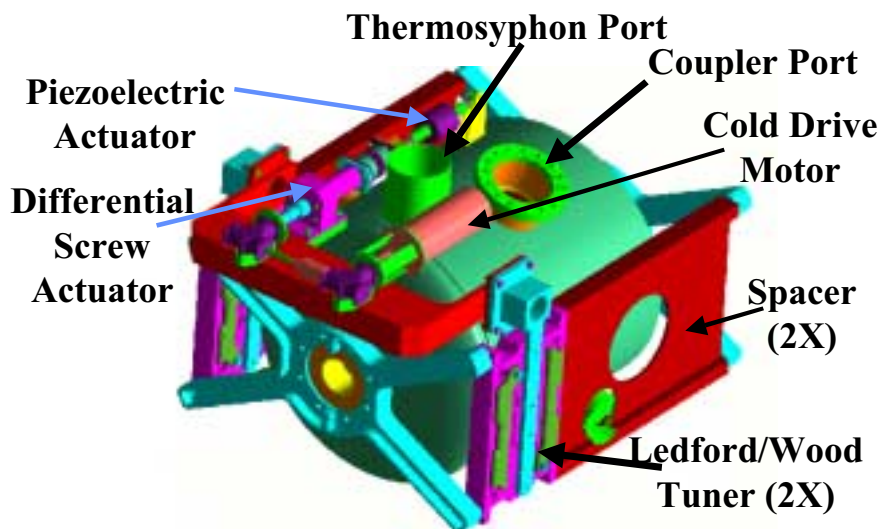


Fig. 20. Assembly of cavity, tuner, and helium vessel

Spoke Cavity Power Coupler - The objective is to develop a power coupler that is capable of the full range of power requirements for the $\beta=0.175$ 2-gap and $\beta=0.34$ 3-gap cavities at both beam currents of 13 mA (ADTF) and 100 mA (APT). The power capacity range is thus from 5–136 kW.

We investigated the possibility of using the LEP2¹⁶ power couplers on a loan from CERN as an option, considering a reduced development effort (these couplers have been demonstrated at our required power level). However, these couplers have some undesirable design features, such as the cooling of the outer conductor with boil-off helium gas and an inner conductor requiring biasing. Also, the design does not provide adequate integral vacuum for our application, and a major re-design would be required. Therefore, it was decided to proceed with the power coupler concept that was presented at the ADTF April review, which is shown in Fig. 21. The physics design is nearly complete. A final design review is scheduled for early August 2001. Preparation of detail drawings, statement of work, and a request for quotation solicitation for fabrication are in process.

Spoke Cavity Cryomodule - A preliminary concept for the ADTF cryomodule concept has been developed. This design utilizes features from the TESLA Test Facility (TTF) and SNS¹⁷ cryomodules. Assembly sequences have been studied to

¹⁵ pion linear accelerator

¹⁶ Large Electron-Positron collider at CERN (Switzerland)

¹⁷ Spallation Neutron Source

assure that assembly is feasible. This concept has been incorporated into beamline layouts from which the beam dynamics analyses can be performed.

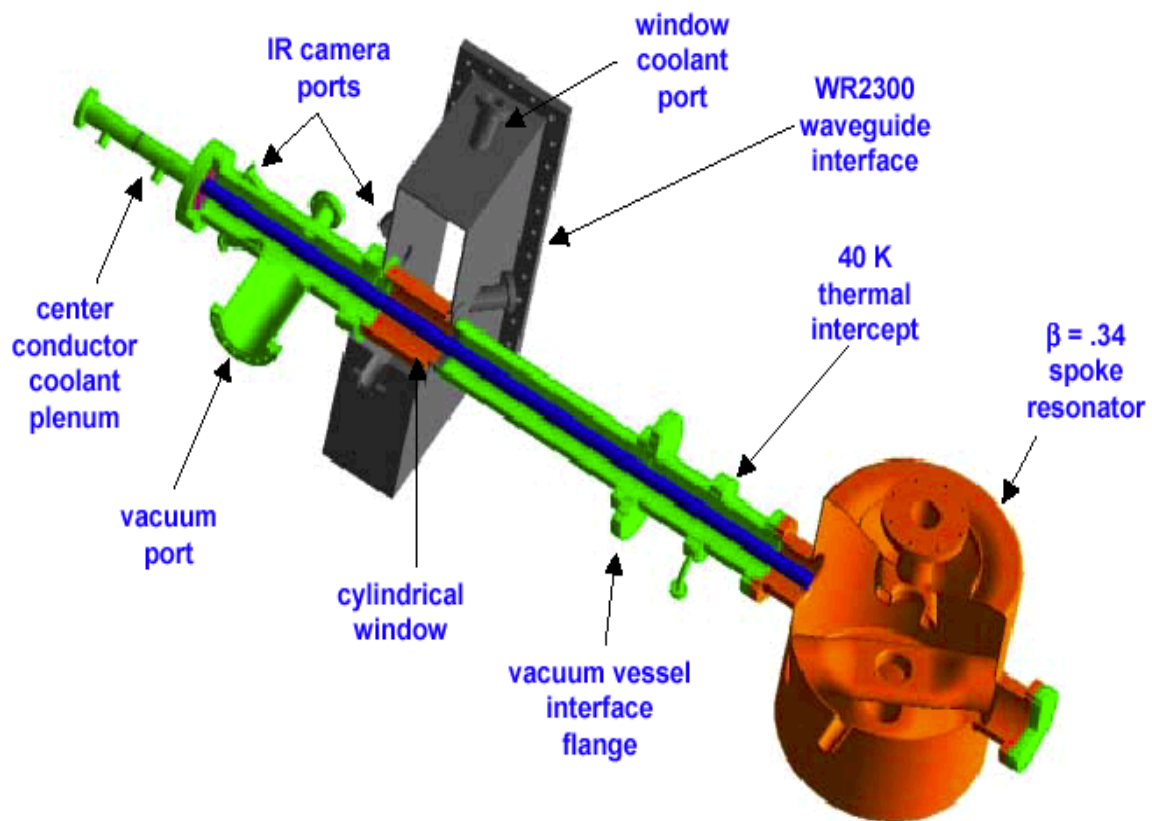


Fig. 21. Spoke cavity power coupler concept

Cavity Testing

Diagnostic System for Elliptical Cavities - We designed and started fabrication of a diagnostic system that can locate problem areas inside elliptical cavities. In a typical cavity test, we measure degradation of quality factors at high fields above the cavity field requirement. This diagnostic system will allow us to identify and locate the cause of such degradation. The system will measure cavity wall temperatures and the emitted x-rays. Cavity wall temperature gives information on anomalous RF losses on the inside surface of the cavity, while the distribution of x-rays gives information of areas where field-emitted electrons impinge and emit x-rays. The diagnostic system was designed to produce maps of temperature and x-ray intensities around the entire cavity. By analyzing these maps, we will be able to locate imbedded impurities and field emitters inside the cavity. Fig. 22 shows an engineering model of the diagnostic system mounted on a cavity. Fig. 23 shows an engineering model of a sensor board that contains carbon resistors (temperature sensors) and pin-diodes (x-ray sensors). Fig. 24 is a photo of a partially assembled sensor board. We are commissioning this diagnostic system.

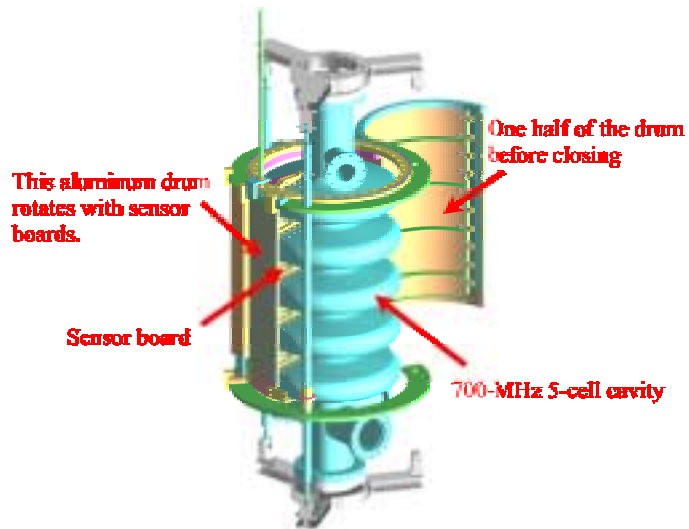


Fig. 22. 700-MHz 5-cell cavity with temperature and X-ray mapping diagnostic mounted

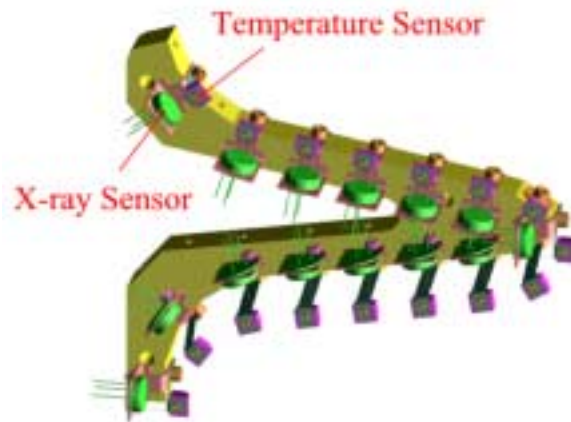


Fig. 23. Temperature and X-ray sensors mounted on a sensor board



Fig. 24. Photograph of a sensor board partially assembled and wired with temperature and X-ray sensors

APT SCRF DDN Work

We are close to completing all the documentation of APT SCRF DDN work. DDN 37 for $\beta=0.64$ elliptical cavity was completed. Final approval of the disposition of DDN 39 for the APT Power Coupler is in progress. Table 20 is a list of reports prepared or in progress to close out the APT SCRF DDN work.

Table 20. APT SCRF Design Data Need Status

Report Number	Title of Report	Format
Completed / Issued:		
TPO-E42-M-TNS-X-00024	Fabrication Drawings for the Accelerator Production of Tritium RF Coupler Window ED&D	CD
TPO-E41-R-TNS-X-00044	Fabrication Drawings of the 5-Cell $\beta=0.64$ Cavity for the Accelerator Production of Tritium ED&D	CD
TPO-E41-R-TNS-X-00047	Test Set-Up Drawings of the 5-Cell $\beta=0.64$ cavity for the Accelerator Production of Tritium ED&D	CD
TPO-E41-R-TNS-X-00041	Disposition of PPO-A21-G-DDN-X-00037: Medium-Beta Superconducting Cavity for HE Linac	Paper
TPO-E41-R-TNS-X-00043	Executive Summary: Development and Performance of Medium-Beta Superconducting Cavities	Paper
TPO-E43-M-TNS-X-00016	Accelerator Production of Tritium; Beta=0.64 ED&D Cryomodule Drawing Book	Paper
TPO-MEM-03901	Cryoplants for APT SRF Program Testing Support	Paper
TPO-E43-M-TNS-X-00018	Cryomodule Design Requirements and Design Description	Paper
TPO-E43-M-TNS-X-00017	Cryomodule Design Reference Manual	CD
In Preparation:		
TPO-E42-R-TNS-X-00052	Disposition of PPO-A13-G-DDN-X-00039: Power-Coupler/Window for HE Linac	Paper
TPO-E42-R-TNS-X-00049	Executive Summary of the Final Report on the APT Power Coupler Engineering Development and Demonstration (ED&D) Activities	Paper

4. Transmuter Development

Scope

- **Analysis Support** – Includes analytical assessments to guide overall transmuter development—specifically, experimental needs and data quality objectives. FY01 focus is assessing damage and gas production in structures surrounding the target.
- **Nuclear Codes and Data** - Includes development of analytical methods for the nuclear design of the transmuter, with focus on nuclear design codes and data, including evaluation of fission cross sections of key Pu isotopes, assessment of the lead-bismuth scattering cross-sections, improvement of the subactinide fission and fission fragment model for MCNPX, benchmarking results and comparing with the higher order methods, and coupling of higher order and deterministic codes and revisions to deterministic codes to account for subcritical source-driven behavior.

- **Thermal-Hydraulic Codes** – Includes assessment of the liquid metal and gas system models incorporated into the Transient Reactor Analysis Code (TRAC), such as benchmarks and quantification of some of the transport equations, thermal-transients in the structures from beam interrupts, natural convection potential in lead-bismuth eutectic (LBE), etc.
- **Laboratory Experiments** - Includes experiments to investigate the fundamentals of chemical reaction between LBE and sodium to address concerns with current design concepts about a possibility of severe sodium reactions with lead or bismuth due to a leak. Preparation for a series of small, scoping-type tests is underway to provide quick, pseudo-quantitative data on the nature and extent of the sodium reaction.
- **Irradiation Experiments** - For FY01, four sets of scoping experiments were approved by the Steering Committee:
 - “Influence of Proton Irradiation on the Corrosion Kinetics of Structural Materials in LBE Coolant Systems” will irradiate material samples with protective oxide layers.
 - “Cross-Sections for the Activation of Sodium by Protons” will investigate the production of the longer-lived isotopes in an AAA target assembly with sodium as a coolant, providing a benchmark for testing the nuclear physics codes used for target design.
 - “High-Energy Neutron Leakage from a Spallation Target” will provide experimental verification of expected flux distributions and evaluate the effectiveness of a buffer in reducing the leakage of high-energy neutrons, which produce gas and limit the lifetime of structural materials.
 - “Measurement of Hydrogen and Helium Production with Neutrons up to 100 MeV” will determine hydrogen and helium production on materials proposed for the AAA program with neutron energies up to 100 MeV.

Highlights

- The intra-nuclear cascade code (CEM2k) was delivered to the MCNPX code developers.
- The ATW changes to TRAC were incorporated into TRAC-M (NRC version). The changes and the test results were documented and submitted to the NRC (*Accelerator Transmutation of Waste Updates for TRAC-M*, LA-UR-01-3660, June 2001).
- A baseline change proposal (BCP) was approved to start a series of irradiation experiments at LANSCE in the blue room at WNR.

Analysis Support

Previous target/buffer design studies investigating the impact of buffer thickness on transmuter performance were done for the ATW Lead-Bismuth-Eutectic (LBE)-cooled system using LBE as the target and buffer material. This work was extended this quarter to the ATW sodium-cooled system also using LBE as target and buffer material. The study evaluated the impact of varying the buffer thickness from 11.5 cm to 28.8 cm on the number of neutrons produced per incident proton, neutron source

distribution, source importance, ATW system performance parameters, and neutron damage rates. In the base study, the energy of the proton beam impinging on the target was assumed to be 1 GeV. The key findings from the study are as follows:

- Compared to the LBE-cooled system, the sodium-cooled system shows a stronger variation in the number of neutrons produced per incident proton, as the buffer thickness is varied. This trend is due to the better spallation-neutron production characteristics of the LBE-cooled blanket, which keeps the number of neutrons produced per incident proton fairly constant with variation in buffer thickness.
- The relative importance of source neutrons to fission neutrons (source importance) increases in the sodium-cooled system as the buffer thickness is reduced, indicating a reduction in the accelerator current requirements, similar to the trend in the LBE-cooled system.
- System blanket performance improves with reduction in the buffer thickness; the transuranics inventory decreases and the discharge burnup increases for a fixed cycle length. The burnup reactivity loss also decreases.
- A reduction of the buffer thickness results in a higher fluence and higher hydrogen and helium gas production and dpa rates at the first row of fuel in the blanket.
- Comparative calculations investigating the impact of the incident proton beam energy on the damage rates indicated that a reduction of the beam energy from 1 GeV to 600 MeV results in an increase in the damage rates at the window and very little impact on the rates at the buffer/blanket interface. This trend is caused by the higher neutron-source intensity required for the lower energy beam to maintain the same blanket power, as a result of the reduction in the number of neutrons produced per incident proton in this case; at the interface, however, the fission neutrons dominate and the impact of the higher source intensity is reduced.

A more detailed investigation of the combined effects of the various irradiation damage components is recommended for future studies.

Nuclear Codes and Data

During this quarter, progress was made in a number of areas as summarized below.

Intranuclear Cascade Code Improvements - During this period, we worked on the development of the CEM2k code, a nuclear-reaction simulation code used in MCNPX for AAA spallation target design. We completed and delivered a new CEM2k module to AAA's MCNPX team. This new version of CEM2k makes two very significant improvements for AAA spallation target simulations: (1) it improves the description of spallation products and nucleon spectra (particularly neutron production) from intermediate energy reactions; and (2) it improves predictions of complex particle (e.g. alpha particles) production in such reactions (important for modeling gas production). Prior to releasing the code to the MCNPX team, we extensively benchmarked the code against a large database of experimental data to validate our improvements. An example is given in this report. Full details are available from the authors and have been presented in seminars and at conferences.

Spallation Radionuclide Products and Neutron Production - The improvements we made to our intranuclear cascade simulations solved two deficiencies. First, until now, all cascade codes have predicted radionuclide-production cross sections to an accuracy less than we would like. Based on new data from the German/European ATW program, we have made theoretical improvements to cascade physics that have allowed us to much more accurately predict these cross sections. These improvements are described below, and extensive benchmarking to experimental data has demonstrated the improvements. Secondly, the cascade physics improvements have led to more accurate predictions of neutron-production per incident proton (n/p). This is very important for modeling the neutron economy of an ATW system.

We incorporated into CEM2k the use of real binding energies (experimental values or reliably calculated values where there are no data) for the nucleons at the intranuclear stage of reactions, instead of using the approximation of 7 MeV employed earlier in the code. Also, we incorporated the use of reduced masses into CEM2k instead of the approximation of real masses used previously by the code. We tested both these refinements on a number of measured reactions, and observed an improvement between CEM2k results and existing data. Very importantly, we modified the length of the cascade phase of the reaction. This results in compound nuclei produced at a higher excitation level, and leads to a higher multiplicity for evaporation particle emission, and hence a higher neutron production (n/p). The increased neutron production has been shown for thin target calculations, e.g. Pb(p,xn). We will be interested to see how MCNPX predicts integral n/p in benchmarks, such as the Sunnyside experiment, when the new CEM2k code is integrated into MCNPX. An example of the excellent agreement that we obtain between CEM2k and experiment is shown in Fig. 25. Here, p+Pb spallation data from GSI are compared with our model predictions.

Gas Production Reactions (Complex Particle Emission) - CEM, as is the case for other similar INC-type codes, historically uses geometrical cross sections to calculate the total reaction and elastic cross sections. This approach provides a reasonably good agreement with available data at incident energies above about 100 MeV, but is not sufficiently reliable at lower bombarding energies. To solve this problem, we have incorporated into CEM2k the NASA systematics by Tripathi et al.¹⁸ for all incident protons, and the Kalbach systematics¹⁹ for neutrons with energy below the maximum in the NASA reaction cross sections. This allowed us to better describe all nucleon-induced reactions. In addition, we have developed new routines to calculate the Coulomb barriers used at the pre-equilibrium and evaporation phases of CEM2k to better describe the thresholds for nuclear reactions. These improvements have had a particularly good impact on our ability to predict alpha and proton production cross sections—important for material damage issues in ATW due to gas production. An example of the improvements we are able to obtain with our new CEM2k code is shown in Fig. 26, depicting alpha particle production from proton reactions on aluminum. The new code predicts gas-production at a significantly higher level of accuracy.

¹⁸ NIM B117 (1996) 347

¹⁹ J. Phys. G: Nucl. Phys. 24 (1998) 847

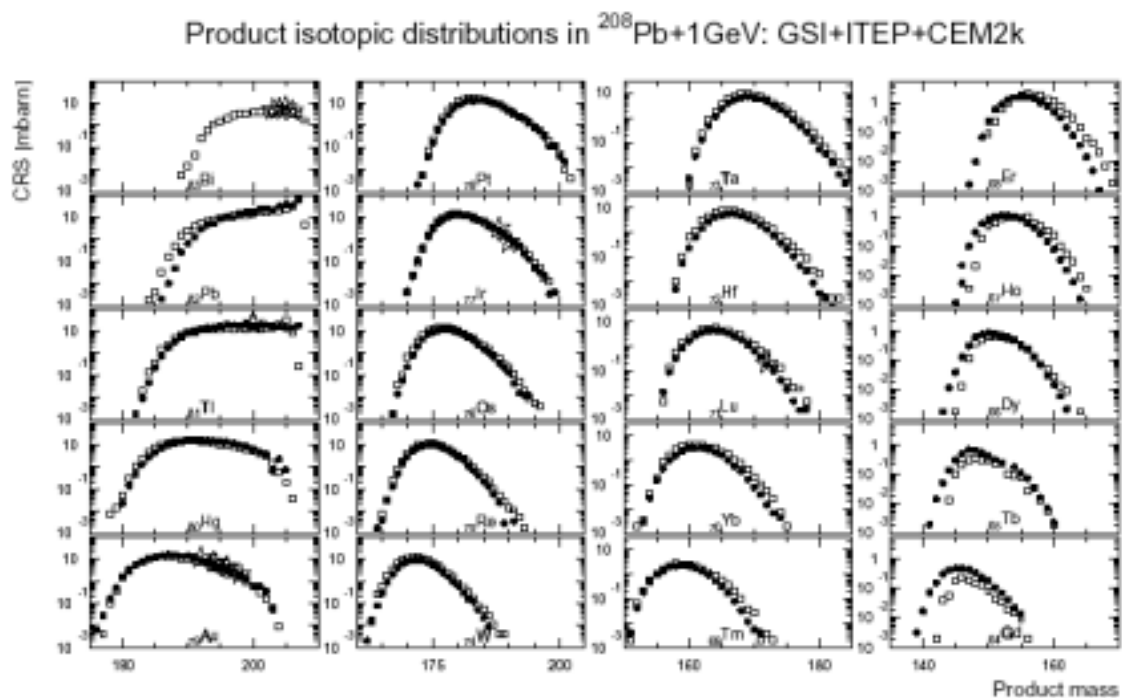


Fig. 25. CEM2k predictions of 1 GeV p+Pb spallation radionuclide production compared with new experimental data. The open squares are CEM2k results, black circles are GSI data, and open stars are new ITEP (Titarenko et al.) data.

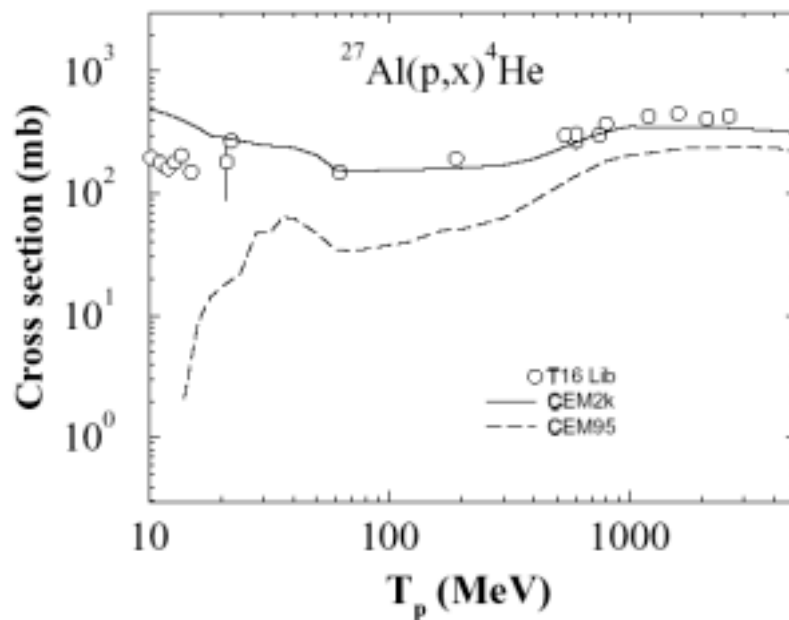


Fig. 26. CEM2k predictions of Al(p,x) alpha production as a function of incident proton energy.

Other Spallation Physics - We have worked on a Los Alamos version of the Quark-Gluon String Model and created a new universal code system, LAQGSM. This milestone is a result of many years of collaboration between several Los Alamos individuals and groups of code developers from Europe. Much of this particular work was supported by PRAD²⁰ funds at Los Alamos, but the code will be useful for AAA spallation target design, and we plan to incorporate it into MCNPX.

Our LAQGSM code includes the Dubna intranuclear Cascade Model (DCM), the Quark-Gluon String Model (QGSM), the improved version of the Cascade-Exciton Model (CEM2k) recently provided to AAA, the Fermi break-up model, and the coalescence model. It simulates nuclear reactions induced by hadrons and nuclei at energies from about 100 MeV/nucleon to 200 GeV/nucleon, and was recently benchmarked in a very detailed comparison with available data and against results by FLUKA (a CERN code) and MARS (a Fermilab code). We have documented the code in the "User Manual for the Code LAQGSM," which will be completed shortly and delivered to potential users. LAQGSM can be used to solve applied problems for AAA and other intermediate-energy projects, e.g., RIA,²¹ as well as for high-energy projectiles, e.g., PRAD. It is similar to the CERN code GEANT4 under development since 1994 by an international team of over 100 physicists (not available from CERN to solve weapon-related problems), but it has a number of new ingredients and refinements, and is therefore expected to provide more reliable results than GEANT4 (as shown by our preliminary study).

Fission Cross-Section Data Evaluations - Our new $n+^{239}\text{Pu}$ evaluated fission cross section for AAA has been validated through extensive comparison against all experimental data (both ^{239}Pu fission data and fission ratio data in $^{239}\text{Pu}/^{235}\text{U}$ experiments), and has been put into ENDF-6 format. Our work used all available experimental data, including some recent measurements from LANSCE and from Russia²². Powerful statistical approaches have been used to evaluate the cross section and its uncertainties, including long-range correlations, important to predict accurately the criticality of any ATW technology. The ^{239}Pu isotope is highly abundant in reactor waste, strongly influencing the criticality of an ATW transmuter, and has therefore been our first focus in this study. More than 50 experimental data sets have been included. Their statistical and systematic errors (including covariance matrices) have been analyzed. The resulting uncertainties on the (n,f) cross section are significantly reduced, compared to the previous ENDF/B-VI analysis. Changes by up to 4% in the (n,f) cross section occur in places (above 14 MeV), mainly due to a revision of ^{235}U after new experimental results obtained by Paul Lisowski (LANL).

Fig. 27 shows our new ^{239}Pu (n,f) evaluation for incident neutron energies 0.8–20 MeV. As a comparison, an older (1990) evaluation is shown. While there is a very good agreement overall between the two evaluations below 14 MeV, large differences appear above this energy. This is mainly due to an improved evaluation of ^{235}U (n,f), largely based on recent data by P. Lisowski. Fig. 28 shows the standard deviations (uncertainties) for both evaluations. This figure demonstrates the significant improvement obtained on the error bars of the new evaluation, owing to the accurate measurements made recently available to us. Our new evaluation of the

²⁰ Proton Radiography

²¹ Rare Isotope Accelerator

²² O.Shcherbakov et al., private communication

ratio cross section $^{239}\text{Pu}(n,f) / ^{235}\text{U}(n,f)$ is plotted in Fig. 29 against two recent experimental data sets: P. Staples' 1998 data and O. Shcherbakov's 2001 data. Staples' data was measured at Los Alamos; Shcherbakov's was measured in Russia through ISTC²³ support for Russian ATW work.

We have worked on combining our new $^{239}\text{Pu}(n,f)$ fission evaluation for AAA into a new ENDF evaluation, for use in AAA transmuter simulations. This has involved translating our results in the ENDF-6 format, and combining the information with other new improvements to the evaluation. The most important of these is a new (n,2n) evaluation, which was completed in LANL Group T-16 through a theory-experiment collaboration (GEANIE at LANSCE). The (n,2n) cross section differs significantly (over 50%) compared to the existing ENDF/B-VI evaluation. The support for this work came from the LANL Nuclear Weapons (NW) Directorate, and resulted in a Defense Program Award of Excellence (2001). In an ATW context, it is important for predicting transmutation of ^{239}Pu into ^{238}Pu .

We held a seminar on our new $^{239}\text{Pu}(n,f)$ evaluation for AAA. In the discussion following the seminar, we were reminded that a new Pu fission neutron spectrum evaluation using the Los Alamos model, will be completed soon (work supported by NW). We will also include this improvement in our final evaluation, to be delivered to AAA by the end of the fiscal year.

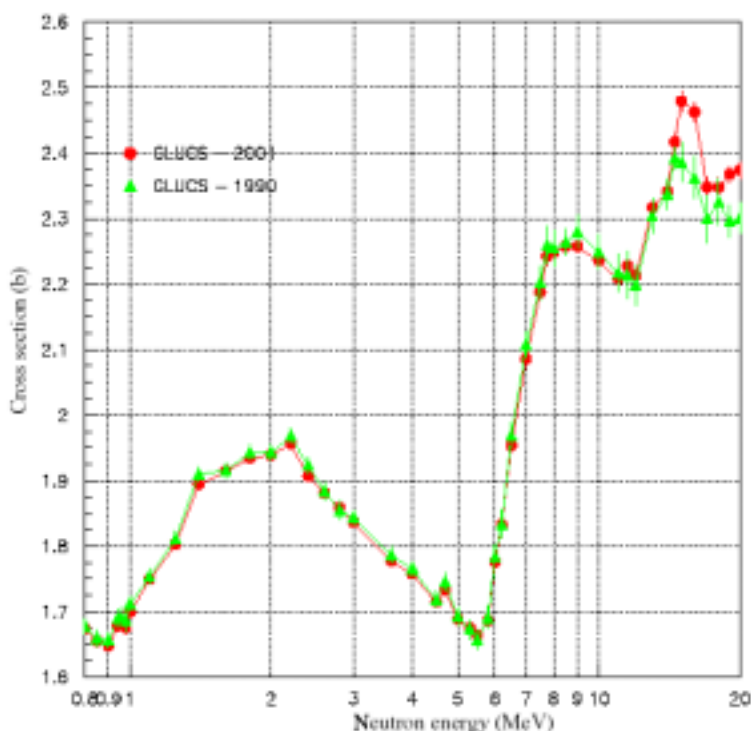


Fig. 27. $^{239}\text{Pu}(n,f)$ cross-section in comparison with the earlier evaluation.

²³ International Science and Technology Centre (Moscow)

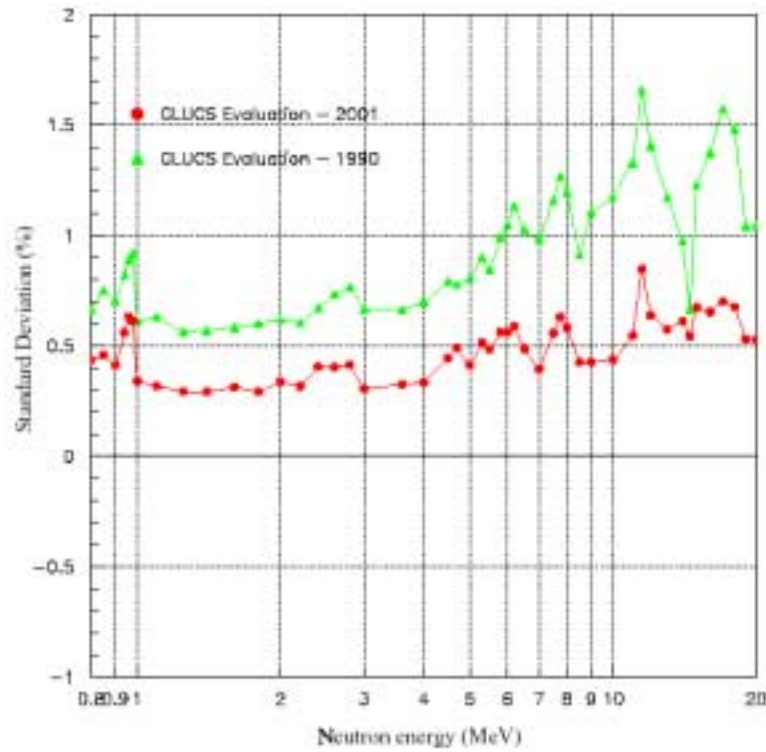


Fig. 28. Standard deviations for the $^{239}\text{Pu}(n,f)$ evaluation in comparison with the earlier evaluation.

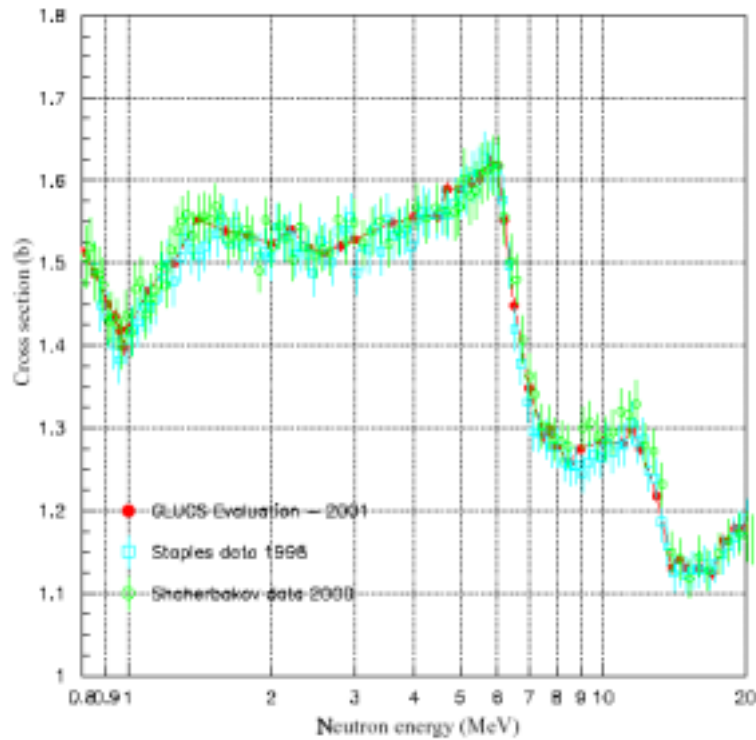


Fig. 29. Comparison of the $^{239}\text{Pu}(n,f)/^{235}\text{U}(n,f)$ evaluation with the recent data.

McGNASH Nuclear Modeling Code Improvements (Fission Model) - We have continued to improve our McGNASH nuclear reaction code to model fission decay and particle emission. Recently, we made progress in incorporating width-fluctuation models into McGNASH. This is particularly important at low energies (keV to a few MeV), and significantly improves the predictions of fission, elastic, inelastic, and capture reactions.

The statistical Hauser-Feshbach theory of nuclear reactions, implemented in GNASH and McGNASH, is based on the Bohr independence hypothesis, which states the independence of the formation and the following decay of a compound nucleus. At low energies (keV to a few MeV), this hypothesis is known to break down because of correlations between incident and outgoing waves. Adequate corrections are crucial to correctly describe fission, elastic, inelastic, and capture reactions at low incident particle energies. To take into account these correlations properly, several models have been developed (HRTW, Moldauer, and GOE). We implemented the Moldauer's approach (fast and accurate) into our McGNASH nuclear reaction theory code, eliminating the need to do separate width fluctuation corrections (WFC) in COMNUC and then reintroducing it into GNASH. The earlier method was both awkward and lacking in consistency. Our WFC calculations have been tested successfully. We are now in the final process of benchmarking our new code against the earlier versions of McGNASH and GNASH.

Thermal-Hydraulic Codes

Progress was made for the following three TRAC-ATW tasks this quarter:

- As a capability demonstration, beam-interrupt transient calculations were performed for the ADTF target and multiplier loops to determine the effect of beam interrupt times on wall-pipe temperatures. The major concern is the thermal fatigue effects on ATW structural components. Wall temperature calculation results for beam interrupt times of 0.3–30 sec will be presented.
- Also as a capability demonstration, the effect of decay heat within the coolant on natural circulation within the ADTF is being investigated. Preliminary results are presented.
- All ATW-TRAC modifications were incorporated into the most recent NRC developmental version of TRAC. These modifications were tested and documented and transmitted to the NRC for inclusion in the NRC official version of the TRAC-M computer code.

Beam-Interrupt Calculations - As an example, nodding diagrams for the target loop and the multiplier loop described in the ADTF pre-conceptual design report for the modular design were developed. In the target loop, the wall temperature evaluated is at the target outlet piping. The wall temperature evaluated for the multiplier loop is at the core outlet piping. A pipe-wall thickness of 6.35 m (0.25 inches) was assumed for both the target loop and multiplier loop. The same wall thickness was assumed for the multiplier loop piping. In the current TRAC models, only the loop piping walls were modeled. Because these were done as demonstration calculations, the walls of the target inlet and outlet plenum were not modeled nor was the heat exchanger tube-sheet structure.

Fig. 30 shows the wall temperature difference, defined as the difference between the wall average temperature and the wall surface temperature, for the target loop as a function of beam interrupt times. Fig. 31 shows the wall temperature differences for the multiplier loop. Table 21 provides a summary of the beam interrupt calculations.

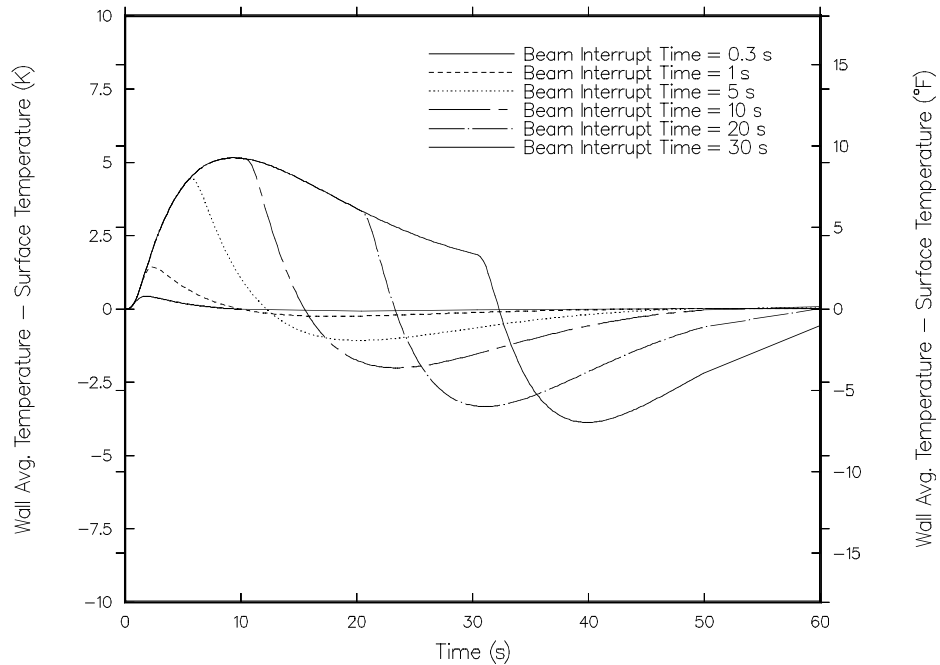


Fig. 30. Effect of beam interrupt times on wall temperature difference for the target loop at the target outlet piping.

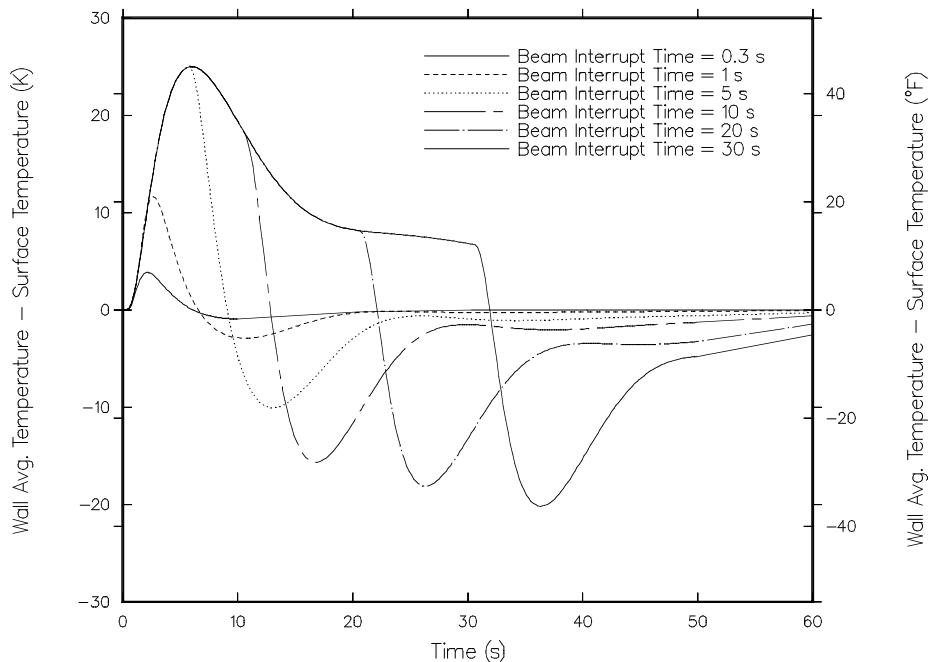


Fig. 31. Effect of beam interrupt times on wall temperature difference for the multiplier loop at the core outlet piping

Table 21. Summary of Beam Interrupt Calculations

Target Loop				
Beam Interrupt Time (sec)	0.3	1	5	≥10
Peak wall temperature difference (K)	0.4	1.4	4.5	5.2
Time of peak wall temperature difference (sec)	1.8	2.3	5.7	9.4
Wall surface temperature (K)	527.3	525.6	517.7	510.8
Wall average temperature (K)	527.7	527.0	522.2	515.0
Coolant temperature (K)	527.0	524.6	514.8	507.5
Decrease in coolant temperature (K)	1.0	3.4	13.2	20.5
Multiplier Loop				
Beam Interrupt Time (sec)	0.3	1	5	≥10
Peak wall temperature difference (K)	3.8	11.6	25.0	25.0
Time of peak wall temperature difference (sec)	2.2	2.6	5.6	6.0
Wall surface temperature (K)	755.3	741.3	699.1	695.6
Wall average temperature (K)	759.1	752.9	724.1	720.6
Coolant temperature (K)	752.5	732.8	681.8	678.8
Decrease in coolant temperature (K)	-9.5	-29.1	-80.2	-83.2

For the target loop, the maximum temperature difference is 5.2 K and it occurs for beam interrupt times of ≥10 sec. For the multiplier loop, the maximum temperature difference is 25 K and it occurs for beam interrupt times of ≥5 sec.

The difference between the average temperature and surface temperature of the structure is used to obtain thermal strains. The method for computing structural strain, deformation, and fatigue limits at elevated temperatures is given in Appendix T of the American Society of Mechanical Engineers Boiler and Vessel code. Fatigue curves from this standard can be used to determine the number of cycles that the structural components can endure based on the calculated thermal strains.

Sensitivity calculations on the effect of wall thickness and wall noding were also performed. Fig. 32 shows the temperature difference for a beam interrupt time of 30 sec for three calculations: (1) base case with wall thickness of 0.25 inches and the number of wall nodes set to 3; (2) a wall thickness of 0.5 inches with wall noding set to 3; and (3) a wall thickness of 0.5 inches with nodes set to 5. The thicker wall results in a higher peak temperature difference. For the 0.25-inch wall thickness, a wall noding of 3 is sufficient until the ADTF design is more accurately defined.

Natural Circulation with Fluid Decay Heat - Two natural circulation cases were run with TRAC-ATW for the lead-bismuth eutectic ADTF target to test TRAC's ability to model natural convection for liquid metal systems. In both cases, the loop was run to a steady state for 2000 sec. Five megawatts were deposited in the beam region with 1% of that power deposited uniformly by volume in the fluid after it exited the beam to model the initial decay heat. At 2000 sec, the beam and pump were tripped. In both cases, the full steady-state flow of helium continued at the same inlet temperature on the secondary side of the heat exchanger.

The first case represented the actual situation for short times after beam trip; the 1% decay heat continued, distributed volumetrically. The velocity in the loop, represented by the pipe exiting the outlet plenum at the top of the target, was 11 cm/s at 4000 sec. The second case was run to illustrate the difference in natural circulation rate between the actual and the more usual situation in a nuclear system

where the decay power is deposited (usually from rods) only in a limited region of the fluid (the core). The same 1%, or 50 kW, was deposited only in the mesh cells representing the beam region. After 4000 seconds, the velocity was 14 cm/s.

The next step will be to investigate the volumetrically deposited and time-dependent decay heat.

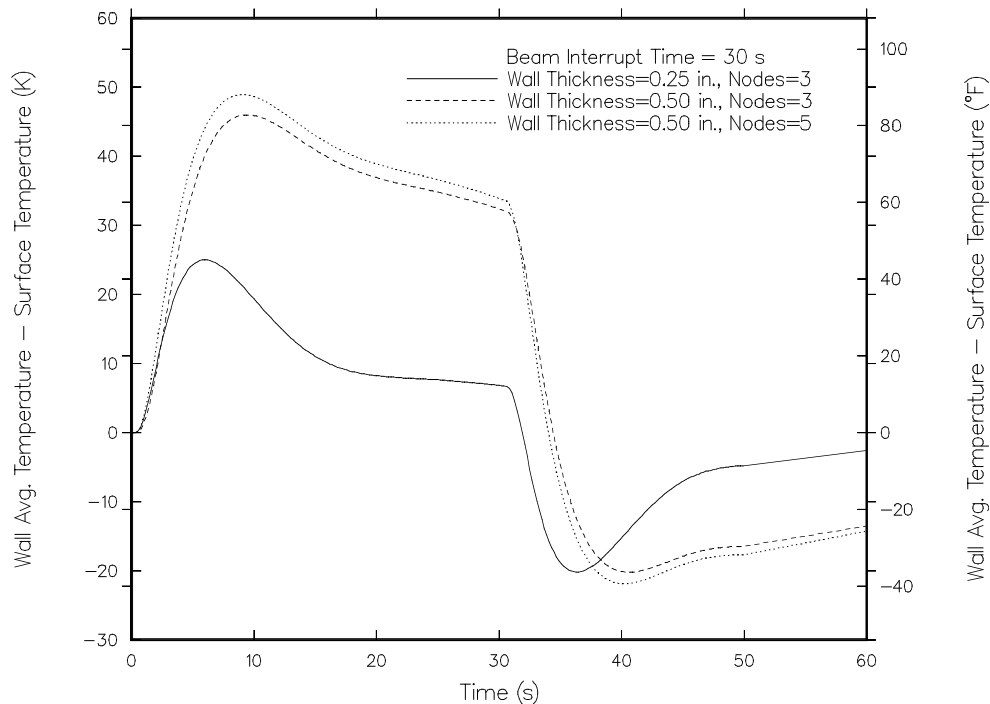


Fig. 32. Effect of wall thickness and wall noding on wall temperature difference for the multiplier loop at the core outlet piping.

TRAC-ATW Models in NRC TRAC-M - The TRAC-ATW models and fixes were incorporated into the latest NRC version of TRAC-M. Over 450 test problems were run that include standard PWR and BWR calculations as well as ATW calculations that include helium, sodium, and LBE. Results were consistent with previous TRAC-M and TRAC-ATW results. Code modifications and test results were documented. The code modifications were sent to the NRC for inclusion into the official NRC TRAC-M code version. It is anticipated that the ATW fixes will be incorporated into the official NRC TRAC-M code version by the NRC staff toward end of August.

Laboratory Experiments

In June, we started the new series of experiments to investigate the fundamental aspects of the chemical interactions between LBE and sodium. An instrumented test apparatus for the scoping tests has been designed and is being fabricated. An existing glove box is being prepared to support the tests during assembly and disassembly operations. A test matrix for the experiments is shown in Table 22. The conditions for Tests 1 and 2 are identical and are intended to determine the repeatability of the experimental process.

Table 22. Test Matrix for Sodium-Lead-Bismuth Compatibility Tests

Test	Initial Temp (°C)	Injection Speed	Sodium Volume (cm ³)	Heavy Metal	
				Injection Material	Volume (cm ³)
1	600	Fast	100	Pb	5
2	600	Fast	100	Pb	5
3	600	Fast	100	Bi	2.5
4	600	Fast	100	LBE	5
5	400	Fast	100	Pb	5
6	400	Fast	100	Bi	2.5
7	400	Fast	100	LBE	5
8	200	Fast	100	LBE	5
9	200	Slow	100	LBE	5
10	400	Slow	100	LBE	5
11	400	Slow	100	Pb	5
12	400	Slow	100	Bi	2.5

Irradiation Tests

During this quarter, we established the LANSCE Irradiation Experiments Working Group to evaluate the proposed irradiation experiments to be performed at LANSCE (blueroom and WNR). The Working Group reviewed a set of proposals and recommended seven sets of experiments for consideration. These experiments are

- Neutron yield and spectrum for LBE targets (including buffer effects)
- Beam effects on oxide layer for LBE corrosion
- Sodium activation in proton beam
- High-energy gas production cross-sections
- Actinide fission cross-section measurements at high energies
- Neutron multiplicity at high energies
- Spallation products assessment for LBE

The Working Group recommendations were presented to the Steering Committee. The Steering Committee authorized scoping tests for the first four experiments in FY01. Depending upon the results of the scoping tests and the funding availability, decisions will be made for continuing with these experiments in FY02. Further details of these experiments were described in the Scope section. For the three experiments not described in the Scope section, a small analytical effort will be devoted to investigate the need, accuracy, experimental technique, and test facility before the actual tests are started in the upcoming years. The design, construction and safety paperwork for these tests was initiated in June.

5. Spallation Target Development

Scope

For the spallation target development, the two main areas are the lead-bismuth eutectic (LBE) technology and materials research.

- **LBE Technology** - In FY01, the main activity in the LBE technology area is the construction and operation of the materials test loop (MTL). This is a large loop capable of delivering 15 m³/h flow rate of LBE using a mechanical sump pump. High velocities (up to 6 m/s) are achievable in the test section whereas the nominal design velocity is 1 m/s. The vertical geometry allows for natural circulation with ~0.2 m/s velocity. The design specification for the power input to the loop is 50 kW (nominal) with 20% extra capacity. This loop is designed and being constructed to support the LBE technology development, in general, by providing a test bed for corrosion, and heat transfer experiments and instrument testing. Oxygen control strategy and probe testing is also a function for the MTL. At present, spallation target technology is the primary motivation for developing the LBE technology, but the loop can also be used to support the choice of LBE as a nuclear coolant, if needed.

- **Materials Research** - In the materials area, we are continuing to develop the Materials Handbook along with supporting experiments.

High-Temperature Testing at PNNL and ORNL - The primary scope of the activities at PNNL and ORNL is to obtain high temperature structural testing data for materials already irradiated at low temperatures under the APT program, including high temperature tensile testing and compact tension testing of 9Cr-1Mo and SS-316L specimens (irradiated and unirradiated), microstructure investigations, reports on fatigue crack growth, fracture toughness, and tensile testing of weld materials. Includes transfer of small-scale testing capability from PNNL to LANL.

Materials Handbook and Related Activities - High temperature structural testing of already irradiated materials (at low temperature) are being conducted. Additional testing of irradiated tungsten samples continue. The Materials Handbook will be maintained and the scope will be expanded to include additional materials of interest to ATW applications.

Temporary Assignment in PSI (Materials Collaboration) - Work at the Paul-Scherrer Institute (PSI) in Villigen, Switzerland, includes assessment of exposure to materials samples to confirm the calculations of neutron and proton flux from LAHET and MCNPX as well as displacement per atom (dpa) and gas production for samples irradiated at the Mark-II SING target.

LANL Hot Cell Analyses - Performing tests after irradiation, such as bend tests, pushout tests, hardness, etc., and analyzing activated samples, such as Alloy-718 window, tungsten, weld specimens, etc. Work being performed as a continuation of the APT program.

Light Water Corrosion - Work is being performed to closeout the water corrosion DDN. Closing the DDN requires a report that summarizes the data and analyses to date with specific corrosion allowance guidance for the target-blanket designers. Continuation of the APT program.

Highlights

- The report, *Preliminary Assessment of the Spallation Target Options for Accelerator Driven-Transmutation*, compiling the initial assessment of various target options, was published and distributed.²⁴
- *Lead-Bismuth Eutectic Materials Test Loop Test Plan*,²⁵ emphasizing the facility description for the Materials Test Loop (MTL), was issued.
- Under the APT ED&D program, Design Data Need, DDN 30, *Light Water Corrosion*, was completed.
- One temporary assignment at Paul-Scherrer Institute (PSI) was completed and a second similar assignment will begin next quarter to perform tensile testing and TEM (Transmission Electron Microscopy) observations on SS-316L and F82H. These assignments are paid for by PSI.

LBE Technology – Materials Test Loop (MTL)

We conducted a second design and engineering review of the Materials Test Loop (MTL) after the responses to the first review, additional analysis, and design modifications were completed. In particular, improved stress analysis with various possible temperature regimes, coupled with adjusting the supports for the piping, resulted in full compliance with the ASME codes. Some additions to the support structure improved the facility and piping network, classifying the MTL to PC-1 status (seismic). A flange-bolt load analysis was also completed with a specified bolt-tightening schedule. The design review comments were documented and addressed. In general, there were no comments that affected the design or the construction of the loop, but valuable recommendations were made for things to be included in the initial testing and start-up procedures.

We completed all major construction and assembly of the MTL this quarter (see Figs. 33 and 34), and put the data acquisition and control center in place. We implemented a formal process to prepare and archive the safety documentation, and to prepare for an operation readiness review and approval with the AAA safety team. A Memorandum of Understanding (MOU) for the MTL safety chain was drafted and signed. A Hazard Control Plan (HCP) for operations as well as Operating Procedures are being finalized. We established a formal procedure for the On-the-Job Training (OJT), daily facility hazard identification, and weekly safety reviews.

Preparations were made this quarter that culminated in a successful pressure/leak test of the MTL. These preparations included:

- a controlled flange-bolt load test to determine the *in situ* friction coefficient for tightening the flange bolts; this test enabled determination of the bolt pre-load for a given tightening torque;
- final installation and wiring of key MTL instrumentation, including pressure transducers, level sensors, solenoid valves, and thermocouples; and
- preparation and approval of the HCP and Test Procedures.

²⁴ AAA-RPO-TRNS-01-0017, LA-UR-01-1634, Rev. 0, March 2001

²⁵ LA-CP-01-134

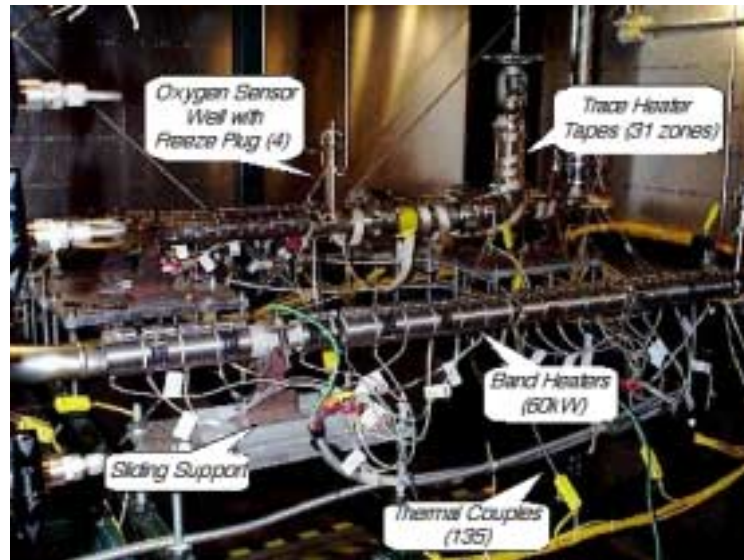


Fig 33. Materials Test Loop (MTL) main heater section before insulation is applied.

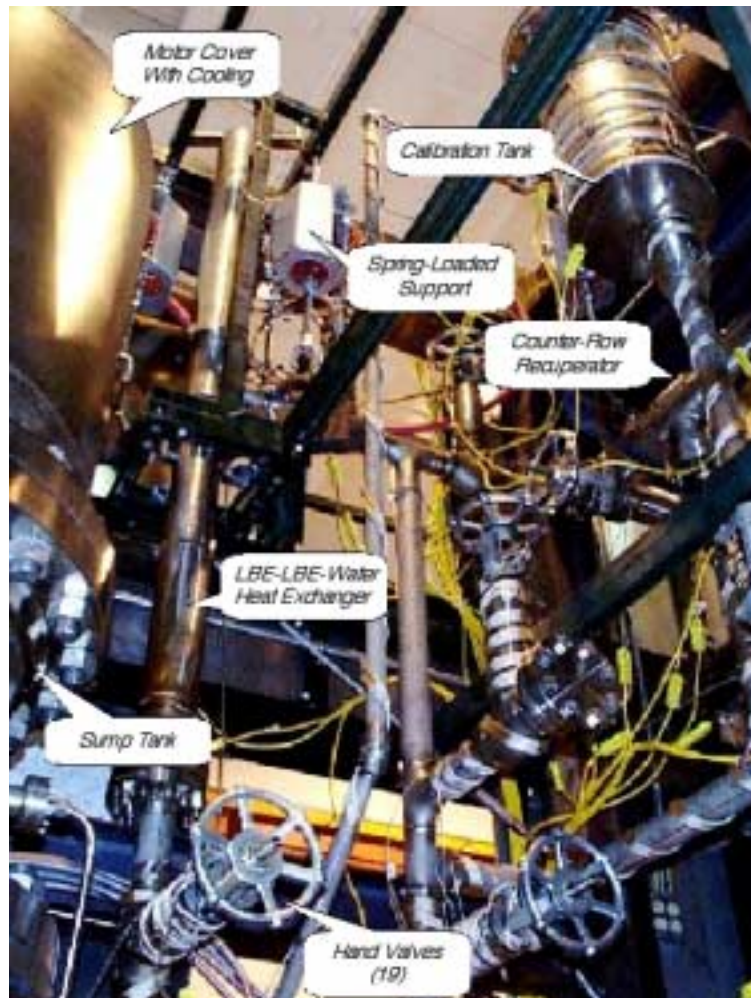


Fig 34. A partial view of the MTL piping network before insulation is applied.

Mid-June marked the transition from the construction phase to system test phase. We successfully performed a pressure test of the loop with water and helium cover gas up to 120 psig at room temperature, surpassing the design requirement in terms of allowable system leakage. All level sensors performed flawlessly. The loop was filled with water and then pressurized with helium gas. On the initial fill with water, two minor flange leaks were detected and corrected (only minor adjustments to the flange bolt pre-load were required). The pressure was then raised in stages up to the final test pressure of 120 psig. During this pressure increase process, no leaks were detected. In addition, helium leak-rate data were obtained at key pressure levels during the test. These leak-rate data indicated good vessel sealing in the cover gas space.

We continue to implement the data acquisition and control (DAC) system. We completed installing the National Instrument (NI) hardware for the DAC and enabled communications with all MTL instrumentation. The LabView program properly controls the hardware and the data is passed in and out correctly. DAC software is about 90% complete for the manned operations of the MTL (see Fig. 35).

An initial test plan emphasizing the facility description for the MTL was issued (*Lead-Bismuth Eutectic Materials Test Loop Test Plan*, Version 1.0, LA-CP-01-134). It is expected that another revision will be made before the end of FY01. The new revision will include more details in terms of the near-term corrosion and heat-transfer experiments. A number of procedures have been written and reviewed to support the operational testing of the MTL.

Materials Research

High-Temperature Testing at PNNL and ORNL - In order to transfer the technology of small-scale tensile testing to LANL, a PNNL expert visited LANL to discuss and obtain information about the LANL facilities where the "hot specimen" tensile-test system will be located. This tensile-test system will be used in the future to perform tensile tests at LANL on highly radioactive tensile specimens. Furnace technology, which will be used for allowing tensile tests to be performed at elevated temperature in the tensile-test system under construction at LANL, has been researched. The design of the fixtures for loading and testing tensile specimens was finished and it is under construction at LANL. The new fixtures represents an improved design compared to the fixtures in use at PNNL where the tensile tests are currently performed.

High temperature testing on SS-316L (at 300°C) and 9Cr-1Mo (at 400°C and 500°C) was completed (see Figs. 36 and 37). These specimens were irradiated at 35-67°C in an 800-MeV 1-mA proton beam with spallation neutrons. The two 9Cr-1Mo specimens tested at 500°C were irradiated to 2 and 9 dpa. These results show an increase in yield stress with increasing dose, but very little change in uniform elongation as was seen for testing at lower temperatures. The SS-316L specimen was irradiated to 2.5 dpa, and exhibited a lower uniform elongation and yield stress than similar specimens irradiated to 2.8 dpa but tested at 50°C.

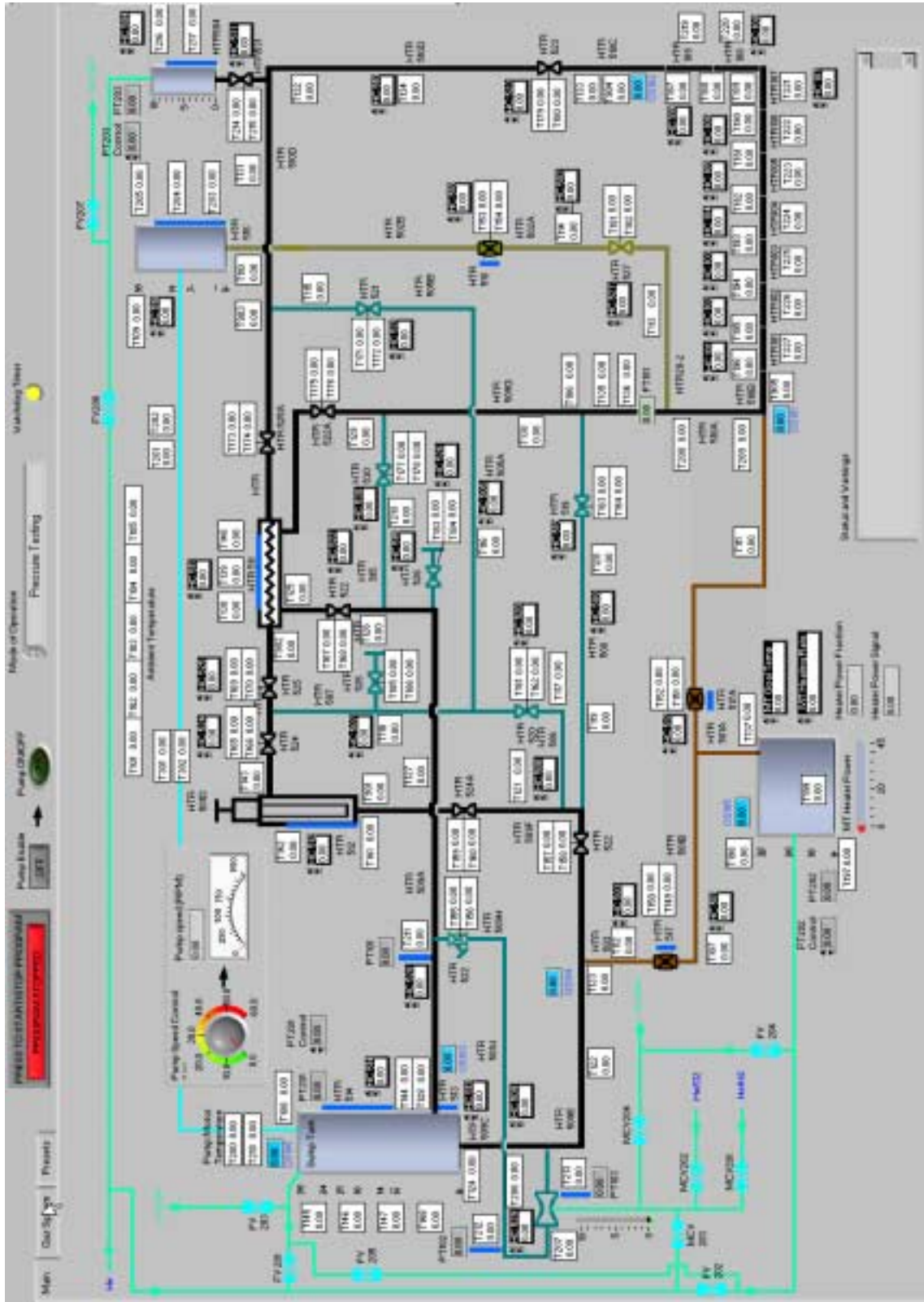


Fig 35. The front panel of the DAC program, showing the schematic MTL with control input for all components and instrumentation.

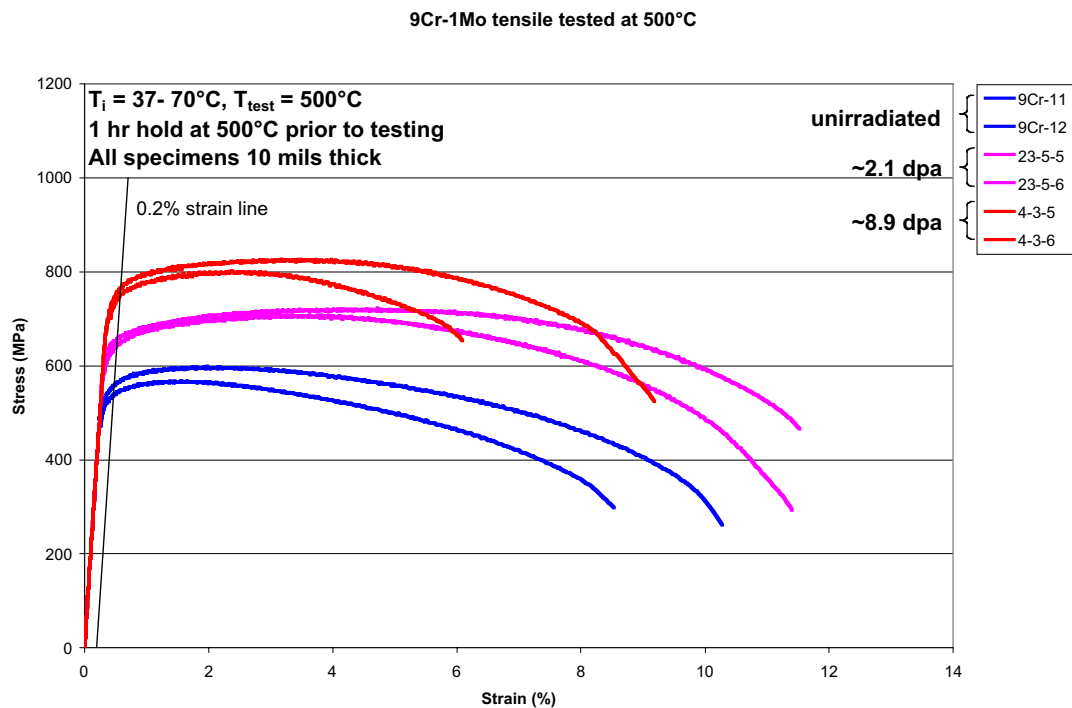


Fig. 36. Stress/Strain curves for Mod-9Cr-1Mo tested in tension at 500°C .

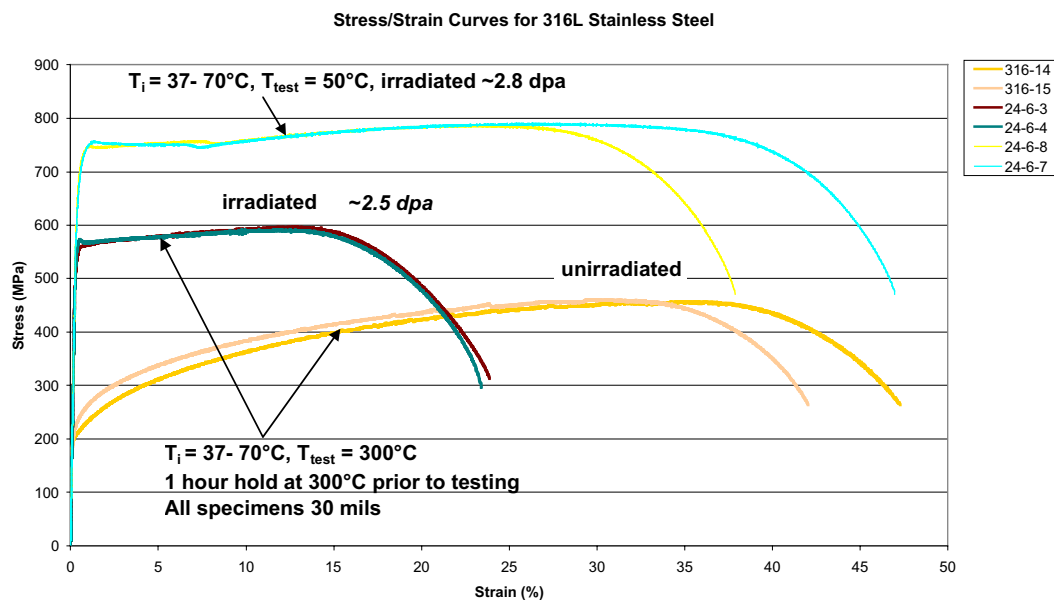


Fig. 37. Stress/Strain curved for SS-316L tested in tension at 50°C and 300°C .

ORNL shipped to LANL twelve "push-out" specimens irradiated at HFIR²⁶ to a maximum dose of 1.5 dpa. (The specimens are made of solid Inconel-718, solid SS-

²⁶ High Flux Isotope Reactor at ORNL

316L, Inconel-718 HIP bonded to tungsten, or SS-316L HIP bonded to tungsten—the specimens containing tungsten were plated with nickel.) In addition, a number of tensile and fracture toughness specimens were returned to LANL after being previously tested at ORNL.

Materials Handbook and Related Activities - The Nuclear Systems Materials Handbook (NSMH) was found to contain data on the corrosion and compatibility of 300 series stainless steels with sodium. The appropriate data have been extracted from the NSMH and will be incorporated into the next revision of Chapters 3 and 16 of the Materials Handbook.

Data and information on modified 9Cr steel [9Cr-1Mo-V ferritic steel] have been collected from Section II of the 1998 version on the ASME Boiler & Pressure Vessel Code. Additionally, an advanced copy of the revision to Subsection NH of the ASME Code has been obtained. It contains ASME-specified values of material properties and requirements for the use of Modified 9Cr in SC III, Division 1, Class 1 construction. Contacts have been made with Cr-Mo steel experts at ORNL to obtain other information relative to the Modified 9Cr material. Finally, drafting of a Handbook chapter [Chapter 19] on the Modified 9Cr ferritic steel has been initiated.

Tensile specimens of HT-9 and EP-823 were normalized and tempered and then shipped to Paul-Scherrer Institute (PSI) in Switzerland to be irradiated in STIP III (Spallation Target Irradiation Program) using the PSI accelerator and target station.

Materials Collaboration at PSI - The materials team at PSI (Switzerland) invited us to assist them in analyzing their irradiation data. One AAA team member spent 3 months analyzing data from the STIP-I irradiation campaign. The work included the counting of activation foils. The activation foils used in STIP-I were composed of Al, Ti, Fe, Ni, Co, Cu, Nb and Au. They were either grouped in stacks in specific locations or, in some cases, distributed along the tube to provide beam-profile information. Of the 101 foils in irradiation, 85 were counted, and of those only 60 were legible/identifiable. As a result, only a few locations could be completely analyzed to refine the knowledge of fluxes in those locations. These locations were the outside locations in rods 1, 2, 3, the center location in tube 4 and the center and outside location of rod 10.

The activities of the radioactive isotopes from the foils were measured and quantified and extrapolated back to time zero (the proton beam shut-off). The saturation activities (and consequently the fluxes) were computed assuming a constant beam current over the length of the irradiation, $4.6633\text{E}+07$ seconds. This means an average delivered beam current of around $525\text{ }\mu\text{A}$.

Neutronics calculations for STIP-I were originally done at PSI using the LAHET Code system. In this work, the model was updated and used in MCNPX. The neutron fluxes in various tubes were calculated to get better thermal flux information. The fluences were tallied at several points along each rod and then folded with dpa, helium and hydrogen cross sections to arrive at the estimated numbers.

In the analysis, the STAYSL2²⁷ package developed at Los Alamos for analysis of the LANSCE/APT irradiations was used. Several additional reactions were available and

²⁷ Computer code analyzing results of activation foil measurements in both a proton and neutron flux

the cross section files were updated to include $\text{Ti} \rightarrow {}^{22}\text{Na}$, $\text{Ti} \rightarrow {}^{46}\text{Sc}$, $\text{Fe} \rightarrow {}^{46}\text{Sc}$, and $\text{Au} \rightarrow \text{Ag}$, $\text{Cu} \rightarrow {}^{46}\text{Sc}$, $\text{Ni} \rightarrow {}^{54}\text{Mn}$, $\text{Nb} \rightarrow {}^{94}\text{Nb}$, $\text{Au} \rightarrow {}^{195}\text{Au}$, although not all of these were useful to the analysis. The adjustments required to the calculated fluxes were not large, and, when folded with the appropriate cross sections for dpa, reveal numbers roughly in agreement with calculations as shown in Table 23. The helium and hydrogen production values were also computed for these locations, but are not given here.

Table 23. Comparison of dpa from Activation Foil Results to Calculations.

Location	Calculated	Final Result
1w	3.12	2.8
2w	2.98	2.8
3w	2.74	3.1
4c	11.66	11.3
10c	5.78	5.0
10w	1.96	2.1

Fig. 38 shows the calculated proton flux and its comparison to the adjusted proton flux from the activation foil information for the center of tube 10. As can be seen, the adjustments made were minor. As shown in Fig. 39, neutron fluxes are approximately the same as calculated at low energies, but above ~ 10 MeV, they are reduced from the calculated values by approximately 50%. The increase in the thermal flux region is inferred on the relative burnup of ${}^{22}\text{Na}$.

Overall, the activation foils gave exposed fluences very close to the calculated numbers. The situation in the SINQ target is very favorable for the calculations, as the rods and target have good alignment with the proton beam, and therefore very little variation in the sample distributions. Aside from small adjustments in proton energy and fluence, and increase in low-energy neutron flux, the agreements were very good in all cases.

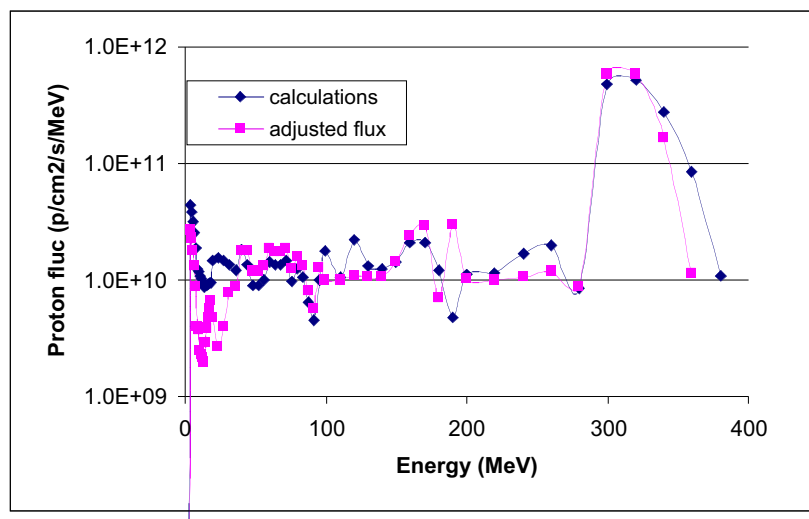


Fig. 38. Proton flux information before and after input from activation foils in center of rod 10.

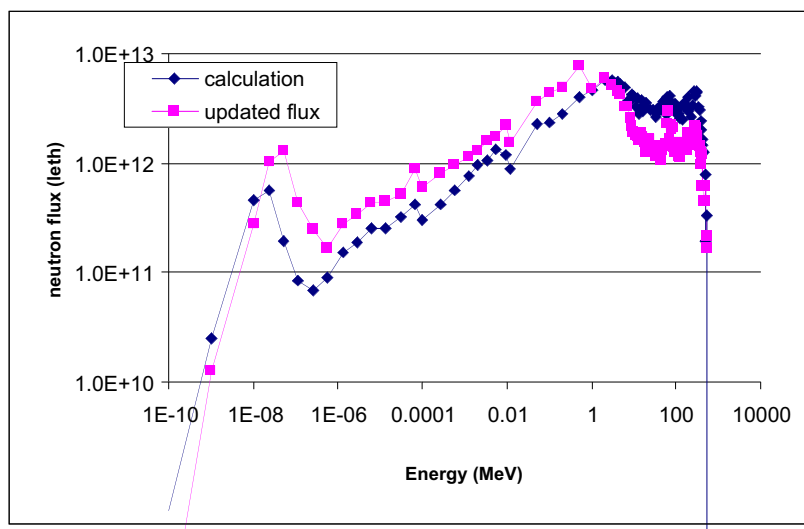


Fig. 39. Neutron spectra shown for center of tube 10 before and after input from activation foils.

LANL Hot Cell Analyses - Tungsten compression samples were sliced from rods irradiated at the LANSCE proton accelerator that were contained in the 18A and decay-heat inserts. Then the ends of specimens were ground parallel. Specimens were tested at room temperature in compression. The compression tests were stopped after deformation to ~20% plastic strain. Results show an increase in yield stress and a decrease in ductility, visible as cracks in the surface of the cylindrical specimens during compression testing (see Figs. 40 and 41). To determine the dose of these specimens, activation foils were sent to LANL TA-48 for counting.

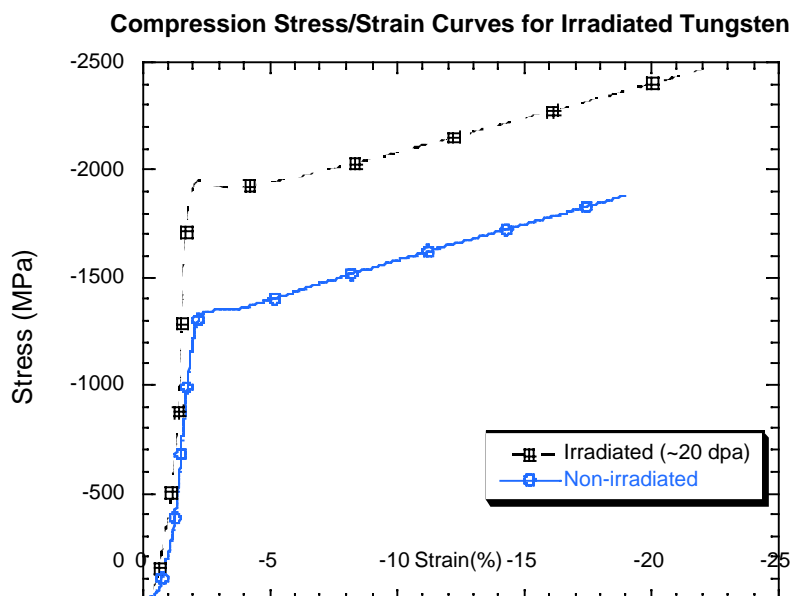


Fig. 40. Stress/Strain curves for tungsten rods tested in compression after irradiation in a proton beam.

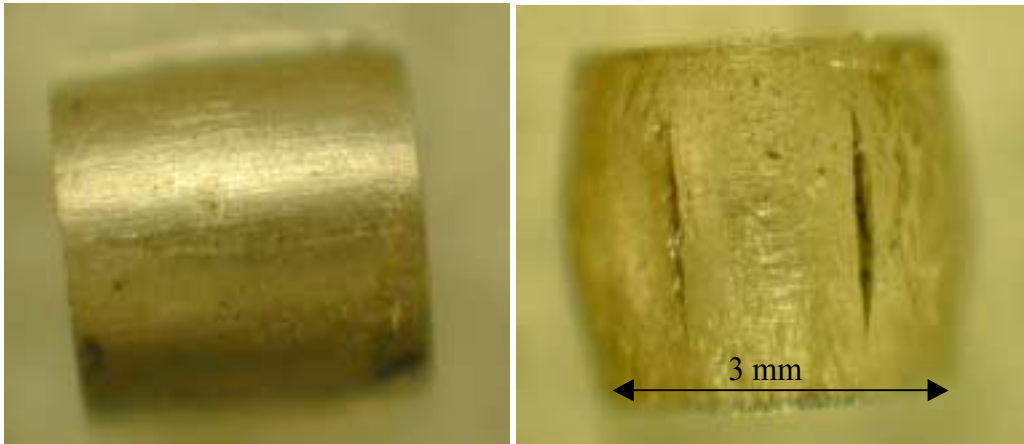


Fig. 41. Optical micrographs of tungsten compression specimens after compression to ~20% strain before irradiation (left) and after irradiation to ~20 dpa.

Slices were also performed on the SS-304L and annealed Alloy-718 cladding. Then, the specimens were mounted in epoxy and polished to a surface finish of 1-micron diamond to prepare them for hardness testing.

Push-out specimens of SS-316L bonded to tungsten and annealed Alloy-718 bonded to tungsten were irradiated to a maximum dose of 1.5 dpa at HFIR in ORNL (see previous section). The specimens were tested in the LANL hot cells. Results show retention of a strong bond after irradiation.

Light Water Corrosion - Work was done to close out the water corrosion Design Data Need (DDN 30). The APT corrosion program made observations that bear on the mechanism of radiation-enhanced corrosion, but not much is known on the specific mechanism. Previously, extrapolation of the corrosion rates measured in the LANSCE high-power beam to the APT production plant was done by correlation with average and instantaneous power densities in the candidate materials. Modifications to extrapolated corrosion rates derived in this way may be necessary because the operable corrosion mechanism may be responsive to other factors present in the APT plant (e.g., the fact that neutrons are more prevalent in the APT production plant than at the LANSCE target area).

Lillard and Daemen (LANL) have correlated increased corrosion rate with cation vacancy concentrations. They have shown that proton irradiation alters the dielectric properties of the passive oxide film which could show up as changes in the oxygen transport properties of the film, and, on this basis, the assumption is made that changes in the oxide are responsible for the observed radiation-enhanced corrosion. There is not a sufficient number of corrosion measurements to implement this idea, that is, to evaluate different weightings of each specific particle type in correlating corrosion rate. Lacking this, the material damage parameter, displacements per atom (dpa) as calculated by Monte Carlo simulation codes, is used to extrapolate corrosion rate under the assumption that changes in the oxide layer are responsible for the radiation-enhanced corrosion. In this way, the corrosion rate of the SS-316L cladding in the 100-mA APT rastered beam is predicted to be 37 $\mu\text{m}/\text{yr}$.

This page left intentionally blank

IV. ENGINEERING DESIGN & DEVELOPMENT

6. APT Engineering Design

Scope

The focus of APT Engineering Design during this phase of the project is twofold. First, we are completing the preliminary design phase to the extent described in the *APT Preliminary Design Plan*. This entails capturing the design in such documents as system design descriptions (SDDs), general arrangement drawings, and piping and instrumentation diagrams (P&IDs), among others, and documenting bases for the design in calculations and technical reports. Release of the *Preliminary Design Status Report*, now in preparation, will formalize completion of the preliminary design phase. Second, we are preparing for close-out of the APT Project, organizing and archiving Project documentation to support an efficient re-start if required.

Highlights

We revised and released the *Facility Design Description*, satisfying a significant Level-2 milestone. The *Safety Requirements Document*, a Level 2 milestone, was also completed on schedule. The *Preliminary Design Status Report*, a Level-1 milestone, is on track for release in September. Four system design descriptions (SDDs), all Level 3 milestones, were revised and released during this quarter.

Preliminary Design Status

Preliminary Design Status Plan - The annual update of the *Preliminary Design Plan* was completed in the previous quarter; however, release of the document was held until the baseline change proposal (BCP) that revised the project scope consistent with the revised plan was approved. Release of the *Preliminary Design Plan* satisfied a Level-3 milestone.

Preliminary Design Status Report - We distributed the first draft of the *Preliminary Design Status Report*, which will reflect the status of APT design at the end of FY01. The report, a Level-1 milestone scheduled for completion the end of FY01, is proceeding on schedule.

APT Archiving - We began archiving hard-copy documentation of the APT Project. To date we have sent seven boxes of archived documents to the LANL Records Center. We estimate approximately 100 boxes are required to capture the entire APT Project documentation.

Target/Blanket Status Review – Preparations for the Target/Blanket Preliminary Design Status, scheduled for August 27-29, is almost complete. The purpose of the review is to provide an update of the status of the design and analyses of the Target/Blanket systems since the last review, and the basis for the SDD revisions this

year. Work remaining to be done to complete preliminary design will be discussed. These meetings will include design authority review of the work.

Top-Level Design Documents

Facility Design Description - We completed revision of the *Facility Design Description* (FDD). The FDD is the top-level document that establishes requirements for the APT plant design. This revision of the FDD satisfies a Level-2 milestone. Significant changes included the following:

- inclusion of a plant-level function-flow block diagram and revision of the top-level functions to be consistent with the diagram;
- rephrasing of some requirements to ensure consistent structure throughout the document;
- update of the *Requirements Allocation Table*, Appendix D, to reflect refinements resulting from SDD reviews;
- elimination of safety requirements duplicating those in the *Safety Requirements Document*; and
- update of the design description section.

Safety Requirements Document - We revised and released the *Safety Requirements Document*, satisfying a Level-2 milestone. The *Safety Requirements Document* formalizes key assumptions made in the APT safety analysis. Revisions to the document were largely in response to comments on safety requirements made during reviews of SDDs.

Environmental Design Requirements Document - We drafted and distributed for review the *Environmental Design Requirements Document* (EDRD). This revision updates the EDRD to assure its currency, remove redundancies with the *Facility Design Description*, and to define APT environmental functions, performance requirements and design requirements associated with preliminary design.

Plant-Level Availability and Maintainability Requirements Document - We revised the *Plant-Level Availability and Maintainability Requirements Document*, satisfying a Level-3 milestone. This revision adds system-level availability allocations and updates requirements to account for design evolution.

System Design Descriptions (SDDs)

Release of updated and revised system design descriptions (SDDs) completes Level 3 milestones for a number of APT systems. For most of these, the task this quarter involved revising Section 1, updating functions and requirements, and developing Section 2, which describes the designs that satisfy the requirements.

SDDs released during the quarter include the Accelerator Tunnel SDD, Target/Blanket SDD, Window Heat Removal SDD, and Primary Coolant Purification SDD. The following SDDs have been revised and distributed for review:

- *Site and Balance of Plant areas*: Demineralizer and Warehouse SDD, Beam Stop SDD, Target/Blanket Module Staging Building SDD,

Accelerator & Facility Maintenance Building SDD, Site Improvement SDD, and Material Handling SDD

- *Accelerator area*: RF Power SDD and High Energy Linac SDD
- *Tritium Separation Facility area*: Glovebox Stripper SDD and Isotope Separation SDD
- *Integrated Control area*: Integrated Control SDD

SDD revision and update work continues in all areas, including such systems as Backup AC Power, Radiation Exposure Protection, Isotope Recovery, Target/Blanket External Shield, and others.

SDD Process - We completed revision of *System Design Description, Preparation, Review, Approval and Release*. This version incorporates improvements to SDD content and to the process used to develop SDDs. We also conducted an SDD workshop at the PPO Oradell office. The workshop presented recent revisions in procedures and addressed areas where difficulties had been identified in previous SDD preparation.

Interface Control

To ensure that interfaces between systems are well-coordinated in the design, interfaces are explicitly captured in interface control documents (ICDs). Eleven interface control documents for the high energy linac were completed and submitted for release. Interface control documents for the electrical distribution equipment layout in the klystron gallery electrical equipment area were also released. These drawings depict physical arrangement of the power distribution equipment serving the accelerator systems and facility loads in the klystron gallery and accelerator tunnel.

Analysis, Calculations, and Modeling

Most of the SDDs are based on analyses that are documented in technical reports and calculation files. During this quarter we performed analyses in areas ranging from calculations of plant availability to modeling of target/blanket hot cell components.

Availability Analyses - In support of the *Plant-Level Availability and Maintainability Requirements Document*, we revised three calculations, the *Accelerator Availability Calculation Report*, *Target/Blanket Availability Calculation Report*, and *Balance of Plant Availability Calculation Report*. These calculations detail availability analyses of the plant segments, and present the basis underlying the duty cycle analysis. Completion of this documentation satisfies a Level-4 milestone.

Coupling Cavities - We released two reports on the inter-segment coupling cavities in the CCL. The reports describe analyses of coupling cells that resonantly connect segments near the beginning and near the end of the CCL. We also released a similar technical report on the inter-segment coupling cavities for the CCDTL.

Cryogenics System Transfer Line - We completed the technical report on the cryogenics system transfer line. This report presents the preliminary analysis to

determine the primary mechanical and thermodynamic characteristics of the of the transfer line.

Low Level RF - The *APT Low Level Radio Frequency System Report* was released.

Window Thermal and Module Stresses Analyses - The retractable window assembly thermal analysis calculation file has been released. We also performed a re-evaluation of the window module stresses with respect to the new Alloy-718 precipitation-hardened allowable stresses. The analysis shows that the allowable stresses are met in the critical window panel, i.e., in the footprint of the beam, using precipitation-hardened Inconel-718. More refined models are necessary to obtain accurate stresses at the intersection of the panel and the window manifold structure. The Window Heat Removal System calculation file was updated to include the stress calculations and was released.

Electrical Power Modeling - In modeling work on the electrical power system, we evaluated the cryogenic section of substation 3-D power distribution for overall optimization of electrical equipment quantities and sizes. The current design includes two 13.8-kV feeders that feed four 13.8-kV/4.16-kV transformers and four 4.16-kV/480-V transformers. We examined the elimination of 13.8-kV conversion, with transformation of the 230 kV directly to the 4.16-kV level, as the cryogenic system does not have any loads that required 13.8-kV power. Preliminary results indicate that this distribution scheme is acceptable. This approach may result in cost reduction.

Energy Use Estimate - We issued the calculation *Energy Usage Estimate for Plant Lighting System (B16)*. This calculation estimates annual electrical energy use by the plant lighting system and associated operating costs.

Waste System Design Alternatives - The Liquid Radioactive Waste System design alternatives study was released.

Equipment and Line Sizing Calculations - We completed the equipment and line sizing calculation for the target/blanket storage pool cooling and purification subsystem. It demonstrated that the cooling and purification functions could be combined into a single subsystem. The pool cooling and purification process flow diagram has been updated. We also released equipment and line sizing calculations for the heavy water recycle subsystem, light water radioactive subsystem, and regulated floor drain-target/blanket building subsystem. These calculations were revised to reflect the Liquid Radioactive Waste System design alternatives study and included updated pump and interface information.

Hot Cell Model - As part of the development of the 3-D electronic model of the target/blanket hot cell, we have developed models of the target/blanket modules that will be moved into the hot cell and the in-cell manipulator.

APT Geotechnical Report - We held a videoconference to resolve comments of the independent review committee on the *APT Geotechnical Report*. The conference included members from each APT organization.

Design Changes

Accelerator Design Change - The design change request, APT-DCR-0037, which relocates the coupled cavity drift-tube linac (CCDTL) and coupled cavity linac (CCL) resonance control cooling system pumping skids outside the tunnel and along the berm, has been approved. Another design change request, APT-DCR-041, to reconfigure the low energy linac into smaller modules, was distributed for review.

Design Drawings

- **Cryogenics** - Nine piping and instrumentation diagrams (P&IDs) for the cryogenics system were completed along with eight subassembly drawings for the transfer line.
- **RF Power** - The RF power assembly and subassembly drawings for the klystron gallery and accelerator tunnel were released. These drawings are for the RF systems that feed both the low energy linac and high energy linac.
- **Power Supply** - Two equipment arrangement drawings were released for information. These drawings show the layout and arrangement of equipment for the DC and Uninterruptible Power Supply (UPS) Safety-Significant System and the DC and UPS Safety-Class System. We also released the high-voltage and medium-voltage ac power system relay and metering diagrams. These show typical relay and metering details for the primary substation 230-kV feeder and transformer, the 13.8-kV/4.16-kV switchgear feeder, and transformers. The Backup AC Power System single line diagrams were submitted for release. These drawings were updated to include the 480-Vac safety-significant HVAC exhaust fan loads, the results of diesel generator sizing calculations, and cable and equipment protection for the diesel generator switchgear. We distributed for review a key single-line diagram drawing of the ac power distribution plan, based on the 1.5-kg/year nominal production capacity design. The distribution scheme depicts power flow from 230-kV ac main power source to 480-V ac distribution.
- **Building General Arrangements** - The general arrangement drawings for the target/blanket building, klystron gallery, klystron gallery mezzanine, and TSF building were released.
- **HVAC** - We distributed for review P&IDs and process flow diagrams for the Target/Blanket Building Heat Removal System, Target/Blanket Building HVAC Air Supply and Exhaust System, Injector Building, Accelerator Level, Accelerator Tunnel HVAC, Klystron Gallery HVAC, Target/Blanket Building HVAC Shutdown, and Electrical and Battery Rooms.
- **Mechanical Service Building** - We released for information the five mechanical service building layouts, which support the site plan layout.
- **Instrument Location** - We released the drawing *Typical Instrument Locations for Instruments in High Radiation Areas*.
- **Hot Cell** - The target/blanket hot-cell general arrangement drawings were approved for release for information.

- **Storage Pool** - The storage pool equipment layout drawings were approved for release for information, as were the process flow diagrams for the Storage Pool Cooling and Purification Subsystem. We completed the equipment and line sizing calculation for the target/blanket storage pool cooling and purification subsystem, which demonstrated that the cooling and purification functions could be combined into a single subsystem. The pool cooling and purification process flow diagram has been updated.
- **Zone maps** - We distributed updated versions of the target/blanket building radiation zone maps.
- **Liquid Waste** - We resolved all reviewer comments and are preparing for approval the Heavy Water Recycle and the Regulated Floor Drain P&IDs. These drawings incorporate recommendations from the Liquid Radioactive Waste System design alternatives study to process flow diagrams and revisions to the equipment and line sizing calculations.
- **Gaseous Waste** - The process flow diagrams for the Gaseous Radioactive Waste System were approved for release for information.
- **Site Overall Plot Plan** - We revised the *Site Overall Plot Plan*, moving the cryogenic building and mechanical service building, resolving the accelerator tunnel centerline dimensions, and making other facility changes. The revised drawing was reviewed and released. We also completed revisions to the site grading drawings to reflect some of the facility adjustments.
- **Accelerator Maintenance Plant** - We completed the accelerator maintenance plant layout floor plan and released the drawing for information.
- **Target/Blanket Building** - The target/blanket building architectural drawings were rotated to conform with the site orientation and were upgraded, with minor interior changes, to become the backgrounds for the general arrangement drawings.
- **Operations Building, Target/Blanket Module Building, Target/Blanket Building, and Klystron Gallery** - We released floor plans for the operations/access building and developed the target/blanket module building floor plan. We also developed architectural sections and elevations for the operations/access buildings and distributed them for review. The target/blanket building and the klystron gallery floor plans were updated for use as backgrounds for general arrangement drawings.

7. Accelerator-Driven Test Facility (ADTF)

Scope

The scope of work covering the pre-conceptual and conceptual design activities for the Accelerator-Driven Test Facility (ADTF) is as follows:

- **Design** - The design covers both the pre-conceptual and conceptual phases of the ADTF project and will include the Target and Material Test (TMT) Station, the Subcritical Multiplier (SCM), the accelerator, and the balance of

facility (BOF) segments. The pre-conceptual design will support a Critical Decision 0 for the Project, "Approval of Mission Need," which is scheduled at the end of the second quarter FY01. The conceptual design will commence thereafter and will continue throughout the remainder of FY01, ultimately leading to Critical Decision 1 (Approval of Preliminary Baseline Range) at the end of FY02.

- **Systems Integration** - Integration activities include:
 - the development of the functional and performance requirements for the ADTF project
 - the definition and control of the design interfaces between the major facility segments
 - the coordination of internal and external design reviews
 - technical risk assessment
 - cost estimating
- **Project Management** - Project Management activities include:
 - definition and control of work scope
 - budget allocation and management
 - preparation and maintenance of integrated project schedules
 - issuance of periodic technical and management progress reports

Highlights

Systems Integration

- The Critical Decision-0 (CD-0) package was submitted to DOE headquarters on March 23, 2001. The material was distributed and used to brief most DOE office directors in preparation for the formal ESAAB²⁸ review, which will not be scheduled until after the FY02 budget congressional appropriation action.
- The revision of the Accelerator-Driven Test Facility (ADTF) Missions, Functions, and Requirements document was completed, incorporating comments received earlier from the External Review Panel. A final updated draft has been issued for final acceptance review.
- Design review meetings were held with the French *Commissariat à l'Energie Atomique* (CEA) in June to discuss collaborative efforts on the project. In preparation for these meetings, the project issued the summary design report of the ADTF pre-conceptual design²⁹.

Target Multiplier Test Station (TMT)

- Thermal-hydraulic studies were performed to evaluate different cooling geometries of the lead-bismuth eutectic (LBE) and sodium-cooled tungsten targets with the objective of optimizing the maximum allowable current density and neutronics performance in the target design.

²⁸ Energy System Acquisition Advisory Board (DOE)

²⁹ TPO-E00-G-CDR-X-00101, Revision 0, May 2001

- Scoping studies were completed to determine the heat transport model that will most effectively accommodate the TMT mission of testing various target technologies. A secondary loop using helium as the coolant has been selected as being the most compatible with all of the envisioned primary coolants and target technologies.

Subcritical Multiplier (SCM)

- A preliminary assessment of the four options being considered for the SCM design (vertical and inclined beam entry, inner vessel, and redan) has been completed. A basic design will be selected for the conceptual design phase.
- A layout for an SCM design with a solid tungsten target and inclined entry was developed.
- Calculations were completed for the shielding requirements to ensure the grid plate design lifetime in the SCM.
- In target designs, the following was completed:
 - A preliminary design of a lead-bismuth target was prepared for both a vertical and an inclined beam entry. MCNPX physics models have been developed and used in the analysis of the performance of the target-multiplier coupling, the estimation of the buffer size, and in calculations of radiation damage. Thermal-hydraulics analysis of the target has been initiated.
 - A preliminary design of a solid tungsten target for inclined entry was prepared. MCNPX physics models have been developed and used in the analysis of the performance of the target-multiplier coupling, the estimation of the buffer size, and in calculations of radiation damage.
- A strategy for return to power after beam interruptions has been developed in order to minimize thermal fatigue in the SCM components.

7.1 Systems Integration

Overall Facility Design and Arrangement

The ADTF is now configured as a multiple station facility. The baseline project scope will include construction of two target stations:

- **Target and Material Test Station (TMT)** – This station will provide a test environment for materials and fuel experiments and the evaluation of alternate coolant and target technologies. The design basis will also include the potential to demonstrate tritium production, as well as the potential for isotope production.
- **Subcritical Multiplier (SCM) -100 MW** – This will provide a test environment for the demonstration of coupled operation of the accelerator, target, and multiplier. Its design basis will have the capability to irradiate significant quantities of fuel with the eventual transition to an actinide core.

A third target station, an international user facility, would be constructed at a later date. A schematic arrangement of the ADTF is shown in the Fig. 42.

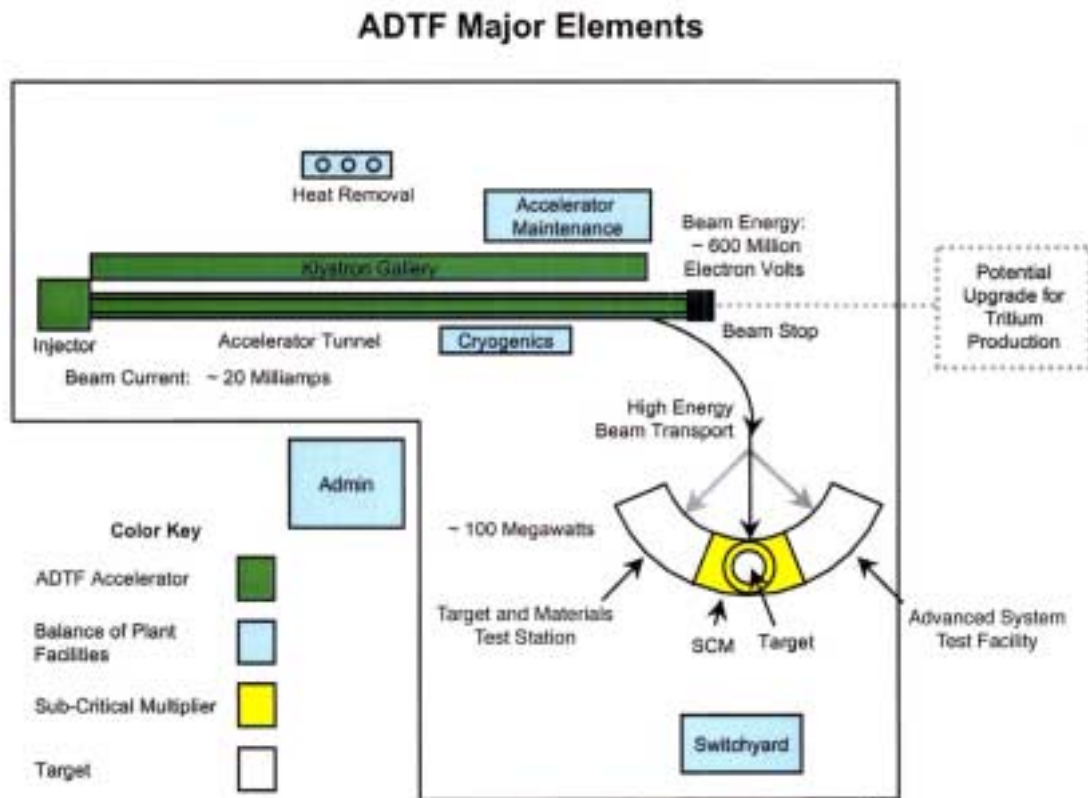


Fig. 42. Schematic of the Accelerator Driven Test Facility (ADTF)

ADTF Missions, Functions, and Requirements

The Missions, Functions, and Requirements for the ADTF have been updated and revised as follows:

- Design segments have been established for both the TMT and SCM stations. The applicable functions and requirements have been allocated to each station consistent with the overall facility mission.
- Some of the high-level mission requirements for the ADTF are related to providing the capability for future plant upgrades to meet alternate production missions (e.g., tritium production). These types of mission requirements are allocated to the design of systems, structures, and components in the form of guidance to the designers to avoid selection of designs that would preclude a future upgrade.
- Revisions to the requirements were incorporated to address the Omberg panel review held last February.
- The document was distributed for final acceptance review with issuance of the approved revision scheduled for July.

Critical Decision - 0 (CD-0) Package

The efforts of the ADTF pre-conceptual design concluded with the issuance of the CD-0 package in March. This report will serve as the basis for the Justification of Mission Need for the ADTF project and the authorization to begin conceptual design. The CD-0 package provides a summary of the cost, schedule, and technical baselines at the pre-conceptual stage, but more importantly, provides the rationale for the facility missions. The report has been distributed to the various department heads at DOE headquarters in preparation for the ESAAB review and approval process.

Cost Estimate

A significant effort is underway to further develop the construction cost estimates for the TMT and SCM stations. The pre-conceptual cost estimate was based on a historical parametric, with APT as the basis. With the further advancement of the multiple station design concept, engineering data (in the form of system and equipment lists) are being generated to provide the basis for an improved pre-conceptual cost estimate. The estimating model, based on the proposed AAA Work Breakdown Structure (WBS), has been developed.

7.2 ADTF Target and Material Test (TMT) Station

Target and Material Test (TMT) Station Design

The target and materials test station (TMT) is being designed with the objective of performing tests on spallation targets, dedicated or advanced fuels, and target/blanket materials. At present, the design studies are concentrating on developing an efficient spallation target where the neutron flux in the test loops adjacent to the target is maximized. Also, the maximum current density sustainable by various target options is being evaluated. The spallation target technologies of interest are lead-bismuth eutectic (LBE), sodium-cooled tungsten, and helium-cooled tungsten. Pre-conceptual design studies are being performed for these different options.

The concepts described for the modular design in the pre-conceptual design report are being used in the current TMT engineering layout. A generic target concept is illustrated in Fig. 43, where the target consists of a number of parallel tubes connecting a lower and upper plenum. This concept is primarily developed for an LBE target where the LBE flows from the lower plenum to the upper plenum through a series of parallel tubes. However, the same concept can be used for the sodium cooled or helium cooled tungsten target as well. For the solid target option, the tubes would house concentric tungsten cylinders with the coolant flowing in the gaps (see Fig. 44). It is also conceivable that the tubes may be used to contain a packed-bed of tungsten spheres for the helium-cooled target option.

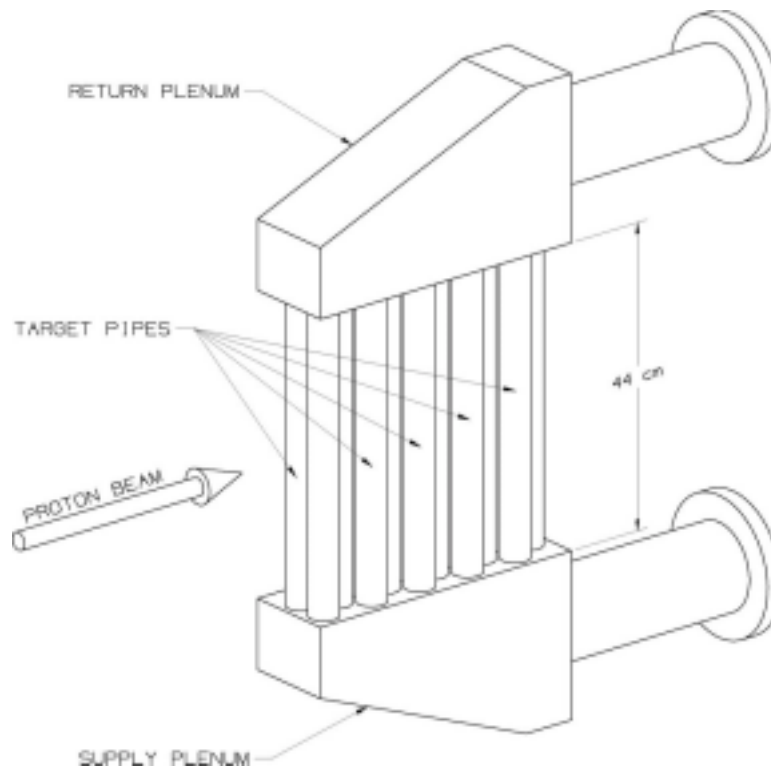


Fig. 43. Conceptual target layout.



Fig. 44. Solid target concept with concentric cylinders

LBE Target Design

For the LBE target, one of the options we considered was to replace the parallel flow tube arrangement shown in Fig. 43 with a double-pass flow (see Fig. 45) where the supply and return manifolds are both located above the target. This configuration (referred to as the concentric flow case), in contrast with the parallel flow case, is

illustrated in Fig. 45. The concentric flow case was investigated with the expectation that it might be able to accommodate a higher current density while reducing the thermal-stresses on the tubes. The maximum allowable beam-current density as a function of tube diameter is illustrated in Fig. 46, where, as can be seen, at tube diameters less than 6 cm, the parallel flow configuration sustains a higher current density. In these calculations, the maximum LBE velocity is set to 2 m/s. The inlet LBE temperature is 200°C. The peak surface temperature (in contact with LBE) is set at a limit of 550°C because of corrosion control concerns. For the concentric flow case, this limit also is applied to the LBE exit temperature (which becomes limiting when the LBE exit temperature is greater than the peak wall temperature on the tubes).

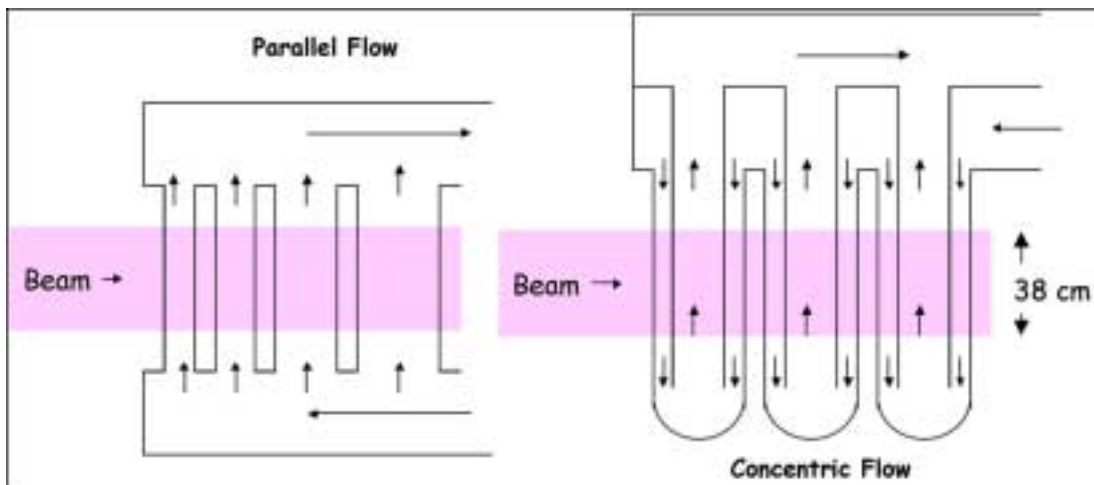


Fig. 45. Parallel versus concentric flow configurations for the LBE target.

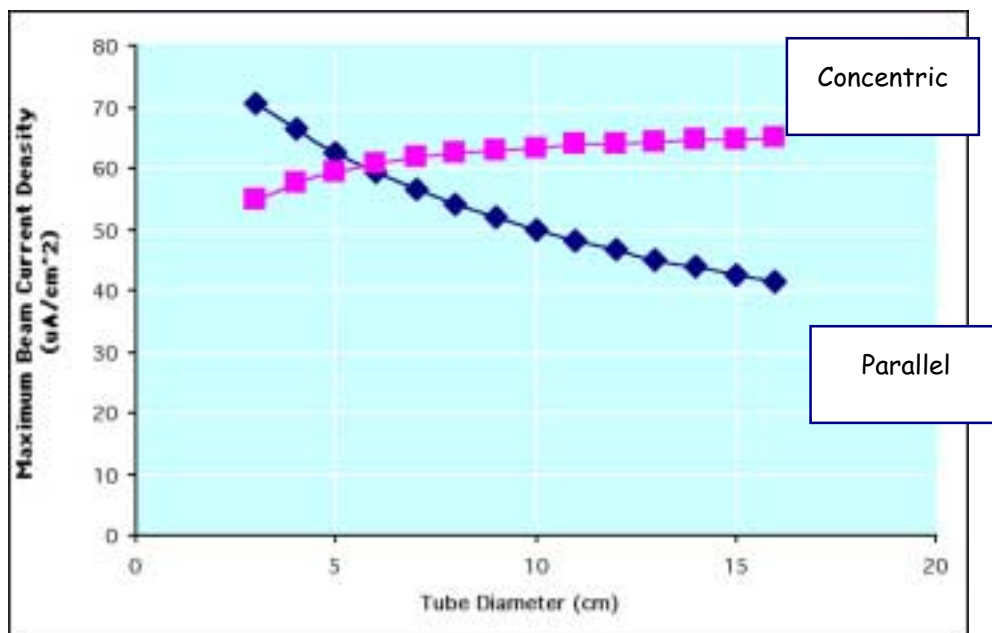


Fig. 46. Maximum allowable current density as a function of tube diameter.

A neutronics assessment was made to investigate the effect of variable-size parallel tubes vs a uniform size set of tubes, which indicated that the impact is minimal on the fast and thermal neutron fluxes in the test locations on either side of the target. Thus, uniform tube sizes with small diameter (<5 cm) are used in subsequent assessments.

We have also investigated the sensitivity of the maximum allowable current density to LBE velocity in the tubes. These calculations are done assuming an HT-9 tube with 1-mm wall thickness and 4.3 cm in diameter. The inlet temperature is 200°C and the surface temperature (in contact with LBE) is limited to 550°C. At 2 m/s, which is the current baseline, the maximum allowable current density is $\sim 66 \text{ mA/cm}^2$. If the velocity limit can be increased to 3 m/s, the beam spot size can be reduced, resulting in a maximum allowable current density of $\sim 86 \text{ mA/cm}^2$.

The power density in and around the target region is shown in Fig. 47 with a logarithmic-scale. As shown, the power density drops considerably outside the target region. Within the target region, there is considerable variation in the power densities even within a given tube. Thus, the thermal stress problem needs to be addressed in designing such a target.

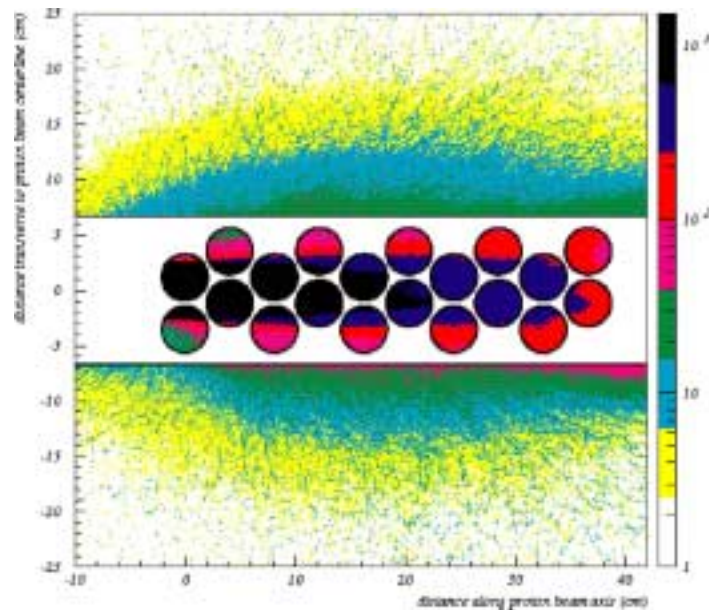


Fig. 47. Power density map (color scale is in W/cc)

The minimum LBE velocity needed to cool the different tubes is also calculated. The results show that the front tubes require a velocity of 2 m/s whereas the back tubes can be cooled using LBE velocities less than 0.5 m/s. If the flow distribution is tailored to power distribution using orifices, the average LBE exit velocity is 320°C.

The thermal and fast neutron fluxes achieved in the experimental regions using the LBE target are shown in Figs. 48 and 49, respectively. The thermal spectrum is defined by neutron energies less than 0.625 eV, whereas the fast spectrum is defined by neutron energies greater than 0.1 MeV. In these simulations, a beryllium reflector is used on one side of the target to achieve the thermal spectrum. The flux averaged over a 4-L volume on the thermal side is $3.6 \times 10^{14} \text{ n/cm}^2\text{-s}$. On the fast side, the flux averaged over a 2-L volume is $7.3 \times 10^{14} \text{ n/cm}^2\text{-s}$.

Currently, we have not done detailed radiological damage assessment in terms of displacement per atom (dpa), and helium and hydrogen production. However, preliminary assessment shows that the target sustaining 66 mA/cm² would result in ~9 dpa/month.

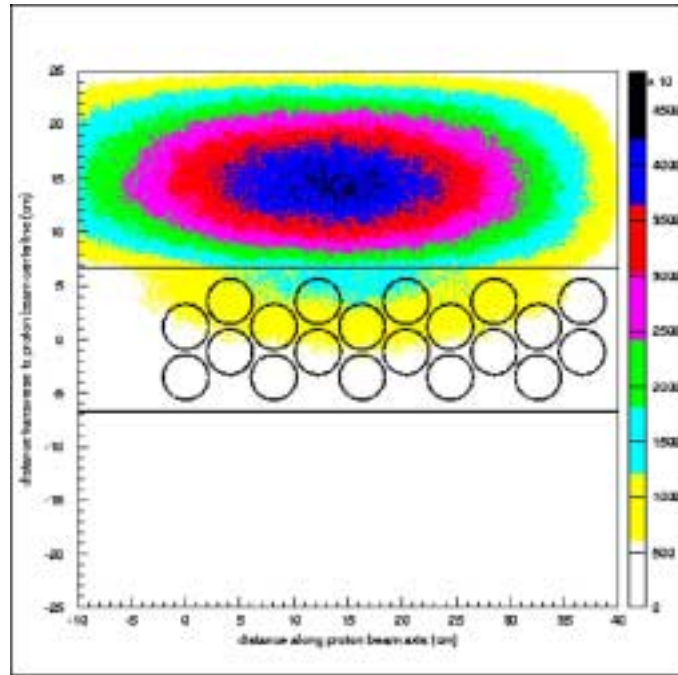


Fig. 48. Thermal-spectrum flux map (color scale in neutrons/cm²-s).

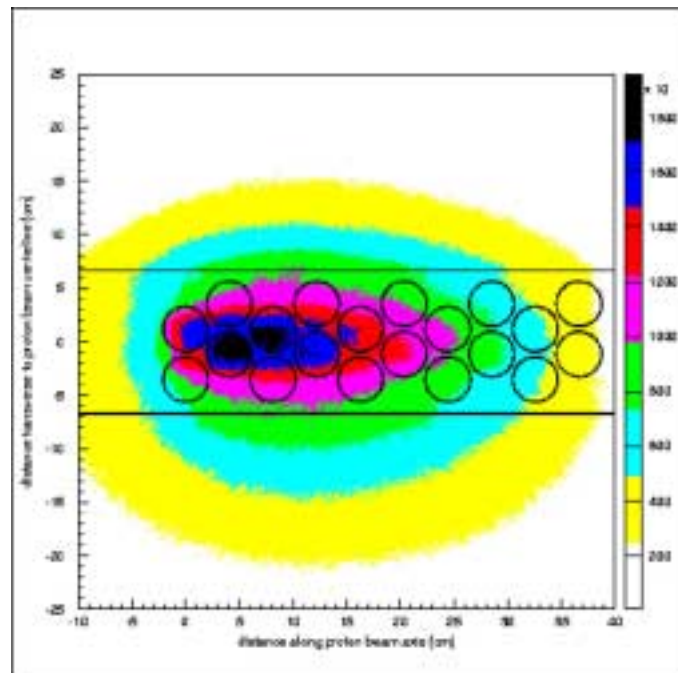


Fig. 49. Fast-spectrum flux map (color scale in neutrons/cm²-s).

Sodium-Cooled Tungsten Target Design

A series of calculations were done to assess the performance of a sodium-cooled tungsten target. The geometry is similar to the one shown in Fig. 43; however, the coolant flow is through a series of parallel tubes containing concentric tungsten cylinders (Fig. 44). Thermal-hydraulic analyses for cases were performed to investigate the maximum allowable current density. In all cases, a beam height (heated length) of 38 cm was used. The maximum temperature for the clad on the tungsten cylinders is limited to 600°C. The tube wall thickness is 0.9 mm and the clad thickness 0.125 mm. The sodium flow velocity in the gap between the tungsten cylinders, the tungsten volume fraction (by varying the thickness of tungsten cylinders), the gap size (flow gap between the cylinders), and the tube size, were varied for the four cases investigated. As shown in Table 24, a sodium-cooled tungsten target may reach a performance (in terms of allowable current density) similar to LBE target performance using a very tight thermal-hydraulic design. To get there, the sodium velocity must be increased to 5 m/s or higher through narrow gaps (1 mm or less).

Table 24. Summary of Sodium-Cooled Tungsten Target Studies.

Parameter / Case	1	2	3	4
Velocity (m/s)	4	5	4	4
Tungsten Fraction (%)	58.4	58.4	63.7	59.3
Channel gap (mm)	1	1	1	1.25
Tube Diameter (mm)	40	40	43	49
Current density (mA/cm ²)	53.0	65.2	43.0	52.3

Using the same current density as for the LBE target, a neutronics simulation of the sodium-cooled tungsten target was performed. The resulting total-, fast- and thermal-fluxes are given in Table 25. The fluxes are averaged over a 4-L volume for the thermal side and over a 2-L volume on the fast side. As shown in Table 25, the neutronics performance of a sodium-cooled tungsten target would be comparable to an LBE target if the same current densities can be sustained in both targets.

Table 25. Neutronics Performance of the Sodium-Cooled Tungsten Target

	Thermal Side Fluxes (n/cm ² -s)		Fast Side Fluxes (n/cm ² -s)	
	Thermal Flux	Total Flux	Fast Flux	Total Flux
Lead-Bismuth Eutectic (LBE)	3.6×10^{14}	1.1×10^{15}	7.3×10^{14}	9.7×10^{14}
Sodium-Cooled Tungsten	3.0×10^{14}	1.0×10^{15}	7.3×10^{14}	9.8×10^{14}

Helium-Cooled Tungsten Target Design

A series of assessments for a helium-cooled tungsten target were also performed. First, a concentric tungsten-cylinder geometry (shown in Fig. 44) is used and the results are summarized below. The initial assessment for the helium-cooled tungsten packed-bed target also is summarized.

Helium Cooled Tungsten Cylinders - The maximum current density sustainable by a helium-cooled tungsten cylinder target is assessed for more than a dozen cases.

Only a limited number of cases are summarized in Table 26 to illustrate the results. Four cases showing the results of two different helium pressures (inlet) and helium velocities (through the annular gaps) are listed. For all these cases, many of the parameters were kept constant and are listed in Table 26. Current densities slightly higher than what is shown in Table 26 are achievable if cladding the tungsten is not necessary and the temperature limit of 600°C is applied to the tube wall. As shown, very high pressure and velocity are needed to approach the performance of a liquid-metal-cooled target. Currently, no neutronics assessment of this concept has been performed.

Table 26. Summary of Helium-Cooled Tungsten Target Studies (Concentric Cylinders)

Parameter / Case	1	2	3	4
Velocity (m/s)	100	300	100	300
Pressure (bar)	40	40	68	68
Current density (mA/cm ²)	9.6	25.8	15.4	41.2
Constants:				
beam height, heated length	38 cm			
max cladding temperature	600°C			
inlet helium temperature	200°C			
tube wall thickness	0.9 mm			
clad thickness	0.125 mm			
tungsten volume fraction	58.4%			
coolant gap	1 mm			
tube diameter	40 mm			

Helium-Cooled Tungsten Packed Bed - The analyzed geometry of the packed bed consists of a 4.3-cm tube filled with tungsten particles (spheres) of variable diameter. The beam height (heated length is 38 cm) and the height of the packed-bed is 44 cm. The tube wall thickness is 1 mm. The helium inlet temperature is 200°C. For the cases where cladding is assumed on the tungsten spheres, the clad thickness is 0.125 mm. The peak temperature either on the tungsten cladding or the tube wall is limited to 600°C. Calculations were done varying the helium inlet pressure, helium flow rate (quantified through fractional pressure drop), and tungsten sphere diameter. The results for the 40 bar and 68 bar helium pressure cases are shown in Figs. 50 and 51, respectively. As shown, for these cases, 15-20 mA/cm² is achievable if a high inlet pressure along with a high-pressure drop (~30 bar) can be justified. If cladding the tungsten is not necessary, the performance improves slightly as shown in Fig. 52, and the sphere diameter has a strong influence on the performance. At large sphere diameters (~15 mm), current densities of 30 mA/cm² may be achievable with high-pressure drop (30 bars!).

Heat Removal System Design

One of the functions of the TMT is to test various target technologies, which may employ one of the coolants discussed above. It is desirable to keep the secondary loop of the heat removal system fixed, independent of the coolant used in the primary system. One coolant that is compatible with all the options being considered is helium. Thus, we envision using helium as the coolant in the secondary loop.

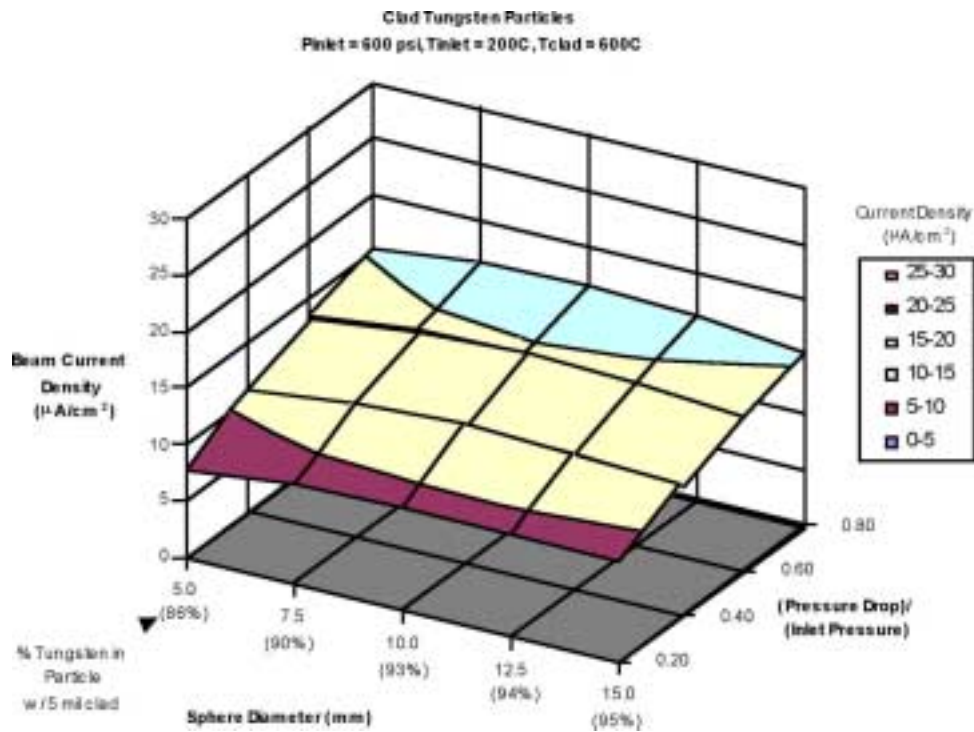


Fig. 50. Helium-Cooled Tungsten packed bed with 40-bar inlet pressure.

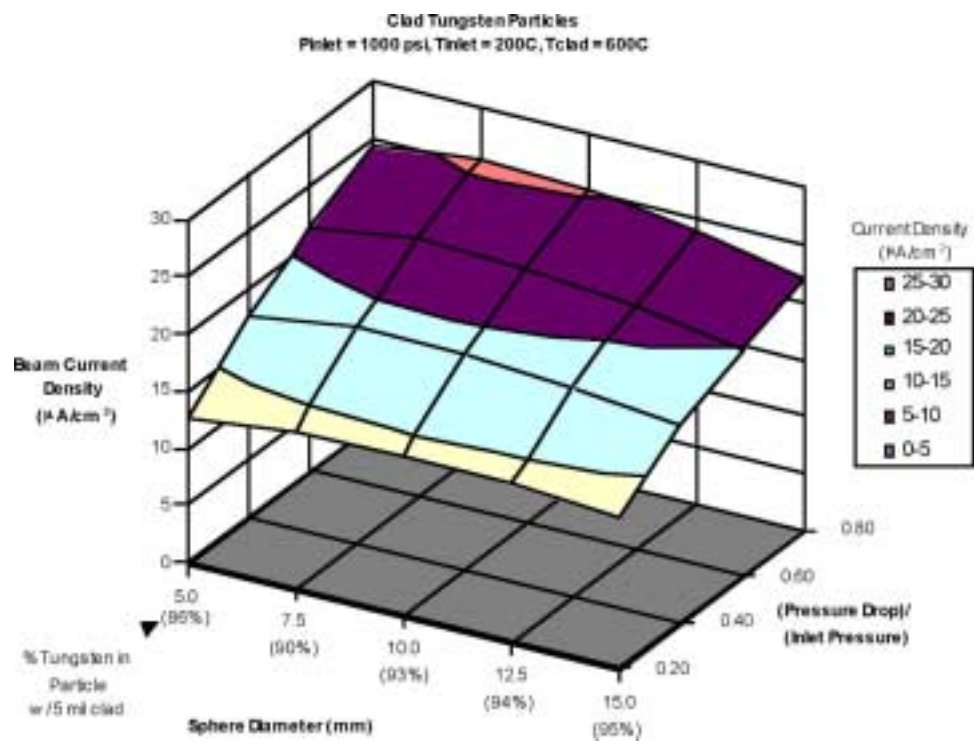


Fig. 51. Helium-Cooled Tungsten packed bed with 60-bar inlet pressure.

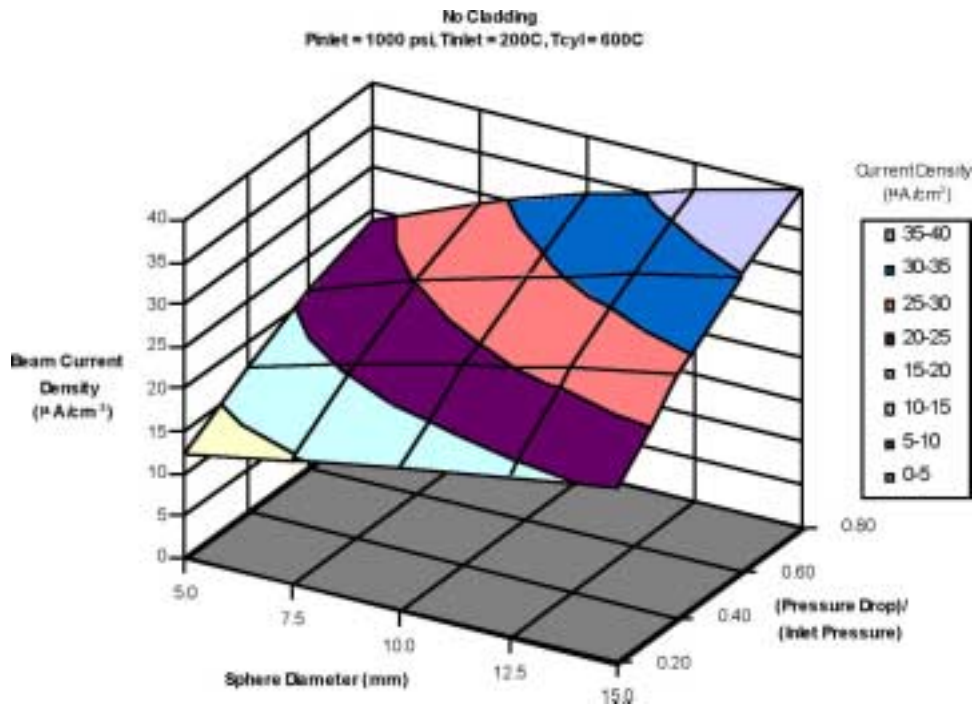


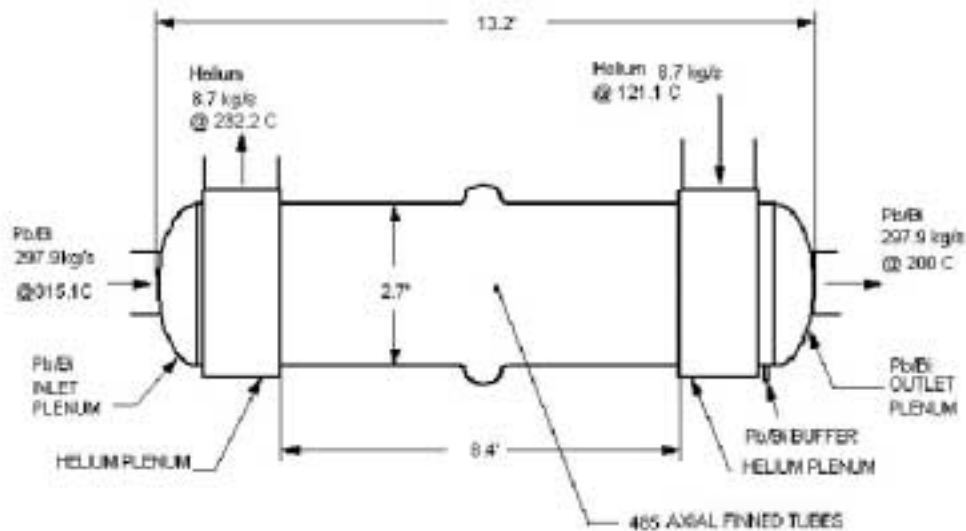
Fig. 52. Helium-Cooled Tungsten packed bed with 60-bar inlet pressure and no cladding.

There are two concerns with the helium secondary loop: (1) the size and weight of the heat exchangers, and (2) the potential for blowing the liquid metal out of the target by high pressure helium in case of a heat-exchanger tube break. To circumvent the second issue, it is currently envisioned that a stagnant liquid metal jacket would be used around the heat exchanger tubes for the liquid-metal cooled systems.

We have also done one sizing study for an LBE-to-helium heat exchanger, assuming a stagnant LBE jacket around the heat exchanger tubes. In this study, the LBE velocity in the heat exchanger tubes is limited to 0.7 m/s. Helium pressure is set to 20 bars. The lead-bismuth enters the heat exchanger at 315°C and exits at 200°C. The thermal-load is 5 MW (corresponding to 8 MW of beam power). The resulting heat exchanger is illustrated in Fig. 53, which shows that such a heat exchanger will be approximately 0.8 m in diameter and 4 m in length. Similar studies for sodium-to-helium and helium-to-helium heat exchanger are in progress.

7.3 ADF Subcritical Multiplier - 100 MW (SCM-100) Design

The pre-conceptual design activities for the sodium-cooled pool-type subcritical multiplier (SCM) have continued during the quarter in several major areas. The overall facility design has progressed, in preparation of the conceptual design phase which will start after the approval of CD-0. The major design options pursued during the pre-conceptual design phase (different geometries for the beam insertion, consideration of an inner reactor vessel in the sodium pool or use of a redan design) have been studied further with the aim of selecting the base design for the conceptual design phase. The target design for the SCM has started and physics models have been developed to analyze the coupling between the spallation source and the multiplier region. Two target designs are being pursued, namely a liquid lead-bismuth



5.02 MW(t) Pb/Bi TO HELIUM HEAT EXCHANGER

MAXIMUM Pb/Bi VELOCITY: 0.7 m/s 15% MARGIN

Fig. 53. Example of an LBE-to-helium heat exchanger with an intermediate LBE jacket.

(LBE) target and a solid tungsten target. For both materials, designs for different beam insertion geometries are being developed.

Work also continued on the analysis of thermal stresses induced by beam interruptions. Frequent and severe thermal cycling induces thermal fatigue that limits the life of SCM structures and components. Design options for SCM systems and components to minimize the thermal stresses have been studied. Strategies for returning to full power after a beam interruption have been developed to minimize the thermal-cycling impact.

Several coordinated activities have also been initiated during the quarter. Coordination meetings have been held with the other ADF design teams in order to establish the interface requirements between the TMT and the SCM and to support the design of common facilities such as hot cells. An initial safety meeting was held to establish the safety team and to determine the safety work required for the CD-1 and CD-2 design stages. The first working meeting with the CEA also took place. The main areas of collaboration were discussed and the specific contributions of CEA to the design and the joint areas of work were identified.

Support for the development of the Environmental Impact Statement (EIS) and the experimental plan also continued during the quarter. Flow diagrams for the mass flows in the fuel-conditioning and fuel-examination facilities have been developed. The mass flows have included activities related to the development of ATW fuel expected to be accomplished in the ADF. Estimates of the core inventories in the SCM have been supported with physics calculations.

Sodium-Cooled Fast-Spectrum SCM Design

The possibility of a horizontal entry of the beam transport tube into the SCM has been thoroughly evaluated and documented. The conclusion is that the engineering problems of a horizontal entry into the sodium pool make the vertical or inclined entries clearly preferable. The report analyzes five concepts that allow for replacement of the beam tube as being representative of the problems associated with breaking and re-making the beam tube connection with the SCM primary Na tank, which is qualified and certified to Section III of the ASME Boiler and Pressure Vessel Code. All solutions were felt to involve replacement procedures that were too complicated and to not have the requisite reliability both to assure replacement under all conceivable conditions, and re-certification to Section III standards, without an extensive test and qualification program using large-scale facilities.

Two options for the beam entry into the primary tank of the sodium-cooled pool-type subcritical multiplier are still under consideration. The first option is a vertical, top-entry of the beam transport tube, and the alternative option is an inclined ($\sim 32^\circ$) entry, but through the tank cover, thus maintaining the primary tank without side penetrations. Two options for the internal pool design have also been further developed. One option involves an internal reactor vessel in a nearly isothermal sodium pool, and the other a vertical redan to separate the hot Na exiting the multiplier and the cool Na exiting the heat exchanger (see Fig. 54 for inclined entry).

A preliminary evaluation was completed of the four (4) SCM concepts under consideration (both vertical and inclined entry for both redan and internal vessel configurations). The conclusion is that the vertical-entry, internal-vessel concept is best suited for implementation as the SCM in the ADTF. The reasons for this conclusion are manifold and will be documented in a report to be issued when the final decision is made. The preliminary conclusion is that, for the inclined entry, the complexity of the thermal expansion of the tube and of the thermal-hydraulics and neutronics of the multiplier appear to be more difficult problems to solve than the placement of equipment around the vertical-entry beam tube. Moreover, the use of an internal vessel allows use of more features proven in EBR-II than does the redan. Although this decision is still only tentative, most SCM upcoming design work will concentrate on improving the definition of the vertical-entry concept.

Progress has also been made on laying out the fuel- and target-handling strategies for all four SCM concepts under consideration. An in-tank storage basket for multiplier fuel instead of peripheral grid locations has been selected. This will allow for restricted fuel handling, i.e., transfer of fuel in and out of the tank during power operation of the accelerator and SCM. Restricted fuel handling appears to be necessary to reduce the duration of fuel-handling outages to acceptable lengths and keep system availability high.

Discussions with the accelerator design team led to the conclusion that incorporation of the requisite bending, focusing, rastering and spreading magnets, and vacuum equipment can be accommodated with the horizontal beam tube no more than 10 m above the operating floor. It was also concluded that the backshine shield could be located at the tank cover (i.e., that the cover would comprise part of the backshine shield) and that ~ 2 m of space directly above the cover could be kept free of accelerator components and available for placement of SCM-related hardware. This information was factored into the tentative decision in favor of vertical entry noted

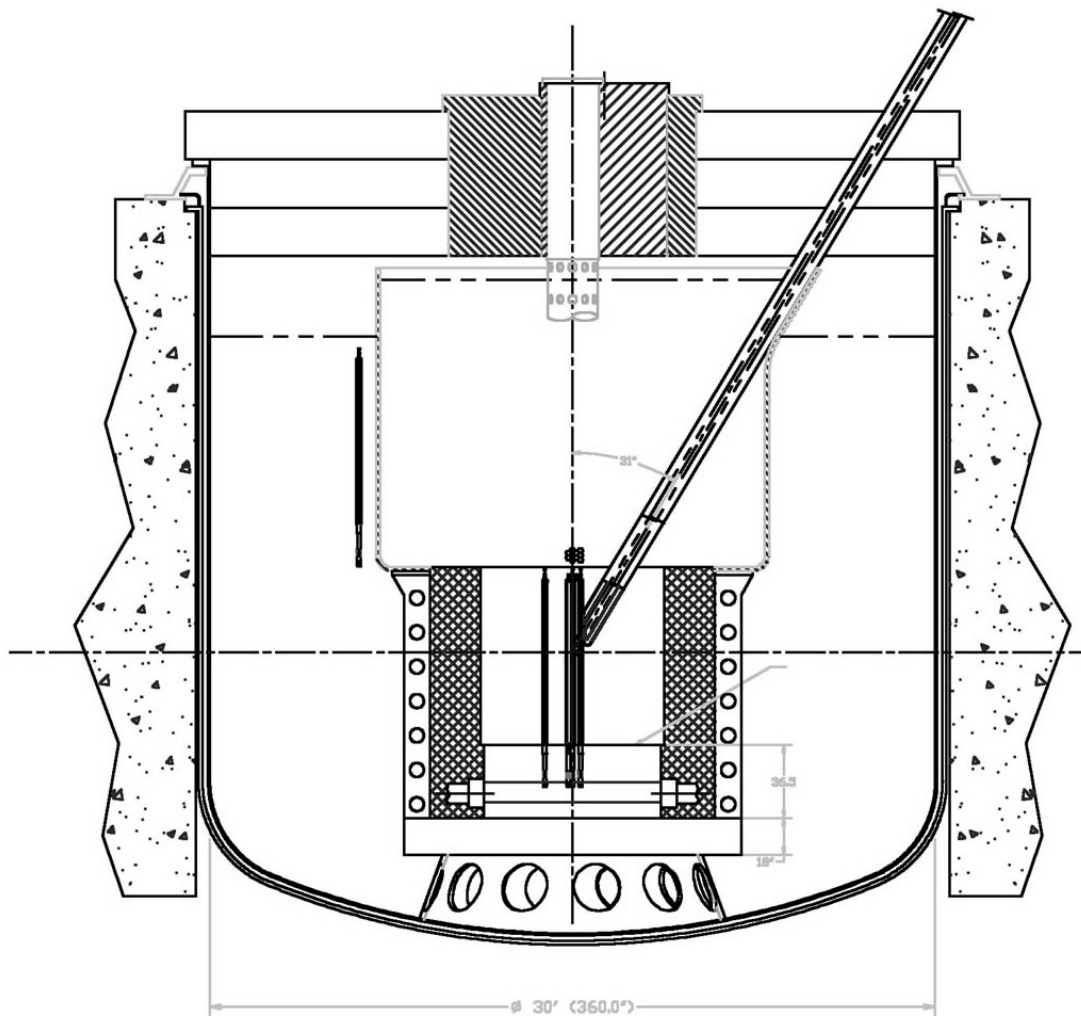


Fig. 54. Vertical section of SCM with inclined accelerator tube entry and vertical redan

above. It also has considerable impact on containment configuration and sizing, and a preliminary estimate of ~27.2 m (90 ft) for the diameter of the containment building (with a height sufficient for a polar crane with a hook height of ~15.3 m) was provided to the balance-of-facility engineering team.

Initial sizing calculations were performed for the design of a Na-to-Na intermediate heat exchanger (IHX) suitable for use in the redan option. The design follows a conservative approach using existing technology. The proposed IHX is a shell-and-tube counter-flow arrangement with the primary flow on the tube side of the unit. The major features and dimensions are shown in Table 27. The tube-side primary flow arrangement was chosen to obtain the low primary-side pressure drop necessary for the redan concept, in which the elevation head must be relied upon to provide flow through the IHX. Consistent with a conservative approach, SS-304 was chosen as the material of construction. This same IHX design can be used for the inner vessel option for the SCM primary coolant. If necessary, the size of the IHX for this option can be reduced by incorporating smaller tubes, since the pressure drop on the primary side can be increased to 2–3 psi (as compared to 1 psi for the redan option).

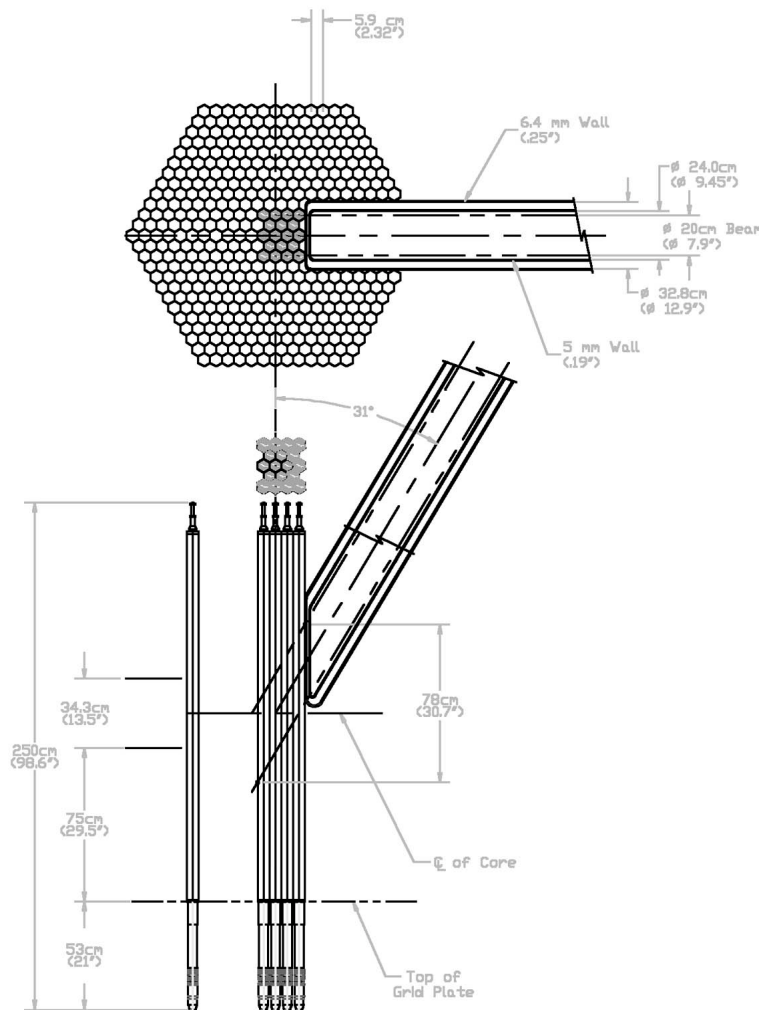
Table 27. IHX Conceptual Design for a Redan-Type SCM.

ADTF IHX Design Parameters (Redan Option)		
Number of Units		2
Rating (ea), MW(t)		50
Primary Temp, EC,EF	Inlet	488, 900
	Exit	371, 700
Secondary Temp, EC,EF	Inlet	331, 627
	Exit	466, 870
Primary Flow (ea)	kg/hr, lbm/hr ($\times 10^6$)	1.27, 2.80
	l/s, gpm (@371°C)	~410, 6500
Secondary Flow (ea)	kg/hr, lbm/hr ($\times 10^6$)	1.04, 2.30
	l/s, gpm (@331°C)	~334, 5300
Primary ΔP , kPa, psi		~6.9, 1
Secondary ΔP , kPa, psi		<138, 20
Material		SS304
Number of Tubes (ea)		1340
Tube OD, cm, in.		2.54, 1
Tube Wall, cm, in. (avg)		0.11, 0.043
Tube Length, cm, in.		277, 109
Pitch/Diameter		1.322
Shell OD, cm, in.		130, 51.25

A multiplier design to accommodate a solid tungsten target has been developed. The preliminary layout for a solid tungsten target for an SCM with an inclined accelerator entry takes the external form of a standard fuel assembly, but is composed of clad tungsten plates. Enough of these assemblies will be required to cover the lateral extent of the proton beam and to provide an axial depth sufficient to stop all protons in the beam, as shown in Fig. 55. This drawing depicts the latest estimate of the shielding below the fuel region necessary to protect the grid plate against damage from neutrons originating in the target and multiplier. Target assemblies are handled identically to fuel assemblies and, hence, target change-out is independent of window replacement.

Two independent SCM geometrical MCNPX models have been used to assess the radiation damage in the grid plate. The first model has a hexagonal representation for the fuel assemblies, while the second model uses an annular representation for the fuel region. Both models have a lead-bismuth spallation target. The first model is intended to analyze the fuel region in more detail. The second model is designed for target and buffer analyses. The atomic displacement rates in the grid plate obtained from both models are consistent.

Using the first model, it has been concluded that a lower axial reflector thickness of 76.5 cm (80% steel, 20% sodium) will yield 0.2 dpa/fpy at a total power of 100 MW. This corresponds to a component lifetime of 20 years for a limit of 3.0 dpa at 75% capacity factor. Hydrogen and helium gas production rates in the grid plate are also calculated.



05-10-01

Fig. 55. Inclined-entry SCM target and multiplier (vertical and horizontal sections)

The second MCNPX model is similar to the previous model except it has annular representation for the fuel materials around the bismuth-lead target. The target details are included in the model. The structural material for the reflector and the target is SS-316. However, the nuclear responses are calculated for iron similar to the previous analyses. The beam power is 5 MW using 600-MeV protons. The fuel volume was adjusted to yield 100 MW from the whole system. In this analysis, the reflector composition is 85% SS-316 and 15% sodium. The 3 dpa limit at the end of life translates into an operational requirement of 0.2 dpa/fpy, based on the SCM operating requirements. This requires about 70 cm of reflector material, which is consistent with the previous results after normalizing to steel fraction.

If helium production is taken into consideration, Type SS-316 can operate up to 10–20 appm of helium without concern about the irradiation damage. Operating at higher values is possible when the radiation damage is taken into consideration in the structural analyses. The above range of helium generation requires about 40–50 cm of the reflector material, which is very close to the 50-cm reflector thickness of the EBR-II design. If the EBR-II reflector design is used, the required reflector thickness

is in the range of 60–75 cm. This thickness is needed in the area under the target zone. However, under the fuel zone, the helium production rate is less, which requires less thickness to protect the grid plate.

SCM Neutron Physics Design

Work on the SCM-100 neutron-physics models continued with the development of MCNPX models for various geometric configurations. The models are being used in the target design and its coupling to the multiplier in estimating hydrogen and helium production rates and damage rates to support the structural design of the target, the sizing of a buffer around the target, and the shielding needed in the SCM to protect key structures such as the grid plate.

SCM Neutron Physics Calculations with an LBE Target

An MCNPX geometrical model for the SCM with a vertical beam using bismuth-lead target material was developed and used to assess the SCM performance. EBR-II Mark-III fuel is used in the multiplier model. The beam power is 5 MW and the fuel loading is adjusted to provide 100 MW of power. The proton beam radius is ~8 cm and the buffer thickness is 7 cm. The inner and outer fuel radii are 15 cm and 25 cm, respectively. The peak fast flux is about 3×10^{15} n/cm²/s. Fig. 56 shows the R-Z neutron flux distribution for neutrons in the energy range 0.1–20 MeV. The nuclear responses in the structural material outside the buffer zone are shown in Fig. 57 as a function of the buffer thickness expressed as 1/outer buffer radius for a 100-MW SCM power level. The nuclear responses show a linear relation to the flux level from the SCM.

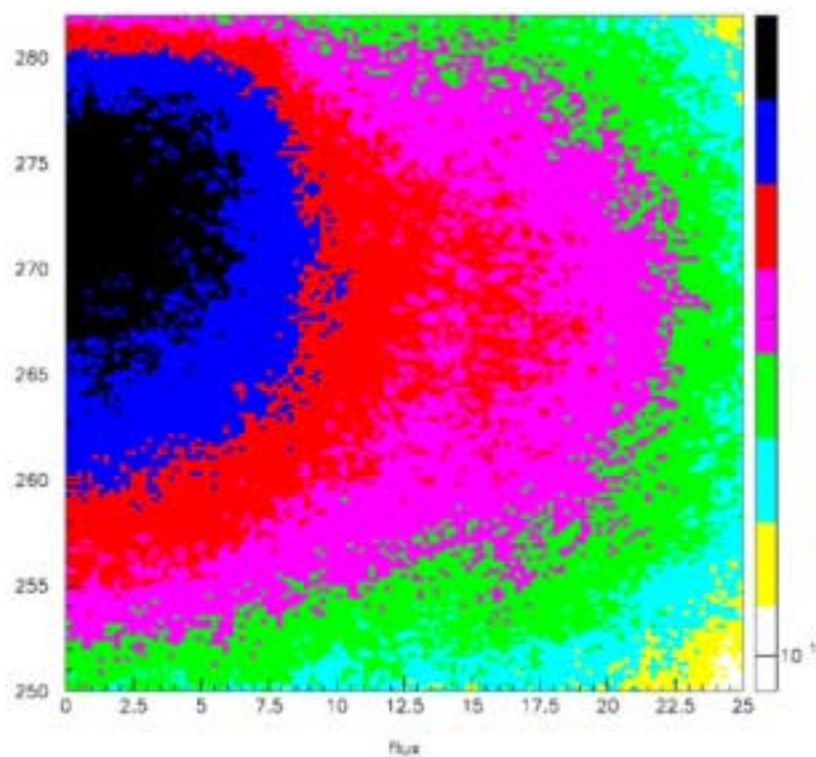


Fig. 56. SCM-100 Fast Neutron Flux (0.1 to 20 MeV) - n/cm²/s

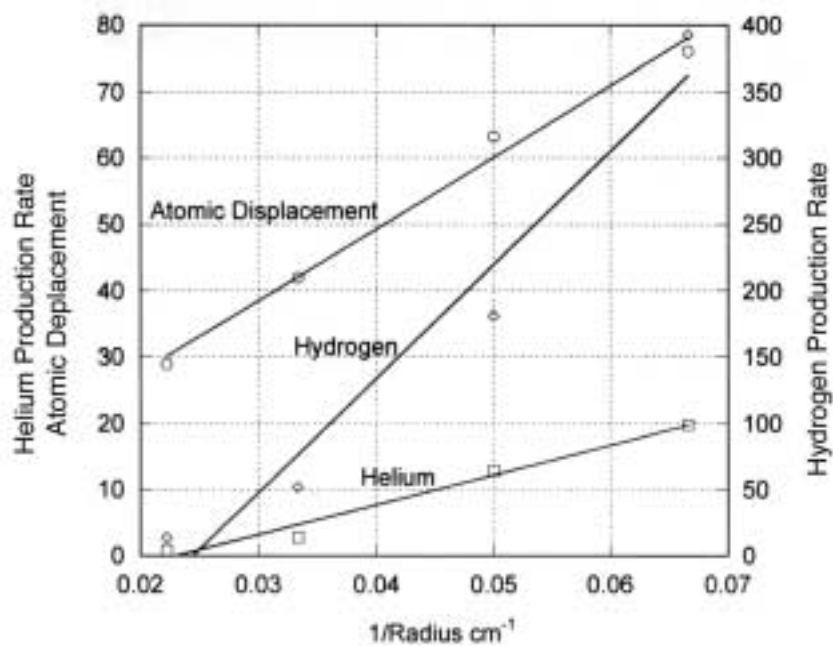


Fig. 57. Maximum nuclear responses in the outer buffer iron structure as a function of the outer buffer radius for a lead-bismuth target with a 5-MW 600-MeV proton beam

The 32° inclined beam-entry configuration has also been modeled with a liquid LBE target. The target itself was shaped like a rhombus in elevation, and was arranged to have its geometrical center at the geometrical center of the subcritical multiplier as in the vertical entry design. Some slight shifting of the target center may be necessary for reducing power-peaking effects and maximizing the total power. A variety of C-shaped core layouts were studied, with a base case of 98 fuel assemblies and 113 reflector assemblies. This configuration uses a steel-sodium reflector element below the beam tube on the open side of the “C.” For present survey purposes, pure sodium reflector was used. Variations have been analyzed by changing the location of the intersection of the beam axis with the subcritical multiplier axis. This shift was varied from -4 to +6 cm, as shown in Table 28. This configuration can provide the necessary thermal power. Obtaining 100 MW at the SCM with a 5 MW beam is readily accomplished using EBR-II-type fuel assemblies of nominal enrichment (~67%).

Table 28. Effect of Target Vertical Location on the Total Power with 5 MW Inclined Beam Power, 98 Fuel Assemblies, 113 Reflector Assemblies.

Beam Axis offset (cm)	Power (MW)
-4.0	104.4
-2.0	106.1
-1.2	107.9
-1.0	107.6
0.0	105.6
+2.0	102.5
+6.0	91.2

Table 29 presents results concerning the relative axial power distribution for a series of cases with an axial target shift of -1.0 cm. The axial peak/average power ratio is 1.093. The axial power profile is very nearly that of a critical system without a neutron source. For the radial power peaking factors, the fuel assembly locations were characterized as shown in Table 30. Clusters 1, 3, 4, and 5 are in the beam path, with 1 closest to the beam. Clusters 6, 7, and 8 are the rows on each side of the beam, with 6 being closest to the beam. The predicted radial peak/average power ratio for these groups of fuel assemblies is 2.15. For comparison, the EBR-II radial power peaking factor was 1.46. These results do not have sufficient spatial detail to find the subassembly with the most power. These results indicate that radial power peaking of the C-shaped core necessary for the inclined entry beam is a design issue. It is probably a key disadvantage for this configuration, relative to a vertical entry configuration.

Table 29. Relative Power in the Top, Middle, and Bottom Thirds of the Active Fuel of the SCM

No. of Reflector Assemblies	P(top) %	P(middle) %	P(bottom) %	Total MW
0	30.32	36.54	33.14	28.97
41	30.50	36.44	33.06	48.24
84	30.68	36.37	32.95	78.00
113	30.82	36.32	32.87	107.60
135	30.84	36.32	32.84	127.70

Table 30. Groupings of Fuel Assemblies in the MCNPX Model with 98 Fuel Assemblies, 113 Reflector Assemblies, and Inclined Entry Beam, LBE Target

Cluster	Number of Fuel Assemblies	Location	Avg. Power (MW)
1	11	column 1 (innermost)	0.963
3	11	column 2	1.563
4	13	column 3	1.455
5	15	column 4	1.263
6	16	row 1 (innermost)	0.843
7	16	row 2	0.817
8	16	row 3	0.726

SCM Neutron Physics Calculations with a Solid Tungsten Target

A model of an SCM with a vertical beam using tungsten-sodium target material has been developed and used in design analyses. The beam power is 5 MW and the fuel loading is adjusted to provide 100 MW of power. The proton beam radius is about 8 cm and the buffer thickness is varied from 0–17 cm. The 2-cm buffer is the minimum thickness required to accommodate the proton beam design uncertainties. A 0-cm buffer was analyzed to study the effect of scattered protons and high-energy neutrons on the structural material. The radiation damage parameters were calculated in the structural material outside the target buffer along the fuel height. The buffer material is the same as the target material. Peak damage parameters are shown in Fig. 58 as a function of the reciprocal of the outer buffer radius. This material is the outer structure of the fuel assemblies next to the target buffer.

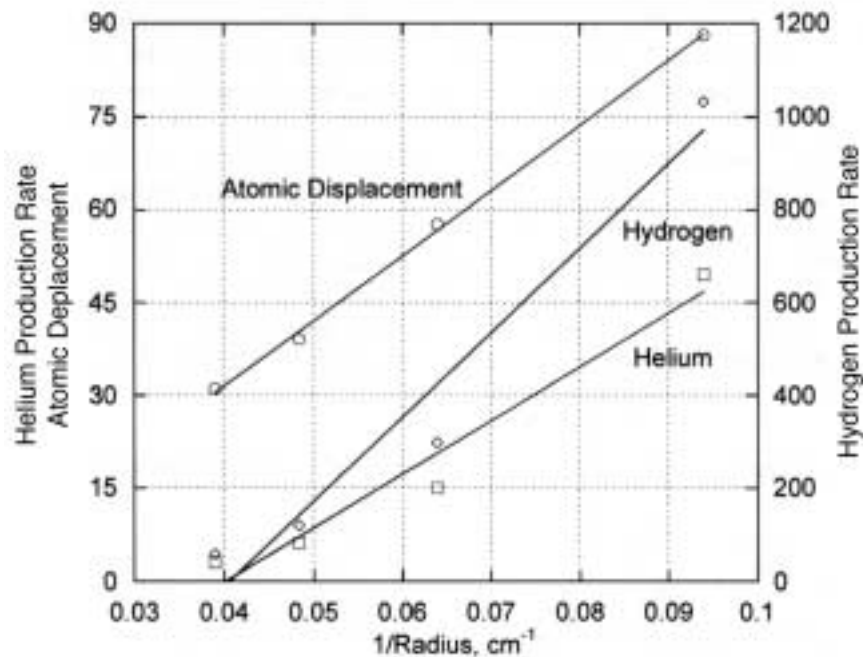


Fig. 58. Peak damage parameters as a function of the reciprocal of the outer buffer radius, tungsten target

SCM Target Designs

LBE Target Design

The MCNPX geometrical model for the SCM design has been used for performing target design analyses. The model has a 5-MW beam utilizing 600-MeV protons. The multiplier dimensions have been adjusted to provide 100 MW of thermal power from the whole system. The beam window has a uniform current density of $40 \mu\text{A}/\text{cm}^2$ and 0.5-cm thickness; both parameters will be adjusted based on the thermal and the structural analyses for satisfying engineering requirements and maximizing the window lifetime. The nuclear heating peak value is $796 \text{ W}/\text{cm}^3$ at 1.75 cm from the LBE surface. Table 31 gives the window nuclear responses (iron is assumed for the nuclear analyses). The neutrons are responsible for 68% of the window atomic displacements and the protons are generating more than 96% of the gas production rate.

The MCNPX analyses have shown that the number of spallation neutrons per proton has little sensitivity to the buffer size, reaching a saturation value at a buffer thickness of about 40 cm. A small buffer thickness of ~7 cm is required to provide inlet and outlet manifolds for the bismuth-lead coolant. However, the number of spallation neutrons reaching the multiplier is significantly reduced as the buffer thickness is increased. This is shown in Fig. 59 where the number drops from 7.8 neutrons per proton with a 7-cm buffer to about 3.3 neutrons per proton with a 40-cm buffer. The neutron leakage is increased as the buffer thickness is increased. This requires the target design to use a minimum buffer thickness.

Table 31. Target Window Nuclear Responses

Proton beam	5 MW power, 600 MeV 40 $\mu\text{A}/\text{cm}^2$
target material	Bismuth-Lead
Energy deposition	766.49 W/cm ³
Atomic Displacement (dpa/fpy)	
Neutrons	46.2
Protons	21.1
Total	67.4
Helium Production (appm/fpy)	
Low energy neutrons < 20 MeV	5.7
High energy neutrons > 20 MeV	50.2
Protons	1437.3
Total	1493.2
Hydrogen production (appm/fpy)	
Low energy neutrons < 20 MeV	6.3
High energy neutrons > 20 MeV	1010.1
Protons	26753.1
Total	27769.5

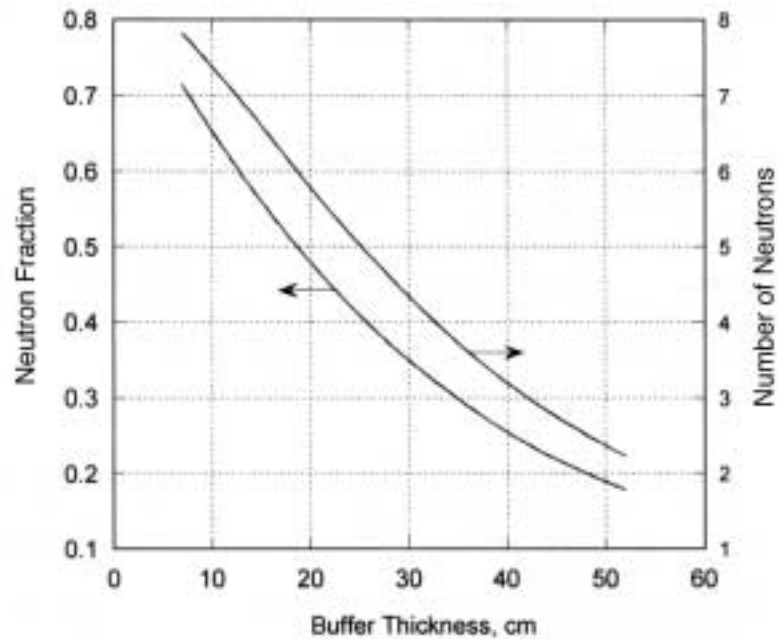


Fig. 59. Neutron utilization as a function of the buffer size for a lead-bismuth target with a 5-MW 600-MeV proton beam

A new target configuration with the lead-bismuth flowing in one direction with respect to the target window has been studied. This configuration enhances the heat removal process from the target window, which reduces the thermal stresses. However, it is more difficult to fabricate relative to the axi-symmetrical design.

Thermal-hydraulics work has been initiated for the SCM LBE target design. Based on an initial configuration (see Fig. 60) and the proton beam heat dissipation curve results, three independent CFD models³⁰ have been built and a series of case studies completed. One of the objectives of the analysis is to minimize heat loads and thermal stresses that could build up at the beam window. Surface temperatures exceeding 550°C are also a concern due to increased rate of corrosion. The current CFD models are intended to provide a preliminary assessment of temperature distributions throughout the target region and lay the groundwork for a more thorough analysis of the SCM target design. The results from three fine-tuned CFD models (FIDAP, STAR-CD, and CFX) will be compared based on a predefined benchmark case. The reference case considers liquid LBE at an inlet velocity of 2 m/s and at a temperature of 370°C.

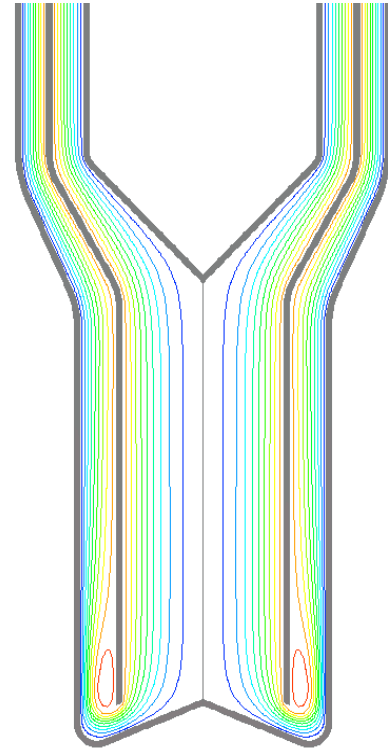


Fig. 60. Axi-symmetric representation of the SCM LBE target design.

The reference case and three variations were analyzed with a FIDAP code model. The reference case resulted in excessive tip temperatures (800°C) and surface temperatures (640°C). Doubling the inlet velocity or reducing the inlet temperature resulted in decreases in the maximum temperature between 110°C–170°C compared to the reference. A variation with interchanged inlet and outlet regions reduced the maximum beam tube temperature down to 670°C (490°C at the surface). However, such a configuration resulted in another stagnation region near the heated part of the middle tube with surface temperatures reaching 510°C. Analysis of alternative, asymmetric geometric configurations indicate that some reduction in the tube temperatures is achieved, but new stagnation regions are developed.

These two alternative configurations, combined with the parametric studies performed on the first design, provide sufficient insight into the conditions that could satisfy the thermal criteria of the target design. With the first design, for example, a reversal of flow direction combined with reduced inlet temperature of 250°C results in a hotspot temperature of 550°C and a maximum surface temperature well below 550°C. Further reductions in peak temperatures are possible with increased flow rate.

Studies with the STAR-CD code address a number of geometric variations, with alterations made in the inclination of the inner or middle walls. Calculations using heat transfer coefficients predicted by STAR-CD show that the design constraints can be met with a reduction in the inner wall thickness from 5 mm to 3 mm.

A preliminary calculation with the CFX code has also been completed, but for a simplified configuration. The CFX results are qualitatively consistent with both the

³⁰ Computational Fluid Dynamics models

FIDAP and STAR-CD results. The velocity of lead-bismuth is reduced significantly close to the tip of the beam window, and that leads to a hotspot in the vicinity of the window tip. However, the calculated hotspot temperature (679°C) is significantly higher than those obtained with the FIDAP and STAR-CD models. The CFX model suggests that the “cool-ability” of the beam window can be enhanced significantly if the coolant flow direction is reversed. In this case, the CFX code predicts the maximum window surface temperature as 400°C, which is well below the design criteria. We assume the maximum temperature that occurs in the guide tube can be avoided by a further design optimization.

Based on these preliminary analyses, the following recommendations are made:

- The window thickness can be reduced from 5 mm to minimize hotspot temperatures if it is required based on the results from the structural analyses.
- The inlet temperature of lead-bismuth can be reduced to 200°C.
- A reversal of flow direction (upward flow in the spallation zone) is preferred to enhance the ability to cool the beam window.

Solid Tungsten-Target Design

A tungsten-target design concept for the inclined beam entry has been developed, which has the same outer geometry as that of a fuel assembly. The design utilizes vertical tungsten plates cooled with sodium similar to the fuel assemblies. The fuel replacement procedure is used for this target design. The shielding material required to protect the SCM grid is integrated in the fuel assembly similar to the EBR-II reflector as shown in Fig. 61.

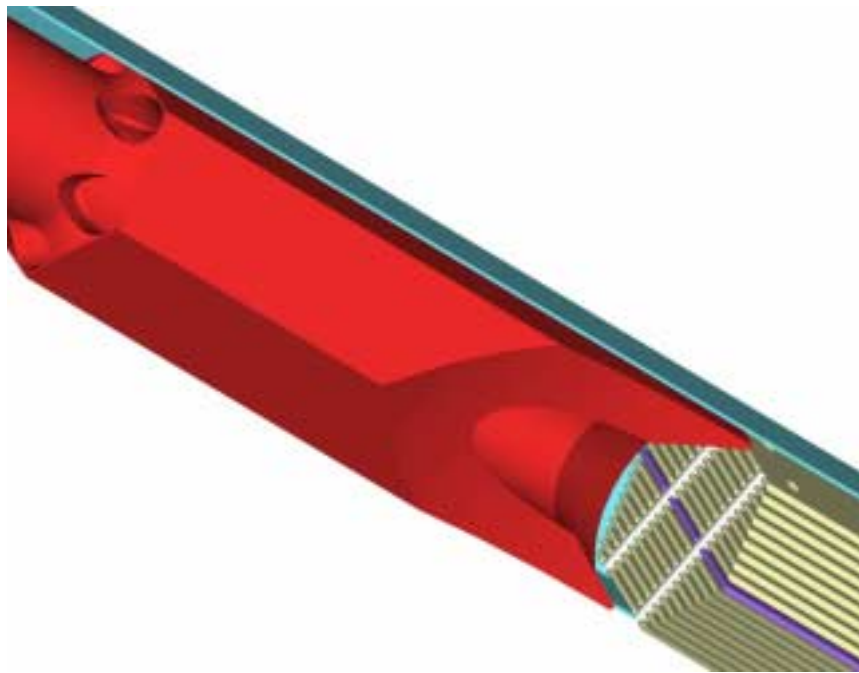


Fig. 61. A section of the tungsten target design concept for the inclined beam entry showing the tungsten plate arrangement and the reflector integration with target design

Tungsten target design analyses have been performed to define the total neutron yield, the SCM neutron fraction, and the spallation neutron leakage as a function of the buffer size. The target has a sodium coolant and steel structure. The proton beam requires a buffer of about 2 cm to accommodate the scattered protons (halo) and the design uncertainties in the operating parameters of the proton beam. The number of spallation neutrons reaching the multiplier is significantly reduced as the buffer thickness is increased. This is shown in Fig. 62 where the number drops from 7.3 neutrons per proton without buffer to about 2.3 neutrons per proton with 17-cm buffer. Also, the axial neutron leakage is increased as the buffer thickness is increased. This requires the target design to use a minimum buffer thickness. The nuclear responses in the structural material outside the buffer require a buffer thickness of about 5 cm. This buffer thickness is adequate for the target, and it provides 6.1 neutrons per proton for the SCM.

Thermal Fatigue Analysis

Thermal fatigue results obtained in the previous quarter for an initial SCM design were not satisfactory if components were subjected to the beam interruption frequency reported for the LANSCE accelerator. Even if the beam reliability were improved by a factor of ten, the lifetime of the upper tube-sheet rim of the IHX and the above core shielding in the hottest subassembly would be less than desired. Alternative thermal-hydraulic designs for a SCM that can tolerate significantly more beam interruptions were analyzed.

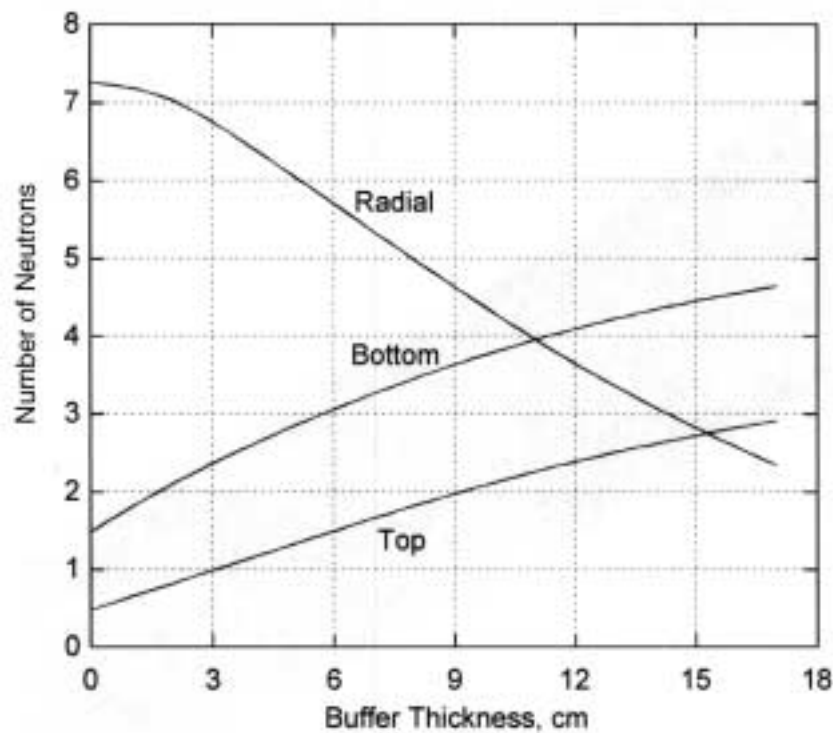


Fig. 62. Neutron source distribution as a function of the buffer size for tungsten-sodium target with a 5-MW 600-MeV proton beam

The two limiting structural components are the IHX upper tube-sheet rim and the above-core shielding in the hottest driver subassembly. The new thermal-hydraulic design consists of 2 IHXs similar in size to that of EBR-II, a lower temperature rise in the core, a lower temperature rise across the intermediate side of the IHXs, a higher primary flow rate, and a higher primary pressure drop. The results indicate that the lifetime of the critical components will be adequate if there is any improvement (a factor of two or more) in beam reliability with respect to LANSCE.

The effect of different schemes for return-to-power after a beam interruption has been further investigated. The pattern in returning to power after a beam interruption (time after interruption, and rate of power change) affect the temperature swing in the critical components and thus has a significant impact on the thermal stresses. Two schemes for returning to power have been investigated (Table 32). The difference between these two schemes is that for short interruptions, the ramp time in Scheme B is 100 seconds instead of 300 seconds. Thus, Scheme A provides more protection to the above-core shielding, whereas Scheme B provides more protection to the IHX upper tube-sheet rim. In conclusion, the scheme used to return-to-power can make a considerable difference in component lifetimes, and there is no one return-to-power scheme that provides optimum protection for all structural components.

Efforts are currently underway to obtain thermal fatigue data for HT-9. The current practice is to analyze HT-9 as if it were SS-316 and then to multiply the results by an uncertainty factor. If there is no HT-9 fatigue failure data, the current practice will be the best available approximation.

Table 32. Return-to-Power Schemes Following Beam Interruption

Duration of Interruption	Return-to-Power Scheme	
	A	B
< 1 s	return to power immediately, if possible	return to power immediately, if possible
1 s ≤ interruption < 50 s	ramp time = 300 seconds for return to power	ramp time = 100 seconds for return to power
50 s ≤ interruption < 400 s	double ramp, 0-.75 power in 100 sec, .75-1.0 power in 8000 more seconds	double ramp, 0-.75 power in 100 sec, .75-1.0 power in 8000 more seconds
≥ 400 s	ramp time = 16,000 sec	ramp time = 16,000 sec

7.4 Balance of Facility Design

A point design has been established for the Balance of Facility design for the ADTF multiple-station concept. The current plant arrangement will have the following features:

- The general site arrangement will be largely based on the APT site plan.
- The target stations will be offset so as to not to interfere with an upgrade path to extend the accelerator tunnel and construct a target station for tritium production.
- The SCM and TMT stations will be arranged such that the beam will enter at the same elevation. This will require a deep subsurface excavation for the SCM containment structure.

- The SCM and TMT stations will be arranged to allow a single hot cell facility to support the operational needs of both stations.

The proposed ADTF site plan is shown in the Fig. 63.

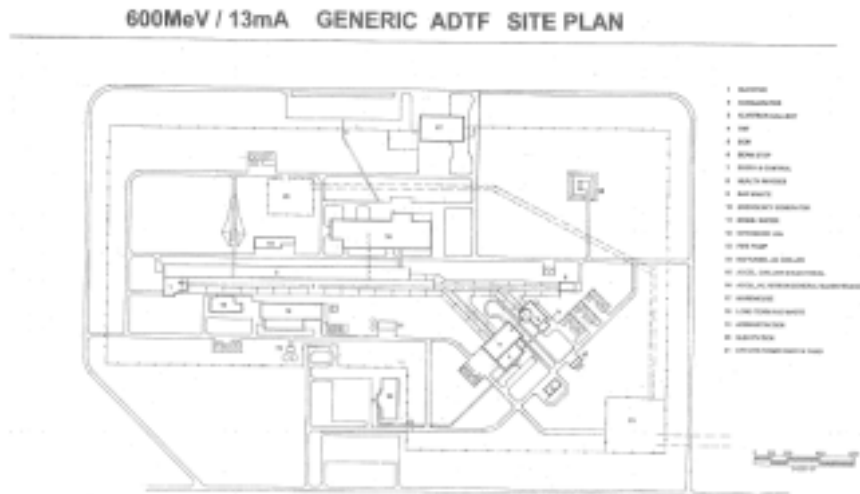


Fig. 63. Proposed ADTF site plan

This page left intentionally blank

V. PROJECT INTEGRATION

8. Systems and Technology Integration

Scope

System and Technology Integration functions to coordinate all technical elements in defining requirements, performing system-level evaluations, developing pre-conceptual designs and establishing technology development activities into a comprehensive Research & Development (R&D)/Proof of Performance (POP) effort. Overall system objectives, system performance requirements, and POP requirements are used to correlate R&D needs, data quality objectives, experimental facilities, resources, and materials. System-level modeling evaluates the performance of multi-strata options in establishing a technically feasible spent nuclear-fuel management program especially with regard to proliferation, economics, environment, safety and institutional issues. Likewise, pre-conceptual designs serve as fundamental bases in defining critical R&D and focusing POP testing. Woven together, the system and technology integration activities can provide a solid foundation for focused and coordinated AAA research and development.

Highlights

- AAA Task Force on AAA System Definition was formed, implementing a “nuclear future” approach to multi-strata evaluations.
- Multi-strata system cases have been specified, and initial results are being generated for Tier I processes.
- Environmental, proliferation, and economic factors are being considered in multi-strata system evaluations.

Multi-Strata Evaluations

The past quarter has seen tremendous change in the focus of Multi-Strata evaluations, based on considering transmutation as part of a “nuclear future” rather than dealing with only the existing legacy of spent nuclear fuel. Three principal cases have been established by the Task Force on AAA System Definition to assess options for an integrated nuclear waste management strategy, as depicted in Fig. 64.

The evaluations utilize an isotopic feed stream of 10-year-cooled spent-nuclear fuel irradiated in Advanced Light Water Reactors (ALWR) in the commercial “Nuclear Future” infrastructure (subsequent evaluations will consider alternative commercial feed streams). The fundamental difference between Case 1 and Cases 2/3 is the separation of plutonium as input to the Tier I thermal spectrum irradiations. In Case 1, the input feed stream of plutonium and technetium is sent to either a gas-cooled or water-cooled advanced reactor (first tier), recycled 1-2 times, with residuals and the minor actinides sent to a second tier, accelerator-driven system (ADS) for further

transmutation. In Case 2, an input feed stream of unseparated transuranics is sent to either a gas-cooled or water-cooled advanced reactor, potentially recycled, with residuals and minor actinides again sent to the ADS. In Case 3, the transuranics, minor actinides and long-lived fission products are sent directly to fast systems with a conversion ratio of 0.0, such as an ADS in the original Roadmap, or with a conversion ratio of 0.5, as with the Integral Fast Reactor.

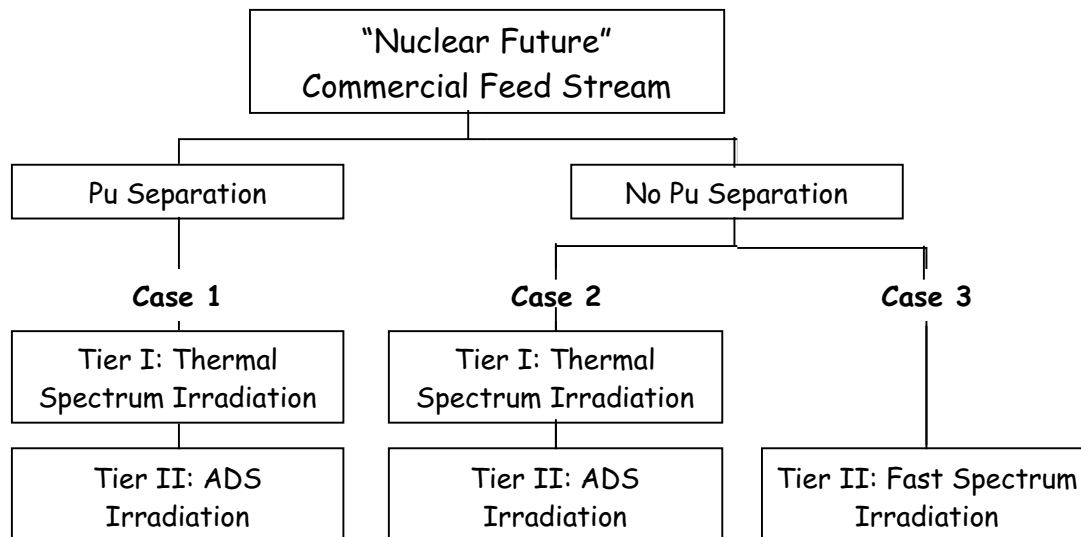


Fig. 64. Principal cases under evaluation by multi-strata task force

Each of these cases can use MOX and/or non-fertile fuels of metal, oxide or nitride composition in the first tier, with appropriate separation technologies. However, timeframe constraints limit the variations imposed on the three primary cases for initial evaluation. Even with the limited evaluation set, the fundamental differences between fuel forms in both tiers will still be demonstrated, as well as the differences between different systems and isotopics assuming a metal fuel in the second tier.

Burnup calculations for Cases 1 and 2, using commercial ALWR commercial feed stream, are essentially complete, and this preliminary input has been provided to staff to assess the isotopic impact on separations and system processes. Resulting isotopics are being fed back to the burnup calculations for the second tier evaluations, which should be complete for the ALWR feed stream late in July. Data will then be incorporated into the integrated system spreadsheet, as available, to baseline the time- and process-dependent mass inventories for assessment of activity, thermal load, radiotoxicity and material attractiveness.

Pin-cell analyses are being performed by separate staff on the first tier water- and gas-cooled systems, using common design and spectrum assumptions to confirm burnup assessments. Proliferation potential will be evaluated using mass inventories and material attractiveness levels. The Delta model, used to support the Organization for Economic Cooperation and Development (OECD) evaluations, is being analyzed for system and economic assumptions and potential applicability.

9. University Programs

Scope

The AAA University Programs consists of four major aspects:

- **University Fellowships Program (UFP)** - The Amarillo National Research Center (ANRC) is acting as the executive agency for the AAA Program to select, award, and administer fellowships for ten graduate students beginning in FY01.
- **UNLV University Participation Program (UNLV UPP)** - The University of Nevada at Las Vegas (UNLV) is supporting the AAA Project through “research and development of technologies for economic and environmentally sound refinement of spent nuclear fuel...”³¹
- **AAA Directed University Research** - Three universities currently support R&D and technology development: University of Michigan, University of California-Berkeley, and University of Texas-Austin.
- **University Research Program (URP)** - A future program to create a NERI-like competition for faculty and student research proposals (not funded in FY01).

The AAA University Program also involves coordination between other AAA projects and academia.

Highlights

AAA University Fellowship Program (UFP)

- The Amarillo National Research Center (ANRC) received 24 applications for 10 fellowships; applications were reviewed and ranked by a Blue Ribbon Panel from DOE/NE, LANL, ANL, and UNLV, and ten fellowship recipients were selected.
- Summer internship positions were established at LANL and ANL for four of the fellowship recipients.

AAA University Participation Program (UPP)

- The AAA UPP was initiated at UNLV with a \$3M budget, committees established, and a UNLV AAA Seminar Series was begun with monthly seminars presented by AAA researchers. Two positions were established for LANL staff at UNLV: a full-time Intercollegiate Programs Coordinator and a part-time International Programs Coordinator.
- A formal submission process for student-based research proposals was established and a call for proposals issued. Seven proposals were received and reviewed, and four proposals were selected for funding.

³¹ ref. H.R. 5483, P.L. 106-377

AAA Directed University Research

- Contracts that were initiated for the University of Michigan and the University of California at Berkeley early in FY01 have not been awarded due to delays in LANL contracting; U of Michigan researchers continued under FY00 funding, faculty at UC Berkeley have exhausted their funding.

University Participation Program

Four research proposals submitted to the AAA UNLV University Participation Program were funded. The UNLV Principal Investigator submitted a Statement of Work for this research to begin in June. The four funded research projects are:

- “Design and Analysis for Melt Casting Metallic Fuel Pins Incorporating Volatile Actinides”
- “Experimental Investigation of Steel Corrosion in Lead Bismuth Eutectic (LBE): Characterization, Species Identification, and Chemical Reactions”
- “Modeling, Fabrication, and Optimization of Niobium Cavities – Phase I”
- “Hydrogen-Induced Embrittlement of Candidate Target Materials for Applications in Spallation-Neutron-Target Systems”

10. Collaborations

Scope

There is great potential for beneficial international collaborations with over a dozen nations currently evaluating nuclear waste partitioning and transmutation. The AAA Program, primarily through the technical community, has informal contacts with many of these programs; however, formal international collaborations, which are in the best interests of the Program, must be carefully developed so as to avoid over-commitments or other programmatic challenges. Through the third quarter of 2001, the following collaborative activities were “formalized” and will be pursued:

- Participation in technical collaborations with the French CEA in developing technologies related to materials, fuels, physics, safety, and a proposed accelerator-driven test facility. Also under discussion are separations, accelerator technology, and systems.
- Participation in a Working Party on Partitioning and Transmutation (WPPT) under the auspices of the OECD/NEA (Organization for Economic Cooperation and Development / Nuclear Energy Agency).

Other collaborative efforts under consideration include the European Union, JAERI (Japan), and work under the auspices of the IAEA. Several other national programs are also of interest, but discussions on collaborations have not progressed as far with those parties.

Highlights

- A delegation from the AAA Program, including representatives from the DOE, LANL, and ANL, participated in meetings with the CEA in France during June. Four of five existing work packages, including materials, physics, safety and the proposed ADTF were discussed.
- An initial meeting of the NEA Working Party on Partitioning and Transmutation (WPPT) set out an ambitious long-term agenda. This study would address many of the issues being evaluated within AAA within an international context.

Meeting with CEA at Saclay

The AAA Team met with Jean-Michel Lagniel, and Henri Safa at the CEA laboratory in Saclay, France. Lagniel is the deputy director of the CEA group that performs research on accelerators. Safa is responsible for the superconducting section. The various projects that they support include IFMIF, ESS, ADS, RIB, CONCERT, and TESLA. The TRISPAL project (French APT—tritium production with accelerators) is no longer being pursued. Although they are continuing accelerator research, there are no projects that have been approved for construction.

In our discussions we learned of the following activities at CEA:

- A recent test of a beta=0.65 cavity achieved 25 MV/m.
- Our 5-cell cavity can be tested in their cryolab in the horizontal position. They expect gradients twice what was measured.
- They still have one of our single cell cavities. It can be used to test different cleaning techniques. This should be discussed for part of our collaboration.
- The first beta=0.47 superconducting cavity will be made without stiffeners and the mechanical properties will be measured. Appropriate stiffening will then be added as required.
- Saclay is building a synchrotron that operates at 352 MHz.

Some effort is going into planning a European IFMIF³² program, but no real money has been provided as of yet. The 150-MHz machine is to produce a 100-mA deuteron beam directed to a liquid lithium target. Bob Jameson (LANL) is the US point of contact.

We visited the injector test stand for the H⁺ source and the H⁻ source. The H⁺ injector is operating smoothly at about 75 mA continuous with about 1 trip per day. After each trip, the control system brings the accelerator back on line within 2 minutes.

The 6.5-kV test H⁻ source is also under development. Joe Sherman (LANL) gave the AAA group a complete tour and discussed many of the problems that they are having in obtaining a workable source. This source is very developmental and can produce milliamps of current. Sherman then discussed their H⁺ source. The H⁺ source ran at 115 mA with only 1 trip per day and 1 trip per week at 75 mA. They measured 10%

³² International Fusion Materials Irradiation Facility

deneutralization at the RFQ entrance position, resulting in lower compensation of space charge in the drift section after the first solenoid.

Eric Pitcher (LANL) met with Sylvie Leray (Saclay) and discussed the physics collaboration. Dick Prael (LANL Group X-5) recently visited Leray, and the two of them have reached an agreement to have Leray's group install Cugnon's latest INCL intranuclear cascade model and the evaporation-fission model of Schmidt from GSI into the latest version of LAHET3. This effort will lay the groundwork for including these two models in MCNPX. Leray is willing to do this work provided her group retains control of updating MCNPX with subsequent versions of the two models. This activity should be pursued through the physics work package.

Leray has collaborated on the inverse kinematics experiments at GSI that have recently produced excellent measured spallation and fission product residue distributions against which the current intranuclear cascade codes have been compared. Of the models that her group has run, the Cugnon INC-Schmidt EVAP models give best agreement with experimental results. Pitcher informed Leray that Stepan Mashnik (LANL) has recently modified his CEM model, and that his new version also gives excellent agreement with these data.

Leray also described experiments carried out at Saturne in the late 1990s measuring double-differential neutron spectra from thin and thick iron, tungsten, and lead targets. A portion of these experiments overlaps well with an experiment proposed by AAA to be carried out in the LANL blueroom in December. Unfortunately, the experimental data are not yet published in the open literature, and so are not available to DOE researchers. Leray will speak to her colleagues about publishing the data so they can be released.

OECD/NEA Working Party on Partitioning and Transmutation

An initial meeting of the NEA Working Party on Partitioning and Transmutation (WPPT) was held in June at NEA headquarters in Paris. The WPPT Chairman, David Hill (ANL), provided a proposed WPPT charter and discussed proposed actions of four working subcommittees. Greg Van Tuyle was designated as the US representative to the WPPT. Since Van Tuyle serves as Chair of the Accelerator Utilization and Reliability Subgroup of the WPPT, his participation is important to initiating the activities of this subgroup.

The members worked through the charters for the WPPT and the WPPR (Working Party on Burning Plutonium in Reactors). While the WPPT plans to communicate closely with the WPPR, care was taken to minimize the appearance of overlapping focus for the two groups. A third group, the Committee on Nuclear Safety led by Tom King (NRC), considers the safety of advanced nuclear systems. The potential overlap will likely be minimal.

The proposed vision for the WPPT involves working the collaboration for about 3–4 years, addressing the need to specify the potential benefits of partitioning and transmutation and determine whether they are realizable. Chairman Hill acknowledged the ongoing evaluations of equilibrium fuels cycles, but stated a desire to extend the analyses to conclude some non-equilibrium cases. Since most national programs are struggling with the same basic challenges, there seemed to be little opposition to the Chair's proposed vision. The likely interest of the IAEA (which

includes 130 member states, and is therefore roughly four times the size of the OECD/NEA) was indicated by a participant who recommended the study be conducted "in cooperation with the IAEA."

The four sub-groups of the WPPT are as follows:

- Physics and Safety, chaired by Marc Delpech from CEA,
- Fuels, chaired by Toru Ogawa from JAERI,
- Separations, chaired by Jim Laidler from ANL, and
- Accelerators, chaired by Greg Van Tuyle from LANL.

Each subgroup chair agreed to complete their efforts by June 1, 2004, and will provide subcommittee reports to the WPPT Chair for inclusion in a final report of the WPPT. The subcommittee chairs agreed to provide detailed plans for their subcommittees to the Chair by Sept 1, 2001, clearly stating any assumptions (e.g., multi-strata systems) and defining the interfaces with each of the other subcommittees (for example, accelerator and physics/safety share an important interest in beam control). Proposed membership of the subcommittee (with affiliations and contact information) will be included in the plans. The WPPT Chair will provide an expanded definition of how the WPPT will guide the effort of the subcommittees to develop the integrated answers regarding benefits and potential.

Regarding the Accelerator Utilization and Reliability Subcommittee, tentative plans for working the issues through a proposed Workshop to be held in Santa Fe, NM, in May 2002, was discussed and thought to be appropriate. When pressed to set a tentative date for the Santa Fe workshop, the period May 13-17, 2002 was identified as target dates.

The next meeting of the WPPT is scheduled for Nov. 15-16, 2001, at the Reno Hilton in conjunction with the AccApp01/ADTTA01 topical meeting to be convened at the American Nuclear Society Winter Meeting. Greg Van Tuyle, who is also General Chair of AccApp01/ADTTA01, will work with the AccApp01/ADTTA01 Technical Program Chair, Warren Funk (TJNAF) on the logistics.